国立大学法人
電気通信大学

Study on RF Energy Harvesting Rectenna System from Ambient RF Signal for IoT Applications

NGUYEN THUY LINH

Department of Computer and Network Engineering
The University of Electro-Communications

A dissertation submitted for the Degree of

Doctor of Engineering

January 2020

国立大学法人
電気通信大学

Study on RF Energy Harvesting Rectenna System from Ambient RF Signal for IoT Applications

by

NGUYEN THUY LINH

A Dissertation Submitted for the degree of
DOCTOR OF ENGINEERING

at

THE UNIVERSITY OF ELECTRO-COMMUNICATIONS

JANUARY 2020

I would like to dedicate this dissertation to my dear family, especially my parents. The dissertation is my present for my father in heaven. I am thankful to my beloved husband for being together with me since married time, bringing up my two daughters - Giang and Duong, and encouraging me during the time of this work.

Tokyo, 2020.1

Acknowledgements

First of all, I would like to emphasize my deepest appreciation to my supervisors, Professor Koichiro ISHIBASHI and Professor Cong-Kha PHAM, for their enthusiastic encouragement, guidance, and support during my doctor course. They have advised and taught me the way to research as a Ph.D. student. Besides, they inspire my interest in the development of innovative technologies. With their guidance, my knowledge is broadened.

I extremely appreciate the supports of Professor Koichiro Ishibashi to me in daily life. He always stands beside me and encourages me to overcome the hardest time in my life, especially, when my father passed away. With me, it is my pleasure to be his student. I hope that we still maintain a good relationship in the future.

I would also like to express my thanks to Doctor Yasuo Sato for his technical support. He taught me to usefully utilize experimental equipment in our laboratory. Besides, he enthusiastic supports me in experiments in the real environment.

I would like to thank the University of Electro-Communications Tokyo (UEC), and JST-CREST Project, Grant Number JPMJCR16Q1, for giving me a chance to join in the Project and study in Japan. Thank them, I have an opportunity to study Ph.D. course. I also would like to send my thanks to the UEC's professors for their guidance and support during my doctor course.

I would like to send my thanks to my teachers and colleagues in the Faculty of Radio-Electronic Engineering, Le Quy Don Technical University, Ha Noi, Viet Nam. I also would like to present my thanks to all of the members of ISHIBASHI's laboratory and my friends in Japan and in Vietnam. Their kindness encourages me to finish my course.

Last but not least, I would like to acknowledge VLSI Design and Education Center (VDEC), the University of Tokyo in collaboration with Synopsys, Inc. and Cadence Design Systems, Inc for their support for this work.

Study on RF Energy Harvesting Rectenna System from Ambient RF Signal for IoT Applications

APPROVED

Prof. Koichiro ISHIBASHI , Chairman

Prof. Cong-Kha PHAM

Prof. Ryo ISHIKAWA

Prof. Nobuo NAKAJIMA

Prof. Motoharu MATSUURA

Date Approved by Chairman

Abstract

Study on RF Energy Harvesting Rectenna System from Ambient RF Signal for IoT Applications

NGUYEN THUY LINH

Doctoral Program in Electronic Engineering
The University of Electro-Communications

In this thesis, a structure of the RF energy harvesting (RFEH) system, which is applied for RF sensor TAG and RF sensor TAG with weak-up receiver (WuR), is studied and proposed. First, characteristics of the RF signal in the environment are analyzed; hence, essential specifications of the ambient RFEH system are pointed out. The analyzation indicates that the Q factor of RFEH system affects bandwidth (BW) of the RF signal, and a wide bandwidth RFEH system is an essential structure to harvest the ambient RF signal efficiently.

Second, principle specifications affecting the efficiency of a rectifier are theoretically studied and evaluated. A 3-stage cross-coupled rectifier (CCR) with the application of dynamic threshold MOSFET (DTMOS) and body-tire-to-source MOSFET (BTMOS) in 65nm Silicon on Thin Buried oxide (SOTB) technology was fabricated and evaluated. The measurement results indicate that DTMOS CCR, which has a higher drain current than that of BTMOS CCR, obtains two times output power higher than BTMOS CCR. Besides, the Q factor of the rectifier is chosen to ensure the BW of the RF signal so that the entire RF power is rectified. As a result, the output power of the rectifier when excited by modulated signals becomes two times higher than that of the rectifier when excited by a pure sine wave signal at -20 dBm input power.

Third, a system design methodology of the ambient RFEH system is analyzed in which relationships between Q factor of the total system, Q factor of the rectifier, and the Q factor of matching circuit are presented. From the methodology, the wide bandwidth RFEH system from 950 MHz cell phone RF signal is designed. In the system, the Q factor of the rectifier dominated Q factor of the total system to ensure the BW of Long-Term Evolution (LTE) signal. A wide BW matching, which is 62 MHz, between a half wavelength wired dipole antenna and the rectifier is designed to fulfill the system.

The measurement results with the 950 MHz LTE signal in the environment show that the output power of the designed system, which is 3.48 μW, is 15 times higher than that of the other study at -20 dBm input power. The designed rectenna with Yagi antenna generates 7.6 μW DC power at outdoor conditions when LTE signal is at a level of -18.6 dBm.

In conclusion, the proposed structure of the RFEH system in this work is a potential candidate for battery-less IoT applications. The designed rectenna is suitable for the RF sensor TAG and RF sensor TAG with WuR.

List of Abbreviation

BPSK	Binary Phase-Shift Keying
BTMOS	Body-Tired-to-source MOSFET
BW	BandWidth
CCR	Cross-coupled rectifier
DTMOS	Dynamic Threshold MOSFET
DTV	Digital Television
GPS	Global Positioning System
ER	Energy Receiver
IERC	European research cluster of IoT
IR	Information Receiver
IoT	Internet of Things
LTE	Long-Term Evolution
MCU	MicroController Unit
OFDM	Orthogonal Frequency Division Multiplexing
QAM	Quadrature Amplitude Modulation
PAPR	Peak to Average Power Ratio
PCE	Power Conversion Efficiency
RF	Radio Frequency
RFEH	RF Energy Harvesting
SWIPT	Simultaneous Wireless Information and Power Transfer
WIT	Wireless Information Transfer
WIPT	Wireless Information and Power Transmission
WPBC	Wirelessly Powered Backscatter Communication
WPCN	Wirelessly Powered Communication Network
WPT	Wireless Power Transfer
WSN	Wireless Sensor Node
WuR	Wake-up Receiver

SOTB	Silicon-on-Thin-BOX
VLSI	Very-Large-Scale Integration

Contents

List of Figures

List of Figures

List of Figures

List of Tables

Chapter 1

Introduction

In this chapter, the background research of Internet of Things (IoT) and energy harvesting technologies are presented. Moreover, the motivation and main contributions of RF energy harvesting in IoT are also described. Finally, the dissertation layout is presented to clarify the composition of this dissertation.

1.1 Research Background

1.1.1 IoT definition and applications

Nowadays, with the vast improvement of technology, we tend to the world in which everything and everyone can be connected and communicated by the application of IoT [1]. The IoT allows people and things to be connected anytime, anywhere, with anything and anyone, ideally with any network, and any service [2], [3]. Fig 1.1 illustrates a definition of IoT of European research cluster of IoT (IERC) [4].

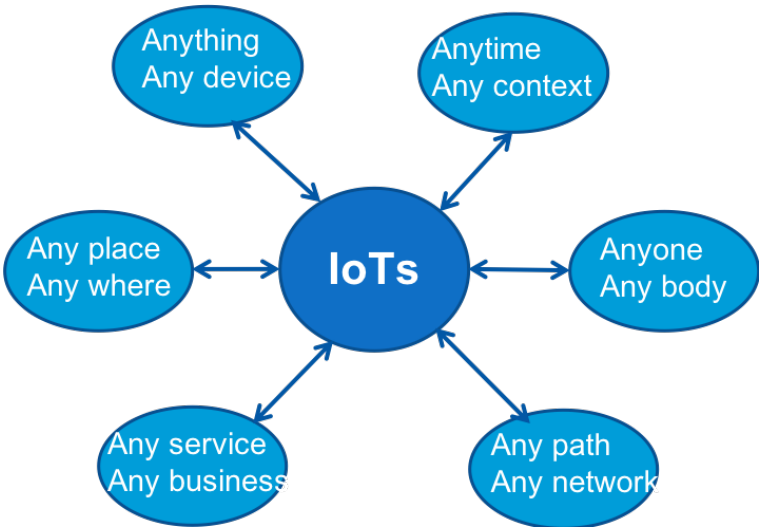

Figure 1.1: IoT definition by IERC [2]

The Internet of Thing (IoT) brings immense utilities for human life, such as makes daily life easier, faster, safer, and smarter [5]. The applications of IoT can be listed as design of smart cities, predicting natural disasters, design of smart homes, design of efficient transport systems, industrial applications, and medical applications [1].

In general, an IoT device consists of four parts [6]:

- A sensor part
- A processing part, which is digital, consists of a processor, memory, filters, accelerators. Besides, a security IP and data encryption are included for security.
- A radio part, which can utilize Bluetooth, Zigbee, Wi-Fi, etc.
- A power management part which is used to control power domains, power supplies, etc.

In IoT applications, a vast amount of sensors is used to collect information from social life as shown in Fig 1.2

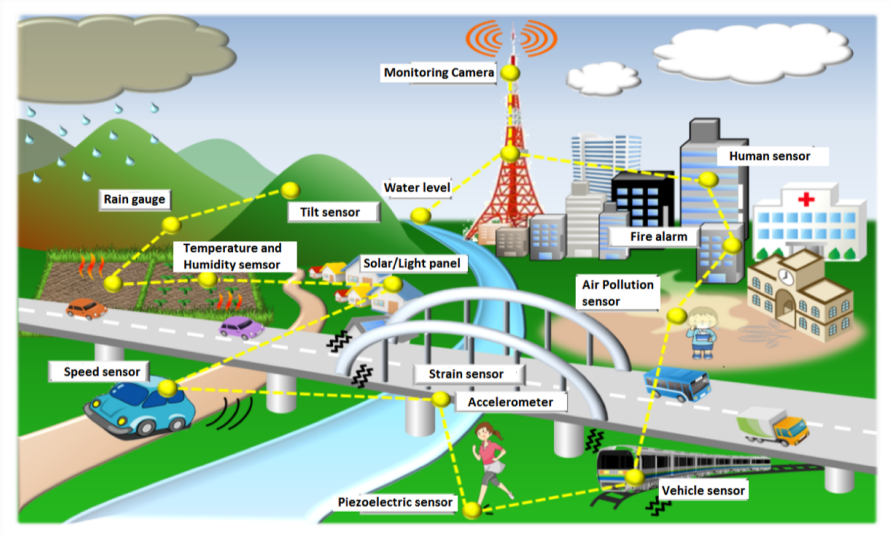

Figure 1.2: IoT applications in human social

The sensors in IoT systems are diversity such as Global Positioning System (GPS) acquisition, weather sensor, liquid sensor, smoke sensor, soil and moisture sensor, distance sensor [7]. The GPS sensor, which used for collecting GPS data, is useful in position applications such as golf car finder, navigator, lost-devices, and belongings tracker. Weather sensors are used to take the surrounding atmosphere information such as temperature, humidity, pressure, light. Applications using weather data are home automation and control, display notifications. Smoke sensor, which is used to collect data about smoke, is handy for warning emergencies in case of fire happened.

Essential design requirements, which are taken into account when dealing with IoT, include [6]:

- Connectivity: wireless;
- Security: secure boot, data encryption, authentication, authorization, physical protection;
- Sensor: sensor hubs, vision & gesture, voice recognition, touch;
- Energy: energy harvesting, wireless charging adoption.

In [8], services specifications for the Padova smart city project, which is one of the IoT applications, are presented. In this project, a requirement of supplying

power for IoT applications is one of the crucial requirements, especially when battery charging or removing is tricky. The energy harvesters are used in waste management, noise monitoring, traffic congestion, and smart parking. The energy harvesting technique becomes an essential solution in this case [9].

1.1.2 Energy harvesting technologies

In the energy harvesting technology, energy from ambient power sources, such as vibration, heat, and electromagnetic waves, is collected and converted into DC power to storage as a power supply for its applications [10], [11]. The available ambient energy sources and their pros and cons are shown in table 1.1.

Table 1.1: Available Ambient Energy Sources [10].

	Solar energy	**Thermal energy**	**Ambient RF energy**	**Vibration**
Power density	100 mW/cm^2	60 $\mu W/cm^2$	0.0002 $\sim$ 1$\mu W/cm^2$	200 $\mu W/cm^2$
Available time	Day time (4 $\sim$ 8 Hrs)	Continuous	Continuous	Activity dependent
Pros	•Large amount energy •Well developed tech	Always available	•Always available •Widely available	•Well developed tech •Light weight
Cons	• Need large area •Non-continuous •Orientation issue	•Need large area •Low power •Rigid & Brittle	•Distance dependence •Depending on available source	•Need large area •Highly variable output

The solar energy harvesting converts light energy to electrical energy by the photoelectric [12]. The power of the solar source, which is 100 $\mu W/cm^2$ to 1000 $\mu W/cm^2$ indoors and 100 mW/cm^2 outdoors [11], is the strongest in comparison with that of other natural source but the power is not continuous. Besides, the solar energy harvesting system usually requires a large area [13], [14]. A thermoelectric generator electrical power from a temperature gradient between

two dissimilar conducting materials [12]. Generally, the thermal power energy density is quite large, but the output power of a thermal energy harvesting is lower than that of the solar energy harvesting system [15]. Besides, the thermal energy harvesting is less intermittent since they work as long as there is a temperature difference across their surfaces [11]. Piezoelectric harvester, which power is from vibration, converts vibrational energy into electrical energy by the piezoelectric effect [16], [17]. The output power of piezoelectric harvester is normally lower than other energy harvesters, but it has a large dynamic range when irregular motions are utilized as the driving force [18].

Ambient radio frequency (RF) energy is quite a low energy density, which is normally form 0.2 nW/cm^2 to 1 $\mu W/cm^2$ [19], [20], [22], compares to other energy sources. However, the ambient RF sources now increasing with the expanding of wireless communication and broadcasting infrastructure. Also, the radio frequency (RF) energy is a promising source for energy harvesting because of its general characteristics in daily life. The RF energy harvesting (RFEH) enables the wireless devices harvesting energy from RF signals for their information processing and transmission. Therefore, the RFEH network can be applied to wireless sensor networks [23], wireless body networks [24], wireless charging systems [25]. Besides, the RFEH system is easily integrated with other harvesting systems, such as the photovoltaic EH system [26], and the thermal EH system [27], to make a hybrid EH system. In conclusion, the RFEH technique shows many advantages and has attracted a considerable amount of attention in a scientific community.

1.2 Motivation and Contributions of this study

1.2.1 Motivation

Wireless power transfer (WPT) is a technology, which is based on electromagnetic theory and radio wave theory, to transfer and harvest electrical power [28,29]. The WPT technologies consist of three main techniques such as resonant coupling WPT, inductive coupling WPT, and WPT via radio wave,

which also called as RF energy harvesting, as presented in table 1.2

Table 1.2: Characteristics of WPT technologies [28, 29].

	RF energy harvesting	**Resonant coupling**	**Inductive coupling**
Field	Electromagnetic (EM)	Resonance (Electric, Magnetic or EM)	Magnetic
Method	Antenna	Resonator	Coil
Efficiency	Low to high	High	High
Distance	Short to long	Medium	Short
Loss during Transmission	Low	Medium	High
Power	Low to high	High	High
Regulation	Radio wave	Under discussion	Under discussion

In the resonant coupling and inductive coupling techniques, transmitter and receiver are electromagnetically coupled, and electrical power is wirelessly transferred via an electric field, a magnetic field, or electromagnetic field. Therefore, these techniques are near-field wireless transmission and not suitable for mobile and remote applications. Besides, the RFEH technique, which utilizes the RF power to generate DC power, is a far-field technique and has remarkable advantages, as mentioned in part 1. With RFEH technique, the radio wave carries both energy and information simultaneously so wireless information transfer (WIT) and WPT can combine in a wireless information and power transmission (WIPT) to efficiently utilize the RF spectrum/radiation and the network infrastructure [30].

The WIPT can be divided into three types:

- Simultaneous Wireless Information and Power Transfer (SWIPT): Energy and information are simultaneously transmitted in the downlink

from multiple access points or multiple receivers. The energy receiver (ER) and Information receiver (IR) can be co-located or separated.

- Wirelessly Powered Communication Networks (WPCNs). Energy is transferred in the downlink, and information is transferred in the uplink.

- Wirelessly Powered Backscatter Communication (WPBC). Energy and information are transferred as the case of WPCN. Backscatter modulation at a tag is used to reflect and modulate the incoming RF signal to communicate with a reader.

In conclusion, the RFEH technique shows many advantages in comparison to other energy harvesting techniques such as well-known and continuous properties of energy source, ability to integrate with IoT sensors and networks. Therefore, the RFEH technique has attracted a considerable amount of attention and the RFEH technique is the target of this study.

1.2.2 Research Contribution

The RF source of RFEH system can be classified into two types:

- Dedicated RF source. The dedicated RF source can be utilized to supply the energy to the network nodes when necessary. The limitations of using a dedicated RF source for RFEH are from criteria of the transmitted frequency and power of the RF source [20]. The frequency of the RF sources can use the license-free ISM frequency band. The output power of the RF sources must be limited due to safety and health concerns of RF radiation. The different schemes of RFEH from the dedicated RF source are studied [31], [32].

- Ambient RF source. In the ambient RFEH system, the energy is from ambient RF sources that are available in the environment. Consequently, there is no need for an energy transmitter and therefor less complexity in system design. This is a strong point of the ambient RFEH in comparison with RFEH from the dedicated source. The RF energy sources are

various, such as TV towers (analog and digital), Wi-Fi, mobile communication. There are majority theoretical studies about ambient RFEH for battery-less devices from Wi-Fi, GSM, DTV sources.

The ambient RFEH technique shows prominent advantages; hence, in this research, we study on RFEH system from ambient RF signal for IoT applications. Primarily, we focus on designing the structure of the RFEH rectenna system that works efficiently in the real environment.

The main contributions of this study are:

- Base on analyzation on characteristics of the RF signal , the study indicates that Q factor of the RFEH system affects bandwidth of the RF signal, and a wide bandwidth RFEH system is an essential structure to efficiently harvest the ambient RF signal.

- Rectifier circuit, in which Q factor is limited by BW of the RF signal, is designed in 65 nm SOTB technology. Evaluation results successfully prove that with the designed rectifier, output power in case of harvesting modulated signal is 2 times higher than that in case harvesting CW signal.

- The study proposed and designed a wide bandwidth RFEH rectenna system that, in measurement with LTE signal, has output power 15 times higher than other study at the same input power of -20 dBm.

- The proposed system generates 3.5 μW DC power at an indoor condition and 7.6 μW at an outdoor condition which suitable to supply for RF sensor TAG and RF sensor TAG with Wake-up receiver (WuR) for IoT applications

1.3 Dissertation Layout

The dissertation contains six chapters which contents are as follows:

- Chapter 1 gives an overview of IoT applications and requirements. The role of energy harvesting in the design requirement of IoT application is presented. Hence, the overview of energy harvesting techniques is presented. The motivation and contribution of the study are presented. From that, the goal of this study, which is to design and implement a structure of the RFEH rectenna that efficiently works in the real environment.

- Chapter 2 provides the power requirement of IoT sensors, and the technical background of the ambient RFEH technique. The general structures of the RFEH system in related studies are analyzed. The characteristics of the ambient RF signal that affect the efficiency of the RFEH system are also presented. Consequently, the required specifications of the ambient RFEH system in order to propose an efficient structure are considered. The wide bandwidth RFEH system is proposed that will be effective for the ambient RFEH rectenna. The target of the study is designing the ambient RFEH system that can supply for RF sensor TAG and RF sensor TAG with WuR.

- Chapter 3 presents the principle specifications of the rectifier circuit. It is the first time that a Q factor of the rectifier is considered in relationship with bandwidth (BW) of the RF signal in the rectifier design methodology. Besides, the effect of drain current in the low-level input range and phase difference between the two RF inputs of the rectifier are analyzed. The circuit was designed in 65nm SOTB technology for measuring the efficiency of the rectifier. The measurement results shows that the DTMOS cross-coupled rectifier with floating sub-circuit is suitable to utilized in the proposed RFEH system.

- Chapter 4 presents the proposed structure of a wide bandwidth RFEH system to harvest ambient RF signals. In the system, the wide bandwidth specification is ensured by the domination of the Q factor of the rectifier when the Q factor of the matching circuit and external component are

high enough. The BW of the design system covers the BW of the target RF signal. From the design methodology, the two structures of ambient RFEH were designed.

- Chapter 5 shows the measurement results of the proposed RFEH rectennas in an anechoic chamber and in the real environment. The proposed systems were evaluated with a 950 MHz Long Term Evolution (LTE) mobile phone signal. Measurement results of the proposed rectenna are compared with the current ambient RFEH studies.

- Finally, chapter 6 summarizes the principal results of the work. From the results, the applications and future works are proposed.

Chapter 2

Requirements of RFEH rectenna system for IoT applications

In this Chapter, the energy requirement of IoT sensor node is presented. Besides, the technical background of the RFEH structure is shown. Considerable specifications of the RFEH structure in some related works are presented. In addition, the characteristics of the RF signal in the ambient environment that affect the output of the rectifier are analyzed. Base on these characteristics, the structure of the RFEH system to harvest the environmental signal is proposed.

2.1 Characteristics of the ambient RF signal

2.1.1 The ambient RF signals in surveys

The RF sources for ambient RFEH were studied earlier [22, 33, 34]. In [22], power densities (PDs) of the RF sources in urban and semi-urban environments of London region was measured, and results are shown in the table 2.1

Table 2.1: RF power density in London, UK [22]

Band	**Frequency(MHz)**	**Average PD** (nW/cm^2)	**Maximum PD** (nW/cm^2)
DTV	470-610	0.89	460
GSM900 (MTx)	880-915	0.45	39
GSM900 (BTx)	925-960	36	1930
GSM1800 (MTx)	1710-1785	0.5	20
GSM1800 (BTx)	1805-1880	84	6390
3G (MTx)	1920-1980	0.46	66
3G (BTx)	2110-2170	12	240
Wi-Fi	2400-2500	0.18	6

From the table, it can conclude that the ambient RF signals in the environment are at μW level range. The three strongest RF signals are a digital television (DTV) signal, a global system for mobile (GSM) 900 and a GSM1800. In [35], the median power of the DTV signal was measured at -38 dBm, and that of a mobile phone signal was -25 dBm. In [36], measured powers of GSM900, GSM1800, 3G are in range of $(-35 \sim -25)$ dBm, $(-25 \sim -15)$ dBm,$(-25 \sim -15)$ dBm, respectively. In [33], levels of the DTV signal was measured in a range of $(-44 \sim 3)$ dBm.

2.1.2 Characteristics of the RF signals at measurement position of the study

The characteristics of the RF signals at measurement position of the study are measured and presented in Fig 2.1. The measurement place was in an office room at the University of Electro-communications, Tokyo, Japan, as shown in Fig. 2.2. In the measurement, a signal analyzer Agilent CXA N900A and a dipole antenna CANDOX 44Sa21 were used. Specifications of the measurement were set up as follows: resolution bandwidth was set at100 kHz, and band power corresponds to 15 MHz. The ambient RF power is the total band power that is set up as previous specifications.

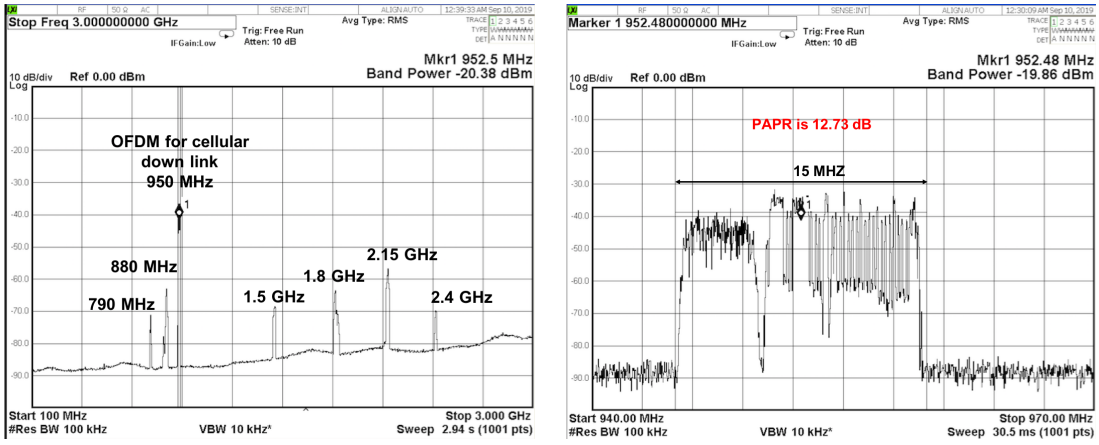

(**a**) (**b**)

Figure 2.1: Measured spectrum of RF signals at the measurement place: (**a**) Spectrum, and (**b**) Magnified spectrum of the 952 MHz signal.

As shown in Fig 2.1, at the measured position, there are some ambient RF signals at 790 MHz, 880 MHz, 950 MHz, 1.5 GHz, 1.8 GHz, 2.15 GHz, 2.4 GHz. Among these signals, the level of the RF signal at 952 MHz is the strongest, which is -20 dBm. The magnified spectrum of the 952 MHz signal is shown in Figure 2.1b. From the characteristics of the signal, it is concluded that the signal corresponds to an LTE downlink mobile phone signal with an orthogonal frequency division multiplexing (OFDM) modulation.

Fig 2.2 presents a map of the measurement place. The measurement point and the base station are approximately 162 m apart.

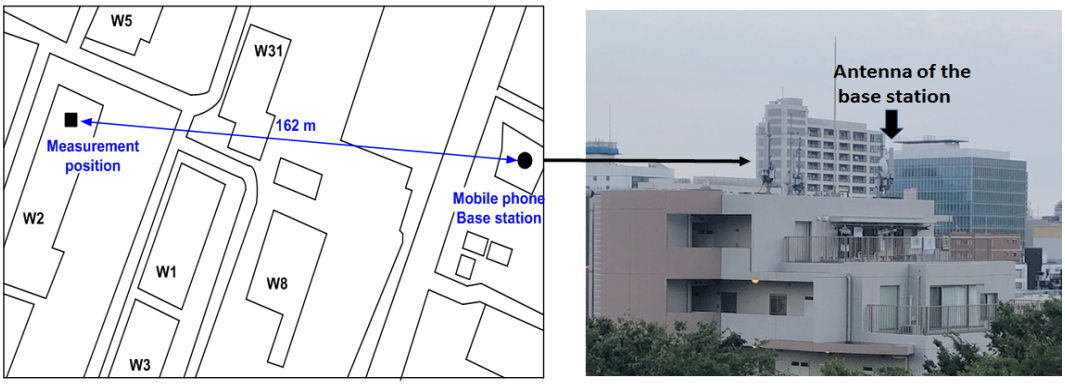

Figure 2.2: Map of the measurement position and picture of mobile phone antenna.

From the measurement results, because the 952 MHz LTE mobile phone signal is the strongest signal at measurement position, so it is the target signal of the proposed RFEH rectenna system. Besides, as indicated in Fig 2.3, RF signals from 4G cell phone base stations are widespread in the ambient environment today. Hence, the cell phone RF energy is one of the ideal energy sources for ambient RFEH.

Figure 2.3: The distribution of mobile phone base station in Tokyo.

2.2 Technical background

2.2.1 Energy requirement of wireless sensor node for IoT applications

The structures of wireless sensor node (WSN) are presented in Fig 2.4. Figure (a) shows a normal structure of the sensor node which consists of parts such as sensor, micro-control unit (MCU), RF module and power supply. The RF module consumes mainly the power of the sensor node to supply for an RF oscillator and power amplifier of the module. At always ON operation mode, the sensor node always transmits so the power consumption is large, which is

in range of (30 ∼ 100) mW in general. To reduce power consumption, the RF signal is only transmitted when the information needs to be transferred. The sensor node works in this mechanism is called an intermittent mode. The RF sensor TAG, which shows in Fig 2.4, consumes a very low power because in this structure there is no need to use the RF module. The RF sensor TAG utilizes incident RF signals to transmits information. The power consumption of the RF sensor TAG is minimized by using a wake-up receiver (WuR) unit.

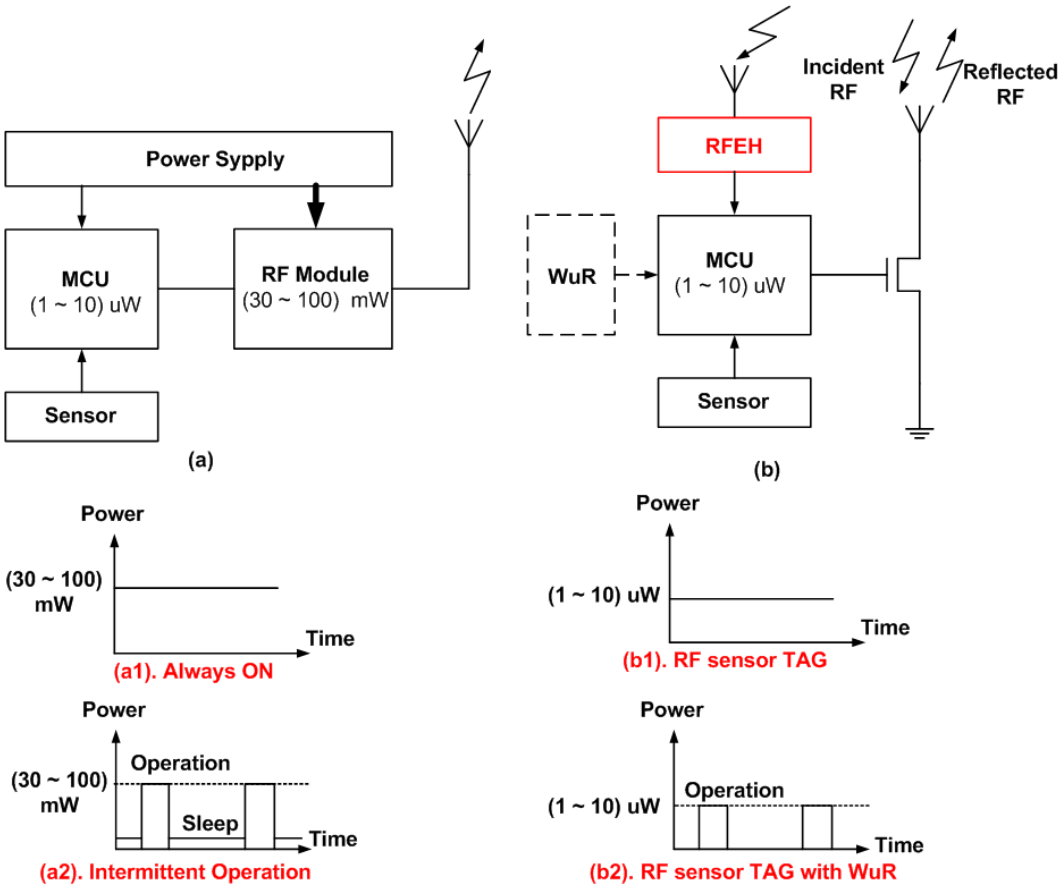

Figure 2.4: Structures of WSNs: (**a**) Sensor node, and (**b**) RF sensor TAG powered by RFEH with/without WuR.

Table 2.2 presents power requirements of WSN structures for IoT applications. The WPT technique is chosen depending on the power requirement of WSN. With ambient RFEH, because the level of RF signal in the environment is at μW level so the power that RF energy harvester can generate is at μW level. Therefore, the RF sensor TAG and RF sensor TAG with WuR are

suitable for utilizing ambient RFEH.

Table 2.2: Power requirement of WSN structures for IoT applications.

	Sensor mode structure	**Required power**
(a1)	Sensor node at always ON mode	30 $\sim$ 100 mW [37], [38]
(a2)	Sensor node at intermittent operation mode	0.1 $\sim$ 1 mW [39], [40]
(b1)	RF sensor TAG	$<$ 10 μ W [41]
(b2)	RF sensor TAG with WuR	$<$ 1 μ W [42]

2.2.2 RFEH technique

The ambient RFEH system utilizes available RF energy in the environment so that the system consists of an energy receiver part. A general structure of the RFEH system includes an antenna and a rectifier circuit; hence, the system also called a rectenna. The block diagram and equivalent circuit of the rectenna is presented in Fig 2.5

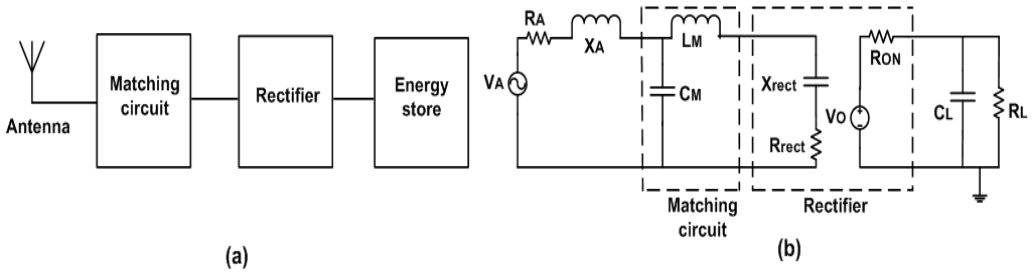

Figure 2.5: Block diagram and equivalent circuit of RFEH rectenna: (a) Block diagram, and (b) Equivalent circuit

In the system, an antenna is used to receive an RF electromagnetic signal in the environment, change it to an RF electrical signal, and supply the RF signal to the following parts of the system. The rectifier, which is used to convert an RF signal to a DC signal, is a main part of the rectenna system. The efficiency of the rectifier decides the efficiency of the total rectenna system. Generally, RF signal available in the environment at μW level, which is smaller than

a threshold voltage (V_{th}) of the rectifier component, resulting in significant decreases in power conversion efficiency (PCE) of the rectifier and the total rectenna system. A matching circuit is utilized to ensure impedance matching between the antenna and the rectifier so that all received power from the antenna is transfer to the rectifier, and reflected power is minimized. The output of the RFEH system is stored in a energy store unit which is general a high capacity capacitor.

There are a large number of study to increase PCE of the RFEH rectenna system, and a majority of the studies is improving implement of separate parts of the RFEH system. Some researches propose solutions to boost the PCE of the rectifier by applying various device technologies or proposing new devices to the rectifier circuit [43–45]. The other studies propose improving architecture of the rectifier such as static V_{th} cancellation scheme [46], differential-drive topology [47–49], and floating sub-circuit bias [50].

In solutions to improve the PCE from antenna design, some authors proposed solutions to collect RF signals in the environment by gathering a multi-band ambient RF signal such as designing multi-antennas. In the multi-antennas, each antenna is a high Q antenna at each frequency of the target RF signals in the environment [22]. Besides, some studies propose designs of multi-band antennas or broadband antennas in which the antenna can receive all the target RF signal bands [35, 51–54]. Multi-band matching circuit was proposed in some studies to match with multi-band antenna in the RFEH [36, 56]

Recent years, study on total RFEH system was proposed in some studies in which the systems can be a single band or multi-band harvesting system. Besdies, some researchers proposed a multi-rectenna system in which rectennas are combined to synthesize the output DC power [57]. Related to single band rectenna, a co-design rectenna, in which antenna is designed to match with rectifier, was proposed and demonstrated outstanding results in terms of sensitivity and PCE [58, 59]. The recent state of art in the RFEH studies is shown as in the Fig 2.6. The survey presents the studies from [33, 48, 51, 58–83]

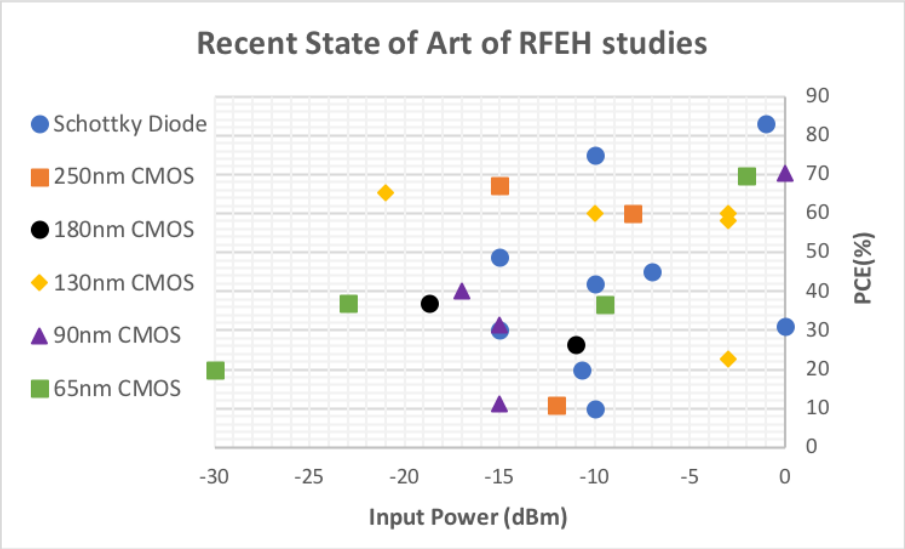

Figure 2.6: Recent state of art in the RFEH studies

2.2.3 Related studies on ambient RFEH

Although there are many studies about the RFEH system which reach outstanding results in the sensitivity and efficiency of the RFEH system, there is a minority of research that the RFEH rectenna system implements in a real environment. The studies, in which the results of the system measured in a real environment, are listed in table 2.3.

The studies in the table harvested the RF signal from various sources such as TV signal, mobile phone signal, Wi-Fi signal, or multi-signal. Structures of the rectenna systems are also diversity from a single rectenna, multi-band rectenna, and co-design rectenna. In [35, 57], the multi-rectenna is utilized as a solution to improve the efficiency of the rectenna. In [35], two rectennas connected in cascade to harvest a mobile phone signal at 845 MHz. In [57], five rectennas are combined to harvest RF signals in 5 bands. In [77], a high impedance antenna is used to improve the PCE due to the high RF voltage fed to the rectifier. The antenna is designed to be a wide bandwidth antenna to receive full bandwidth DTV signal at 500 MHz bands. In [58, 80], co-design rectenna is utilized. In these studies, high Q antennas are designed to match with high Q rectifier to improve efficiency of the systems.

Table 2.3: Studies about ambient RFEH.

	Antenna	**Rectifier**	**Matching circuit**	**Measurement with CW signal from SG or RFDS**	**Measurement with RF ambient signal**
Kitazawa [35]	Dipole antenna	6-stage charge pump (Schottky diode HSB276AS)	Unspecified circuit	With SG at 900MHz: 0.79V, 19.7% @ $P_{in} = -5dBm, R_L = 10k\Omega$,	Mobile phone 845MHz: 0.32V, 0.22μW@ $P_{in} = -20dBm$
Kitazawa [57]	Wire and tape folded dipole	2-stage charge pump/band (diode HSMS285C)	LC matching network	With SG: 9.1%@$P_{in} = -20dBm$, 215MHz	5 bands: 1.9 μW@ $P_{in} = -15dBm$
Stoopman [58]	Square loop microstrip antenna	5-stage CCR (90nm CMOS)	Control loop by capacitor bank	In chamber room: 1V@ -27dBm, open load; 40%@-17dBm; 1V@27m	A phone call GSM 900: -4.6dBm, 2m distance: 2.2 V@ 25 seconds, 350 nF capacitor
Furuta [77]	High impedance dipole antenna	2-stage Cockcroft-Walton	LC matching network	With AR-FEH 500 MHz: 49.8% @ $P_{in} = -15dBm$	DTV signal: 22.53 μW @ $P_{in} = -13dBm$
Sadagopan [80]	High Q loop antenna	6-stage CCR (GP 65nm CMOS)	-	RFDS: 1V@-36dBm, 2.4 GHz (primary mode)	Wi-Fi 2.42 GHz: 3.3 nW@ $P_{in} = -18.6dBm$

In the studies in table 2.3, the rectenna mostly tested with continuous sine waves (CW) signals in the laboratory. Measurement with RF signal in the environment is implemented in a very short time, and evaluation conditions are extremely unclear. Figure 2.7 presents measurement results of the ambient RFEH studies when the system harvest (CW) signals in the laboratory and real ambient RF signals in the environment. As shown in the figure, output powers

of the studies when harvest real RF signals in the environment are much smaller than that of the case harvesting CW signals in laboratory measurement.

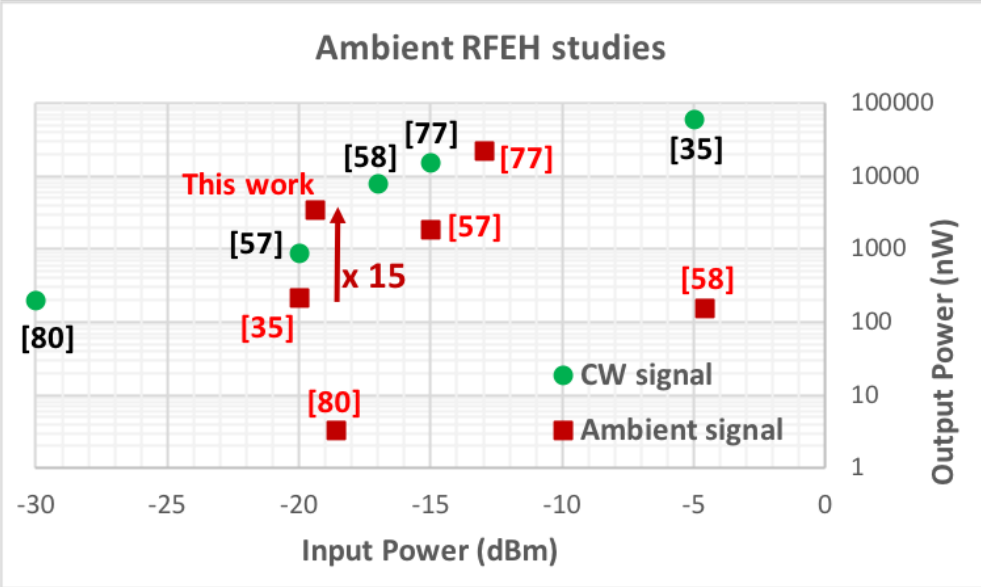

Figure 2.7: Recent state of art in the ambient RFEH studies

The results indicate that the characteristics of the real RF signal in the ambient environment strong affect on the efficiency of the ambient RFEH rectenna system. In conclusion, to design the structure of the ambient RFEH rectenna system, the relationship between characteristics of the ambient RF signal and specifications of the RFEH rectenna must be analyzed.

2.3 The proposed technique of the study

2.3.1 The proposed technique for ambient RFEH system

In ambient RFEH, the rectenna harvests RF signal available in the environment to generate DC power, so characteristics of the RF signal decide specifications of the rectenna system. There are two main characteristics of the RF signal that system design of RFEH rectenna must be considered as presented in Fig 2.8:

- Level of the RF signal.
- Modulation type of the RF signal.

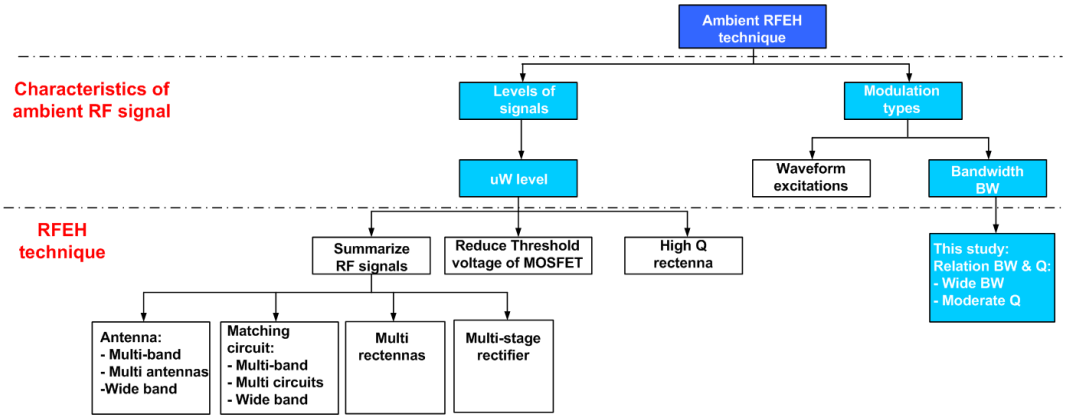

Figure 2.8: Ambient RFEH technique

The level of ambient RF signal in the environment is at μW level, therefore the ambient RFEH system has to work efficiently at this level. Many techniques are proposed such as synthesis the signals, reduction threshold voltage of MOSFETs, and high Q rectenna. The high Q rectenna system, in which a high Q antenna and high Q rectifier are designed, shows a prominent result. The passive voltage gain, which is proportion with the Q factor, is high, resulting input voltage of the rectifier increasing. Hence, the efficiency of the rectenna system improves. In recent times, researchers tend to design the RFEH rectenna system in which the Q factor is increased. In [58, 80], Q factors of antenna are 81 and 120, respectively. Sensitivities in these studies are outstanding values, which are 1V at -27 dBm and -36 dBm, respectively.

Related to waveform modulation of the ambient RF signal, there are two characteristics that affects to the efficiency of the rectenna which are waveform excitation and bandwidth BW. The effect of the waveform excitation of RF signal to the performance of the RFEH system is mentioned in [84–86]. In these studies, theoretical analyzation or measured evaluation was performed just in the rectifier circuit. The effect of the waveform excitation of the RF signal to the performance of the total ambient RFEH rectenna has not mentioned in any related study. In the ambient RFEH, the RF signal is available in

the environment, hence the waveform excitation is not a specification that the system can manage.

In this study, we point out the required specifications of the ambient RFEH system in which the relation of the Q factor of RFEH system and BW of RF signal should be considered simultaneously.

The relationship between Q factor and BW is shown as in equation 2.1 [87, 88]

$$Q = \omega_c \left(\frac{E_s}{P_D} \right) \quad or \quad Q = \frac{f_c}{\Delta f} = \frac{f_c}{f_2 - f_1} \tag{2.1}$$

where E_s is energy stored in the circuit, P_D is average power dissipated in the circuit, ω_c is the resonant frequency in radians/second, f_c is the resonant frequency in Hz, and Δf is the BW.

The BW of the system can be determined by the reflection coefficient as indicated in Fig 2.9.

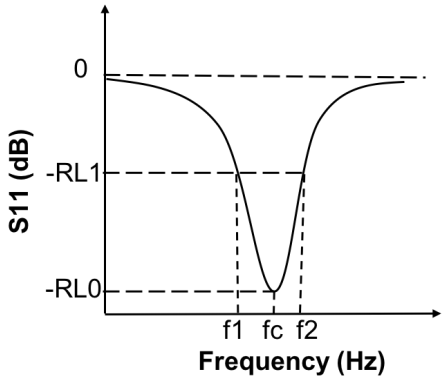

Figure 2.9: Definition of BW on the reflection coefficient to calculate Q factor of the system

In the figure, frequencies f_1 and f_2 are determined at which the return loss RL1 is calculated by equation 2.2.

$$RL1 = -10log \left(\frac{10^{-\frac{RL0}{10}} + 1}{2} \right) \tag{2.2}$$

The Q factor followed by 2.1 is a limited value to ensure the bandwidth of the target ambient RF signal. If the Q factor of the system is larger than the

value of Q in equation 2.1, then BW of the system is smaller than BW of the RF signal resulting in power loss.

In the ambient RFEH technique, the Q factor of the RFEH system should be limited by BW of the target RF signal in the ambient environment so that no power loss. The solution to maximizing the Q factor of the RFEH system is not valid with the ambient RF signal. For this reason, in [58, 80], output powers are outstanding with the CW signal, but that of the case harvesting real RF signals in the environment dramatically decreases.

In conclusion, to efficient harvest RF signal in the ambient environment, in this study, we propose the structure of the RFEH rectenna that consists of three main characteristics:

- Wide bandwidth RFEH system: BW of the system has to be large enough to cover BW of the target RF signal. Therefore, the Q factor of the RFEH is limited by BW following equation 2.1
- Q factor of rectifier dominates Q factor of the RFEH rectenna system to minimize power loss.
- Rectifier circuit works efficiently in μW level, and Q factor of the rectifier is chosen to ensure BW of the target RF signal

2.3.2 Required specifications of the proposed RFEH system

From the designed methodology, two RFEH rectennas was designed to harvest the 950 MHz LTE signal. The specific specifications of the designed RFEH rectenna system are:

- Target RF signal is LTE signal with OFDM modulation at 950 MHz band, from 945 MHz to 960 MHz
- Bandwidth of the RF signal is 15 MHz. The BW of the rectenna is chosen 20 MHz at least to ensure discrepancy.

- Q factor of the rectifier, which calculated follow equation 2.1, is maximum 47. The Q factor of the RFEH system is as much as the Q factor of the rectifier.

- Target application of the study is to supply power for RF sensor TAG and RF sensor TAG with WuR. Therefore, output power of the designed system are required in a μW level.

Chapter 3

Rectifier circuit

3.1 Types of rectifier circuits

3.1.1 Half-wave rectifier

A rectifier is a circuit which converts alternative current (AC) signal to direct current (DC) signal. The circuit uses components, which enables current in only one direction, such as a diode, transistor. The simplest rectifier circuit, which consists of a diode, an ac source, and a resistive load, is presented in Fig 3.1. First, we consider the circuit in a simple condition to figure out some specifications of the circuit. Input source is an AC source, which generates a sine wave signal. The diode has zero resistance in the forward direction and infinite resistance in the reverse direction. The input voltage and the diode current are shown in Fig. 3.1 (b) and (c).

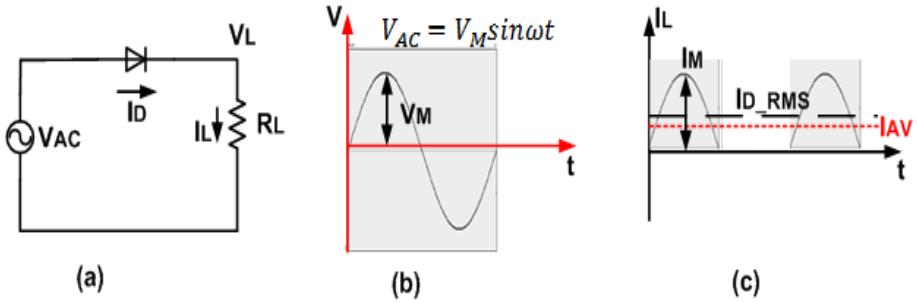

Figure 3.1: Half-wave rectifier circuits with resistive loads: (a) Half-wave rectifier, (b) Wave form of input voltage, and (c) Wave form of diode current

The excited voltage is $V_{AC} = V_M sin(\omega t)$, and a root mean square (RMS) of the voltage is $V_{RF\_RMS} = V_M/\sqrt{2}$. The excited current is $I_{AC} = I_M sin(\omega t)$, and RMS of the current is $I_{RF\_RMS} = I_M/\sqrt{2}$. In the half-wave rectifier (HWR), the current only flows into the load in the forward direction when the input voltage is positive, in the reverse direction, the current is nearly zero because of infinite resistance of the diode. Therefore, the output voltage in the load only has one direction. Specifications of the rectifier are listed as follow: [89]

DC current in load current is an average of the load current, which is calculated by equation 3.1

$$I_{DC} = I_{AV} = \frac{1}{2\pi}\int_0^{\pi} I_M sin\,(\omega t)\,d\,(\omega t) = \frac{I_M}{\pi} \approx 0.38 I_M \tag{3.1}$$

The RMS of diode current is

$$I_{D\_RMS} = \sqrt{\frac{1}{2\pi}\int_0^{2\pi} I_{AC}^2 d\,(\omega t)} = \sqrt{\frac{1}{2\pi}\int_0^{\pi} I_M^2 sin^2\,(\omega t)\,d\,(\omega t)} = \frac{I_M}{2} \tag{3.2}$$

Form factor is the ratio between the RMS and the average. Form factor of the diode current in HWR is

$$F = \frac{I_{RF\_RMS}}{I_{AV}} = \frac{0.5 I_M}{0.318 I_M} = 1.57 \tag{3.3}$$

Ripple Factor. The rectifier is a nonlinear circuit, so the output of the rectifier consists of DC component, first-order frequency, and harmonic frequencies. These components make ripples in the output. The ripples can smooth by using a filter in the output. The ripple factor is calculated by

$$r_f = \frac{Effecitve \quad rectified \quad AC \quad load \quad components}{Average \quad load \quad current} = \sqrt{F^2 - 1} \tag{3.4}$$

For HWR, $r_f = 1.21$

Power conversion efficiency (PCE), which indicates the ability of the rectifier to convert AC power into DC power, calculated by the ratio of output DC power to AC input power. The maximum PCE of the HWR is shown in 3.5

$$PCE = \frac{P_{DC}}{P_{AC}} = \frac{I_{DC}^2 R_L}{I_{RMS}^2 R_L} = 0.405 \tag{3.5}$$

In conclusion, the HWR uses to rectify a half-wave of the RF signal. Besides, another half-wave power has not been utilized to produce the output; hence, the PCE of the HWR is not high, which is a maximum of 40.5 %. Main advantages of HWR are:

- Simple: circuit structure and number of components;
- Low cost: because of using fewer components in comparison with other rectifier structures.

Disadvantages of HWR are:

- Power loss: the circuit utilizes the power of one-half cycle of the RF signal, and waste the power of the remaining half cycle;
- Low output voltage in comparison to other rectifier structures;
- High ripple in the output.

Applications of HWR:

- For rectification applications;
- For demodulation applications;
- For signal peak applications.

3.1.2 Full-wave rectifier

For rectification applications, to increase rectified efficiency, a full-wave rectifier is used. Fig 3.2 shows schematic diagram of some basic rectifiers.

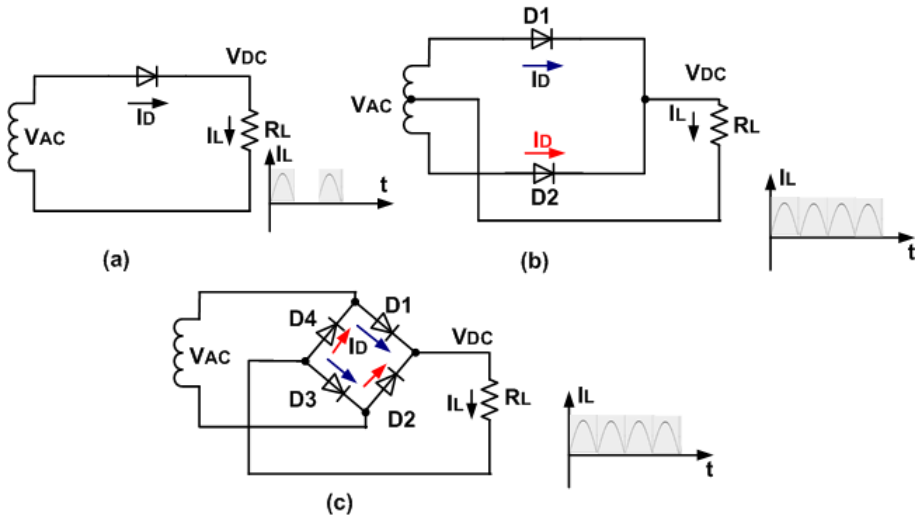

Figure 3.2: Basic rectifier circuits with resistive loads: (a) Half-wave rectifier, (b) Full-wave center-tap rectifier, and (c) Full-wave bridge rectifier

In a full-wave rectifier (FR) and full-wave bridge rectifier (FBR), two half cycles of the RF signal are utilized to generate DC output power. In FR, diode D1 is in a forward direction in a half cycle while diode D2 is in the forward direction in the remained cycle. In FBR, diode D1 and D3 work in one-half cycle while diode D2 and D4 work in another half cycle. The current in the load resistor is combined with currents in diodes, as shown in fig 3.2. Specifications of the full-wave rectifiers are indicated in table 3.2

Table 3.1: Characteristics of basic rectifier circuits with resistive load

	Half-wave rectifier	**Full-wave rectifier**	**Full-wave bridge rectifier**
Diode average current	$0.318I_M$	$0.636I_M$	$0.636I_M$
Diode rms current	$0.5I_M$	$0.707I_M$	$0.707I_M$
Form factor of diode	1.57	1.57	1.57
Form factor of Load current	1.57	1.11	1.11
Ripple	1.21	0.48	0.48
Maximum PCE (%)	40.6	81.2	81.2

From table 3.2, full-wave rectifiers show better performance in comparison with the half-wave rectifier, especially in PCE. In the full-wave rectifier, the total cycle of the signal is used to generate output signal so that PCE of the

rectifier increases while ripple decreases. The main disadvantage of the full-wave center-tap rectifier is the requirement of using center-tap transformer; while, the main disadvantage of the full-wave bridge rectifier the requirement of using more diodes than other rectifier circuits.

A voltage multiplier rectifier circuit has a high voltage ratio, low voltage stress, high-efficiency [90, 91]. Two common types of voltage multiplier rectifier circuits are the Cockcroft-Walt rectifier and the Dickson charge pump rectifier, which shown in Fig. 3.3. The Cockcroft-Walton rectifier is a combination of voltage multiplier circuits in series, while, Dickson charge pump is a combination of voltage multiplier circuits in parallel.

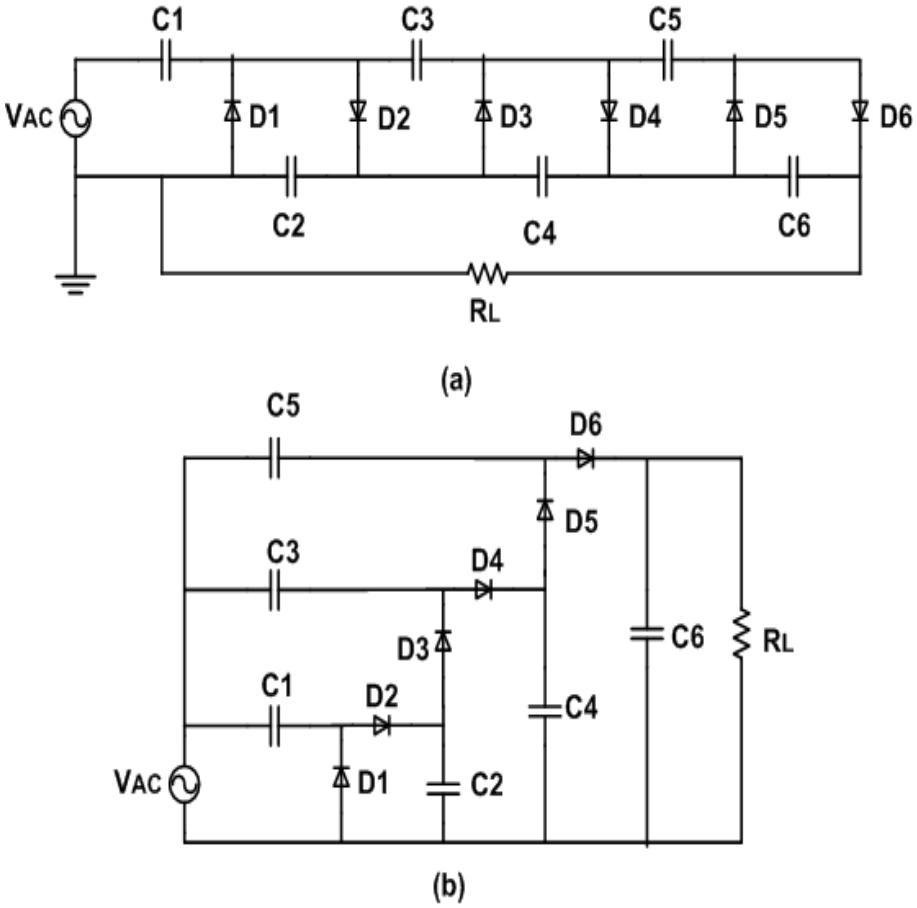

Figure 3.3: Schematic of multiplier rectifiers: (a) 3-stage Cockcroft-Walton multiplier rectifier, and (b) 3-stage Dickson charge pump rectifier

3.1.3 MOSFET rectifier for RFEH system

In a conventional rectifier, the Schottky diode is an attractive candidate to utilize in the rectifier circuit due to low forward voltage drop and fast switching speed. However, Schottky diode can not properly be modeled in all CMOS technologies, which shows powerful usefulness in low-cost applications, where high integration levels are desired [92, 93]. In recent times, researchers have been best desired to replace Schottky through CMOS technology in the rectifier circuit. In IoT applications, CMOS technology is a preferred technology because of integrated ability into sensors. In addition, in a low input power range, as shown in Fig. 2.6 in chapter 2, results have got from CMOS technology in RFEH show satisfactory in comparison with the results got from using Schottky diode.

CMOS technology was successfully applied into many structure of rectifier circuit such as Dickson charge pump [62, 91], static V_{th} cancellation rectifier [46], cross-coupled rectifier (CCR) [47]. Schematic diagrams of CMOS Dickson charge pump and CCR are shown in Fig 3.4

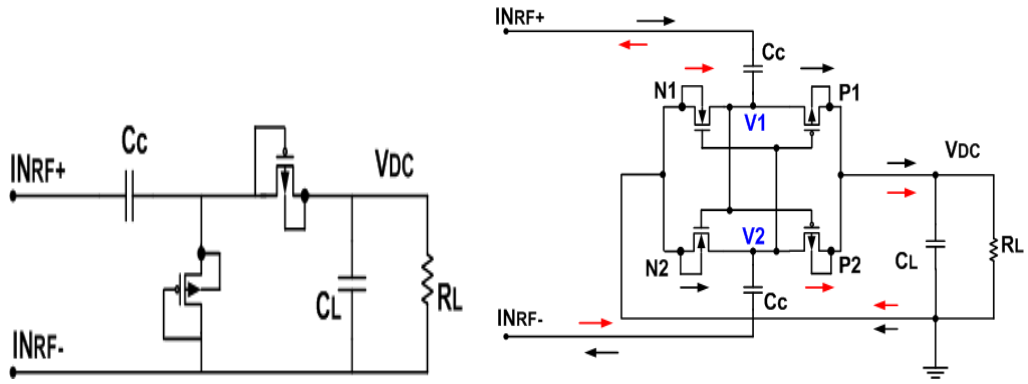

(a) (b)

Figure 3.4: CMOS rectifier circuits: (a) Dickson charge pump rectifier, and (b) Cross-coupled rectifier CCR

In a low input level range, which can compare to the threshold voltage V_{th} of the diode/MOSFET, the cross-coupled structure shows an advantage in comparison to other structures. For instance, in a Dickson charge pump in

Fig 3.4, diode-connected PMOS turns on only when $V_{in} - V_{DC} \geq V_{th}$ where $V_{in} = V_{INRF+} - V_{INRF-}$. Besides, in CCR, P_1 or P_2 turns on when $V_{in} \geq V_{th}$, which means circuit can work at a low input level. In summary, the CMOS CCR is a popular choice of researchers in order to design RFEH systems for IoT applications.

In a CCR, a couple of cross MOSFET works in a half cycle of the RF signal, the other couple of MOSFET works in a remained half cycle. For instance, in Fig 3.4 (b), when positive half cycle is supplied into INRF+, PMOS P_1 and NMOS N_2 will turn on, while P_2 and N_1 turn off. Currents in the circuit flow follow the black arrow. In a half-cycle after, the currents flow in the direction of the red arrow. The operation principle of CCR is the same as the full-wave bridge rectifier, so the efficiency of CCR is improved.

Base on CCR, [50] proposed the structure of CCR with floating sub-circuits, which has a schematic shown in Fig 3.5.

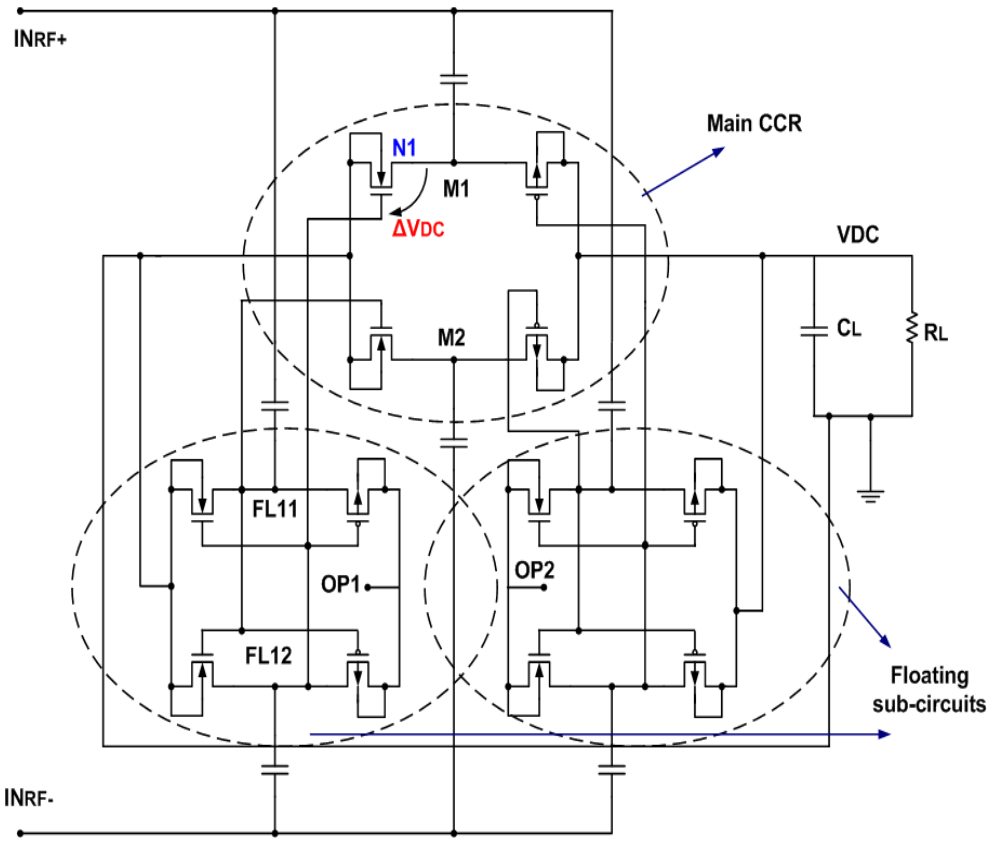

Figure 3.5: Schematic of a CCR with floating sub-circuits

In one stage of CCR with floating sub-circuits, there are three CCRs which are the main CCR and two CCR sub-circuits. Each CCR sub-circuit has an open load so that DC level at point OP1 (or OP2) is maximized. Hence, DC levels at FL11, and FL12, which are almost half of OP1, are also maximized. These voltages are supplied to the gates of the MOSFETs in the main CC. Hence, in comparison to a conventional CCR, CCR with floating sub-circuits reaches a higher gate-to-source voltage of MOSFET in the main CCR, as indicated in equation 3.6.

$$V_{GS}(N1) = V_{in} + \Delta VDC \tag{3.6}$$

where ΔVDC is a DC difference level of the voltages at FL12 and M1. The voltage ΔVDC shows the effectiveness of CCR with floating sub-circuits in comparison to a conventional CCR.

In this study, CCR and CCR with floating sub-circuits are utilized to designed rectifier circuit on an application of 65nm Silicon-On-Thin Buried Oxide (SOTB) technology.

The SOTB, which is one of the FD-SOI CMOS processes, has been developed recently due to its advantages in comparison to a conventional bulk CMOS [94, 95]. In [95], the RF characteristics of 65 nm SOTB CMOS are measured and presented as shown in table 3.2.

Table 3.2: RF characteristics of 65 nm SOTB [101]

	PMOS	**NMOS**
Gate length	60 nm	60 nm
Gate oxide thickness	2.0 nm	2.0 nm
Threshold Voltage	-0.32 V	0.35V
F_T	26 GHz	40 GHz
F_{max}	20 GHz	28 GHz

As indicated from the table, because F_{max} of PMOS and NMOS of SOTB devices are 20 GHz and 28 GHz, respectively, so, it is indicated that the SOTB technology works effectively at 1 GHz frequency range.

3.2 Principle specifications affect to efficiency of rectifier

3.2.1 Drain current

The relationship between drain current and output of the rectifier is indicated from a current-voltage relationship in CCR. A single-stage schematic of CCR is shown in Figure 3.6. IV relation in NMOS N1 is considered to simplify the work of CCR. Positive drain current in N1 is a forward current that charges the load. In contract, negative drain current in N1 is the flow-back current that discharges the load.

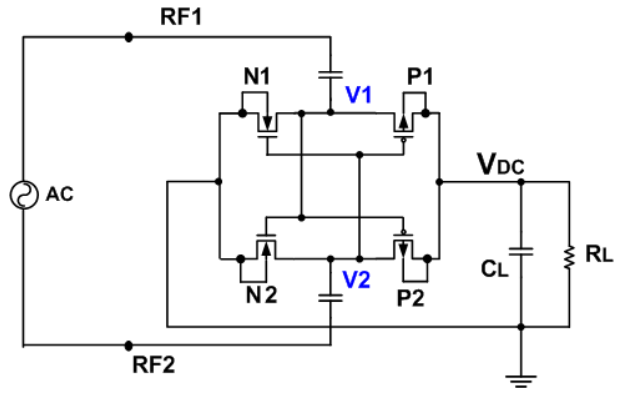

Figure 3.6: Schematic of a single stage CCR

RF differential signals at V_1 and V_2 are supplied by AC source through coupling capacitor C_c and can be denoted by $V_{RF}sin2\pi ft$ and $V_{RF}sin\left(2\pi ft+\pi\right)$, respectively. V_1 and V_2 also have DC voltages. We denote these voltages are DC_{offset} voltages. Consider CCR is symmetrically designed, so voltages at V_1, V_2 have the same absolute value and can be express as equation 3.7, 3.8. Due to the symmetry of CMOS devices, the drain and source of MOSFET can be switched depending on the potentials at these ports.

$$V_1 = V_{DC\_offset} + V_{RF}sin2\pi ft \tag{3.7}$$

$$V_2 = V_{DC\_offset} + V_{RF}sin\left(2\pi ft+\pi\right) \tag{3.8}$$

If $V_1 \leq 0$ which is equivalent to $sin2\pi ft \leq -\frac{V_{DC\_offset}}{V_{RF}}$, then V_{GS} and V_{DS} through N1 are:

$$V_{GS} = V_2 - V_1 = -2V_{RF}sin2\pi ft \qquad if \qquad V_1 \leq 0 \tag{3.9}$$

$$V_{DS} = -V_1 = -V_{RF}sin2\pi ft \tag{3.10}$$

If $V_1 > 0$ which is equivalent to $sin2\pi ft > -\frac{V_{DC\_offset}}{V_{RF}}$, then V_{GS} and V_{DS} through N1 are:

$$V_{GS} = V_2 = V_{RF}sin\left(2\pi ft + \pi\right) \qquad if \qquad V_1 > 0 \tag{3.11}$$

$$V_{DS} = V_1 = V_{RF}sin2\pi ft \qquad if \qquad V_1 > 0 \tag{3.12}$$

Depend on the gate-source V_{GS} voltage and drain-source V_{DS} voltage, MOSFET works in one of three regions: week inversion region, triode region, saturation region [96].

Current in week inversion region, when $V_{GS} < V_{th}$, is calculated by

$$I_{D\_WI} = \frac{W}{L}I_t exp\left(\frac{V_{GS} - V_{th}}{nV_T}\right)\left[1 - exp\left(-\frac{V_{DS}}{V_T}\right)\right] \tag{3.13}$$

where I_t is a drain current when $V_{GS} = V_{th}$, $W/L = 1$, and $V_{DS} \gg V_T$; $n = (1 + C_{jx}/C_{ox})$ is a voltage division between the oxide capacitance C_{ox} and depletion-region capacitance C_{js}; V_T is a thermal voltage, which is nearly 26mV at room temperature.

Denote I_{s0} is

$$I_{s0} = \frac{W}{L}I_t exp\left(-\frac{V_{th}}{nV_T}\right) \tag{3.14}$$

then I_{D_WI} can rewrite as

$$I_{D\_WI} = I_{s0}exp\left(\frac{V_{GS}}{nV_T}\right)\left[1 - exp\left(-\frac{V_{DS}}{V_T}\right)\right] \tag{3.15}$$

Current in triode region

$$I_{D\_T} = \frac{k'}{2}\frac{W}{L}\left[2\left(V_{GS} - V_{th}\right)V_{DS} - V_{DS}^2\right] \tag{3.16}$$

where $k^{'} = \mu_n C_{ox} = \mu_n \frac{\varepsilon_{ox}}{t_{ox}}$

Current in saturation mode

$$I_{D\_S} = \frac{k^{'}}{2}\frac{W}{L}(V_{GS} - V_{th})^2 (1 + \lambda V_{DS}) \tag{3.17}$$

where λ is a channel-length modulation coefficient.

The current flows in load is a combined current in two branches of the CCR. The DC output current is an integral of the load current, which calculated by equation 3.18. The output voltage and power are calculated by equation 3.19, 3.20

$$I_{DC} = I_{AV} = \frac{1}{T}\int_0^T I_L dt = \frac{1}{T}\int_0^T 2I_D dt \tag{3.18}$$

$$V_{DC} = I_{DC} R_L \tag{3.19}$$

$$P_{out} = \frac{1}{T}\int_0^T I_L^2 R_L dt \tag{3.20}$$

In a low input level, $V_{RF} < V_{th}$, so the MOSFETs usually work in the weak-inversion region. Therefore, the drain current is mainly calculated by equation 3.15. The equation indicates that current in this region depends on I_{s0}, V_{GS}, and V_{DS}. I_{s0} presents characteristics of the MOSFET, while V_{GS} and V_{DS} depend on levels of the RF signal. It can conclude that I_{s0} increases letting DC current in load increases.

The driving body of MOSFET is a popular technique to increase the drain current of MOSFET. The dynamic threshold voltage MOSFET (DTMOS) technique, in which the body of the MOSFET is tied to the gate, is an effective technique to drive the drain current. In [97], it has been proved that a very low voltage on the DTMOS technique can obtain a much higher current drain than regular MOSFET. In RFEH technique, DTMOS is utilized to the rectifier as a diode-connected rectifier [98], self V_{th} cancellation rectifier [99].

In the SOTB technique, the threshold voltage of the MOSFET can be modulated by body bias, such that DTMOS becomes more effective than the

normal MOSFET structure. The body bias constant, which is calculated by equation 3.21, is almost 150 mV/1V in SOTB [100]. In [101, 102], we proved the effectiveness of DTMOS in terms of decreasing V_{th} of the MOSFET in comparison to body-tired-to-source (BTMOS) in the 65 nm SOTB technique.

$$\alpha = \frac{\Delta V_{th}}{\Delta V_{BS}} \tag{3.21}$$

Figure 3.7 present simulated results of IV characteristics in 4 configuration types: diode-connected BTMOS, diode-connected DTMOS, DTMOS in CCR and DTMOS in CCR with floating sub-circuits

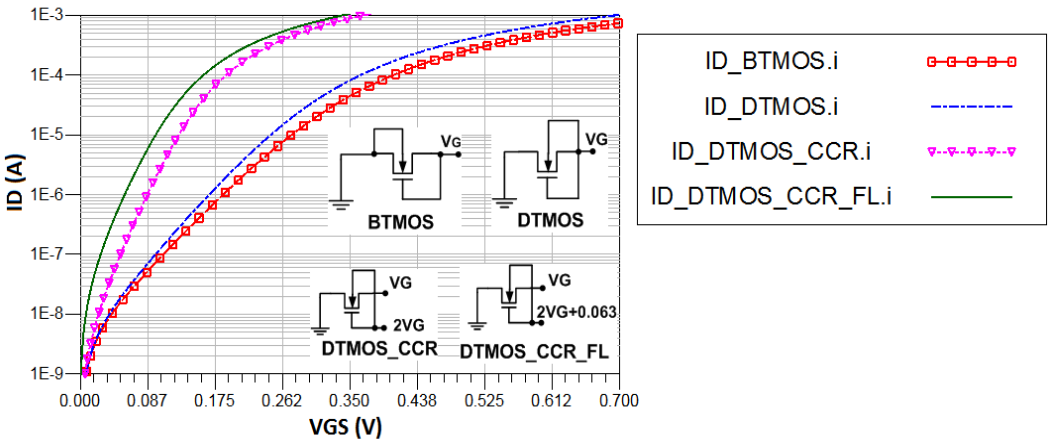

Figure 3.7: Simulated IV characteristic of the DTMOS diode, BTMOS diode, DTMOS CCR configuration, and DTMOS CCR with floating sub-circuits configuration

The figure indicates that applying DTMOS gains a higher drain current than BTMOS. Besides, as shown in the figure, in DTMOS CCR and CTMOS CCR with floating sub-circuit, the drain current is much higher than a diode-connected configuration. In simulation conditions, a 63 mV DC voltage of CCR floating sub-circuit is the amount of ΔVDC that the circuit achieved when input power is -20 dBm, as presented in Fig 3.8.

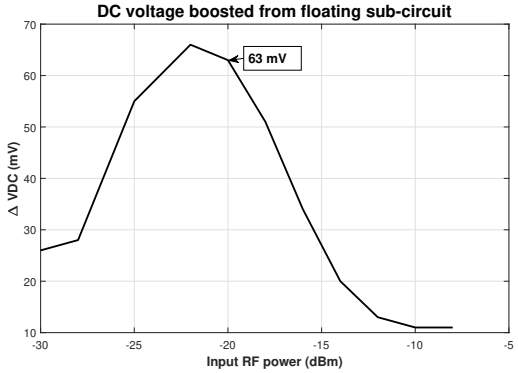

Figure 3.8: Simulated DC level-up amount (ΔVDC) from the floating sub-circuit

Fig 3.9 shows the simulated the dependence of output power of the rectifier on I_{s0}. As in equation 3.15, I_{s0} presents the characteristics of the MOSFET on weak inversion region. The simulated results got from a conditions that input power is -20 dBm, and load is $100k\Omega$

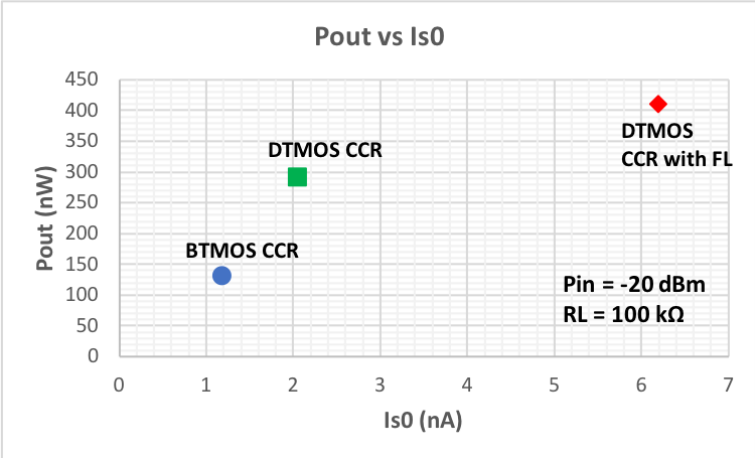

Figure 3.9: Simulated the dependence of output power of the rectifier on Is0

As shown in the figure, the output power of the CCR with floating sub-circuit is the highest because of the drain current of this structure is the highest. To conclude, DTMOS CCR and DTMOS CCR with floating sub-circuit on 65 nm SOTB technique is the best choice for the low input level range. The rectifiers in this study are chosen from these structures.

3.2.2 Q factor

The Q factor of a resonator, which is also a passive gain, is calculated by equation 2.1 in relationship with power and bandwidth of the resonator. Besides, in a relationship with resistance and reactance of the resonator at a resonant frequency, Q factor can be calculated by:

$$Q = \frac{X}{R} = \frac{B}{G} \tag{3.22}$$

where R, X, G, B are resistance, reactance, susceptance, conductance of the resonator.

In the RFEH rectenna, when a matching condition between antenna and rectifier is satisfied, the system is equivalent to a resonator, and at this condition, the passive gain Q will achieve. In chapter 2, the limitation of the Q factor of the rectifier to ensure BW of RF signal is proved. In this section, the relationship between the Q factor and the number of CCR stages is presented. First, the effect of the Q factor on the input voltage of the rectifier is considered. A equivalent of the rectifier is shown in Fig 3.10 to simplify analysis.

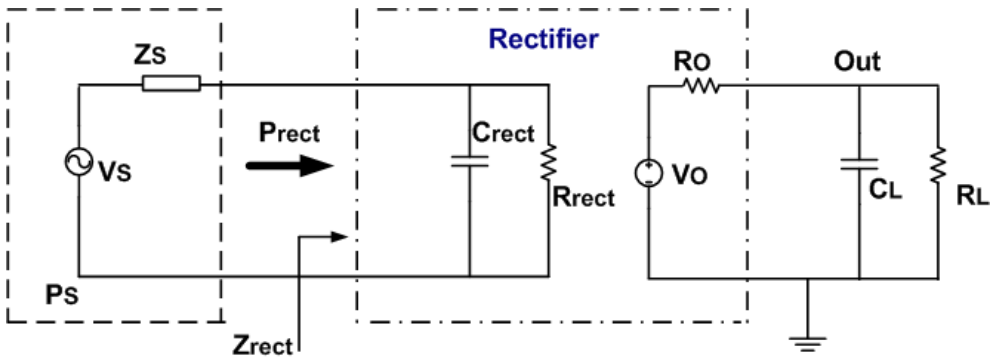

Figure 3.10: Equivalent circuit of a rectifier in the RFEH rectenna

A condition to ensure matching happen is analyzed in Chapter 4. In this section, we consider that matching condition is satisfied so that a source V_S supplies a power P_{rect} to the rectifier. At this condition, from input view, rectifier equivalent to a capacitor C_{rect} and R_{rect}. Relationships between

$P_{rect}, C_{rect}, R_{rect}, V_{rect}$ are shown in equation 3.23, 3.24, 3.25

$$Q_{rect} = \frac{B_{rect}}{G_{rect}} = \omega C_{rect} R_{rect} \tag{3.23}$$

$$P_{rect} = \frac{V_{rect}^2}{|Z_{rect}|} cos\,(\theta) = \frac{V_{rect}^2}{G_{rect}\,(1 + Q_{rect}^2)} \tag{3.24}$$

$$V_{rect} = \sqrt{P_{rect} G_{rect}\,(1 + Q_{rect}^2)} \tag{3.25}$$

From equation 3.25, V_{rect} is proportion with Q_{rect}. With the same input power P_{rect} value, Q_{rect} is higher resulting V_{rect} higher; hence output is higher. The output voltage of the rectifier also increases when number of rectifier stage increase. The block diagram of n-stage CCR is shown in Fig 3.11

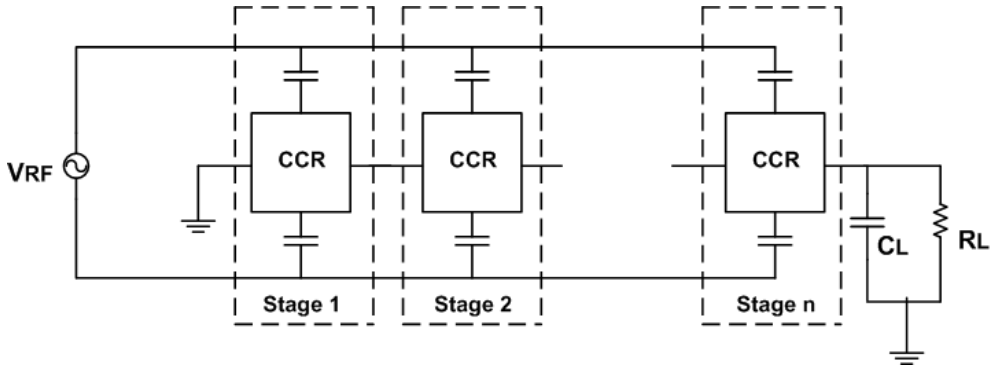

Figure 3.11: Block diagram of N stage CCR

In n-stage CCR, the RF signal is supplied in parallel while the DC signal is added in serial through n stages. If RF power supplied into each stage is unchanged, so the output of n-stage is equal to n times of one stage. However, because n-stage is connected in parallel, so input impedance of rectifier Z_{rect} also changes. To analyze the Q factor in n-stage, first, we consider a small-signal model of MOSFET as Fig. 3.12 [87], [103]

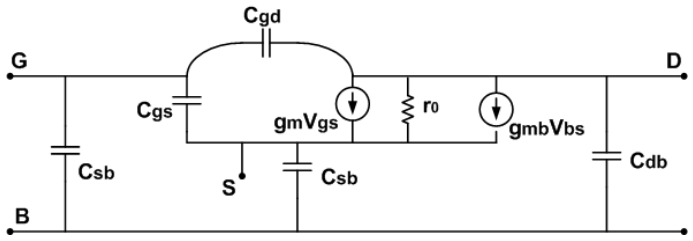

Figure 3.12: Complete MOS small-signal model

In the model, the effect of capacitors is taken into account. These capacitors are in a range of nF/m^2. A stage of CCR consists of four MOSFETs and two coupling capacitors. To analyze the effect of the number of stages to Q factor, we assume that each stage of CCR is equivalent to a capacitor C_{r1} in parallel with resistor R_{r1} as shown in Fig 3.13

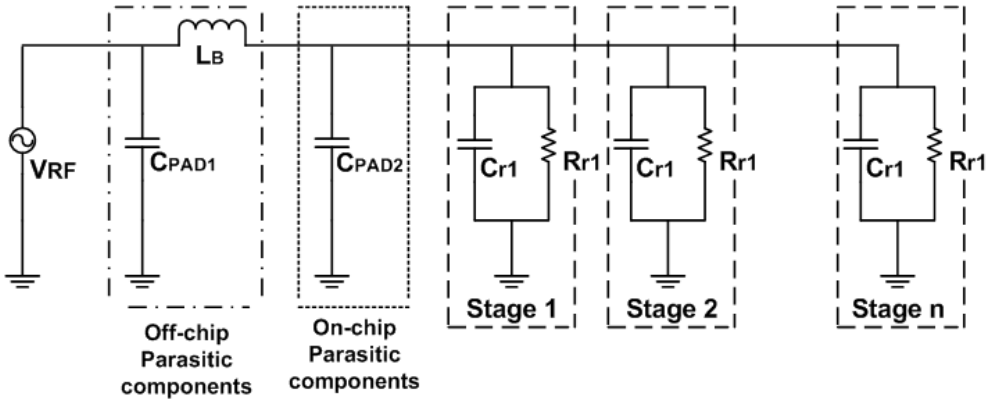

Figure 3.13: AC equivalent circuit of N stage CCR with effect of parasitic components

In the figure, the effect of parasitic components is taken into account. The parasitics components include on-chip components and off-chip components. The off-chip parasitic components are from bonding wires and pads to attach a rectifier chip onto a PCB board. The effect of the bonding wire is equivalent to an inductor L_B, which value is approximate to 1nH/mm for gold wire. The bonding wires can be designed as shortening as possible to reduce parasitic effects. The effect of pads in the PCB is equivalent to a capacitor C_{PAD1}, which value depends on the size of the pad and specifications of the board. Typically, pads in PCB is designed so that parasitic capacitors are small enough to not

affect to implementation of the circuit. The on-chip parasitic components in the CMOS process are mostly from parasitic capacitors C_{PAD2} of pads in the frame of the chip. In SOTB chip, these capacitors are generally in a range of few pF. In 65nm SOTB technology, for an in/out pin with ESD protection, we assume parasitic capacitor is around 2.1 pF.

In conclusion, the effect of parasitic components is mostly from on-chip parasitic capacitors of IO pins, which can not reduce. Besides, the parasitic capacitor C_{PAD2} is in pF range, while C_{r1} is in a range of fF in CMOS technology, so the capacitor C_{PAD2} takes into account to the input impedance of rectifier. The admittance of n-stage CCR is calculated in equation 3.26

$$Y_{n\_stage} = \frac{n}{R_{r1}} + j\omega \left(C_{PAD2} + nC_{r1}\right) \tag{3.26}$$

Q factor of n-stage CCR is

$$Q_{n\_stage} = \frac{\omega \left(C_{PAD2} + nC_{r1}\right)}{\frac{n}{R_{r1}}} = \omega R_{r1} \left(\frac{C_{PAD2}}{n} + C_{r1}\right) \tag{3.27}$$

From equation 3.27, the Q factor is inverse proportion with the number of stages. When n increases, the Q factor of rectifier decreases.

To conclude, the Q factor of the rectifier should be high to level up the input voltage of the rectifier. Besides, the Q factor is limited by BW of the target RF signal and the number of stages of the rectifier. As the specifications pointed out in chapter 2 to harvest LTE 950 MHz signal, the maximum Q factor is 47. The number of rectifier stage is chosen to satisfy this value.

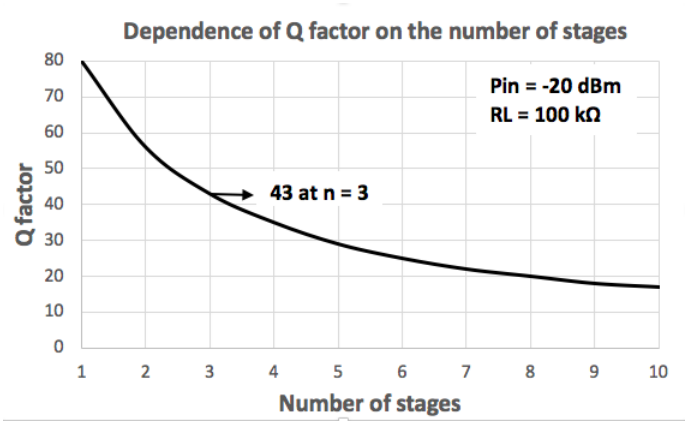

Figure 3.14: Simulated dependence of Q factor on the number of rectifier stages N-stage CCR with floating sub-circuits

Fig 3.14 shows simulated results of the dependence of Q factor on the number of rectifier stages N-stage CCR with floating sub-circuits in conditions of -20 dBm input power and $100k\Omega$ load. From the figure, a 3-stage rectifier, which has a Q factor of 43, is satisfactory requirements of the Q factor to ensure the efficiency of the rectifier.

3.2.3 Waveform excitation

As presented in the Fig 2.8, the waveform excitation is also the specification that affects the efficiency of the rectifier circuit. The RF signal available in the environment is a modulated signal. The modulated signal can be characterized by a Peak-to-Average-Power-Ratio (PAPR). With the same average power of a signal, the different modulation type can have different PAPR as shown in Fig 3.15 [86].

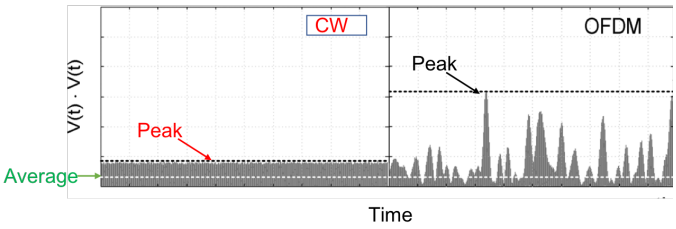

Figure 3.15: Instantaneous power of the CW signal and OFDM signal

As shown in the figure, with the modulated signal, the peak power of the modulated signal is higher than the peak power of the CW signal. In the study [84–86], the PAPR is defined at a level that a Complementary Cumulative Distribution Function (CCDF) of the signal is 0.001 %. Fig. 3.16 presents the PAPRs in the measurement of this study in which the modulated signals are generated by the signal generator SMJ100A. As shown in the figure, PAPRs of the CW, binary phase-shift keying (BPSK), 64 quadrature amplitude modulation (QAM), 256 QAM signals are 0.09, 2.83, 6.21, and 5.72, respectively.

The instantaneous voltage of the modulated signal differs from the CW signal then V_{GS} and V_{DS} in equation 3.9, 3.10, 3.11, and 3.12 are changed.

3.2. Principle specifications affect to efficiency of rectifier

The output current is exponential proportion with the voltages at V_{GS} and V_{DS} as indicated in equation 3.15, 3.16, and 3.17. Therefore, the different PAPRs led to different output voltages.

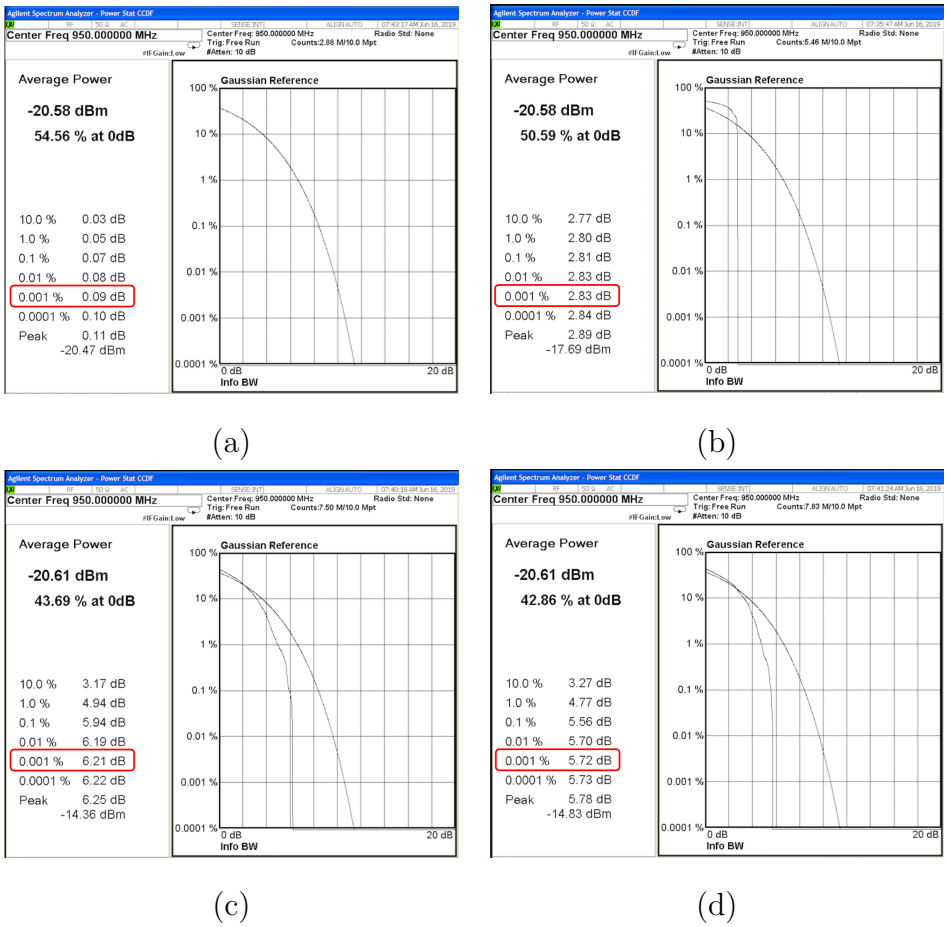

Figure 3.16: PAPRs of the measured RF signals with signal generator: (a) PAPR of CW signal, (b) PAPR of BPSK signal, (c) PAPR of 64 QAM signal, and PAPR of 256 QAM signal

Although the waveform excitation is the specification which affects the output of the RFEH system, but this is a fix characteristic of the ambient RF signal in the environment. Therefore, the waveform excitation of the RF signal does not a specification that designers can manage in the ambient RFEH system design.

3.2.4 Phase difference

In section 3.2.1, the two input power at points RF_1 and RF_2 are assumed differential signals which mean phase difference between these two signals are 180^0. In the RFEH system, the RF signals supplied to the rectifier are from the former parts such as antenna, matching circuits. Hence, the condition to ensure the two signals are symmetrical is needed. In this section, we analysis circuit performance when the two paired signals of the CCR have an arbitrary phase difference, denoted by $\Delta\varphi$. In this case, V_1 and V_2 rewrite as equation below.

$$V_1 = V_{DC\_offset} + V_{RF} sin 2\pi ft \tag{3.28}$$

$$V_2 = V_{DC\_offset} + V_{RF} sin\left(2\pi ft + \Delta\varphi\right) \tag{3.29}$$

Therefore, gate-to-source voltage V_{GS} of NMOS N1 is presented as equation 3.30

$$V_{GS} = \begin{cases} 2V_{RF} sin\left(\frac{\Delta\varphi}{2}\right) cos\left(2\pi ft + \frac{\Delta\varphi}{2}\right) & when \quad V_1 < 0 \\ V_{RF} sin\left(2\pi ft + \Delta\varphi\right) & when \quad V_1 \geq 0 \end{cases} \tag{3.30}$$

Equation 3.30 indicates that V_{GS} depends on $\Delta\varphi$; hence outputs of the rectifier also depends on $\Delta\varphi$. V_{GS} is maximum when $\Delta\varphi = \pi$ meaning the paired RF input signals of the rectifier are symmetric.

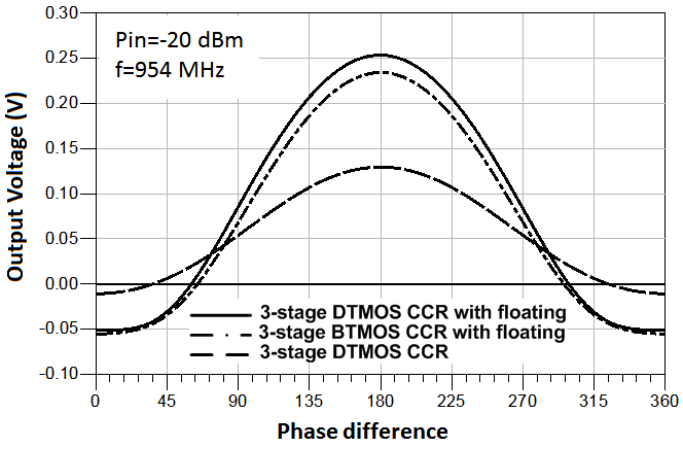

Figure 3.17: Dependence of DC output voltage with $\Delta\varphi$ in 3-stage CCR, 3-stage CCR with floating sub-circuit using DTMOS and BTMOS.

Fig 3.17 presents simulated results of three 3-stage-CCR types: simple CCR, CCR with floating circuit using DTMOS, CCR with floating circuits using BTMOS. The simulation conditions are an input power of -20 dBm, a load of 10 MΩ, and a frequency of 954 MHz. It can conclude from Fig. 3.17 that with all rectifier types, the DC output voltage strongly depends on the phase between the paired RF inputs. The output voltage reaches the peak value when $\Delta\varphi = \pi$ and significantly decreases when $\Delta\varphi$ changes.

From the analysis of the effect of the phase difference between the two paired inputs of the rectifier, we can conclude that when designing the CCR to ensure the highest PCE, the circuit must be symmetrically designed.

3.3 Evaluated results of fabricated rectifiers

3.3.1 Design of 3-stage DTMOS CCR and BTMOS CCR

The cross-coupled rectifier was fabricated in 65nm SOTB technology to evaluate the effect of the specifications indicated in section 3.2. In the fabrication, 3-stage CCR with DTMOS and 3-stage CCR with BTMOS were designed as the schematic diagram in Fig. 3.18. The layout of the designed CCR is shown as in Fig 3.19 and 3.20. In the circuits, MOSFET specifications of DTMOS and BTMOS are chosen exactly the same so that comparison conditionals between the performance of the two circuits are equally. The W/L ratio of MOSFET is 1.5 μm/60 nm. Coupled capacitors of the CCR are designed 1 pF each.

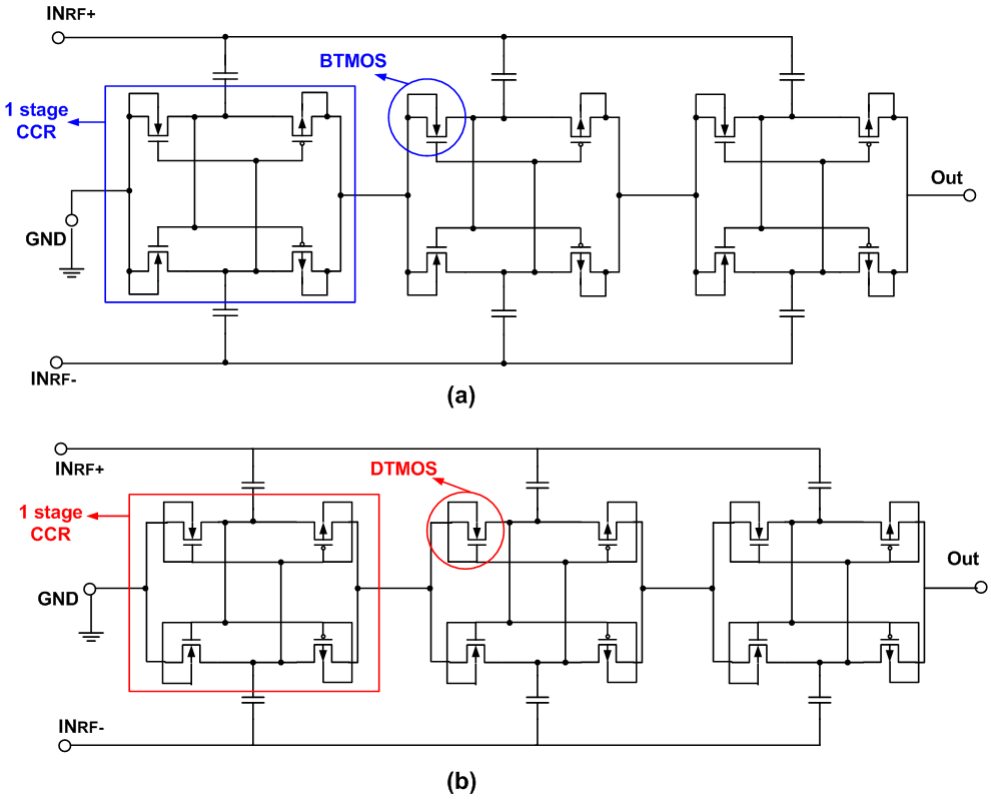

Figure 3.18: Schematic of 3-stage CCR: (a) with BTMOS, (b) with DTMOS

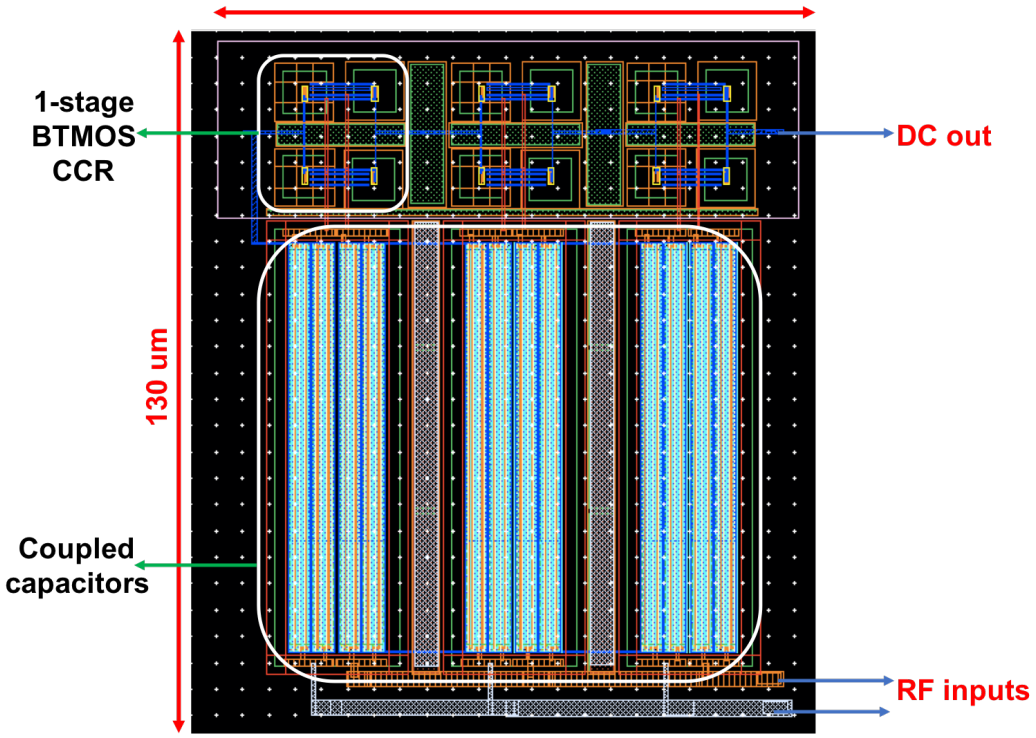

Figure 3.19: Layout of 3-stage BTMOS CCR

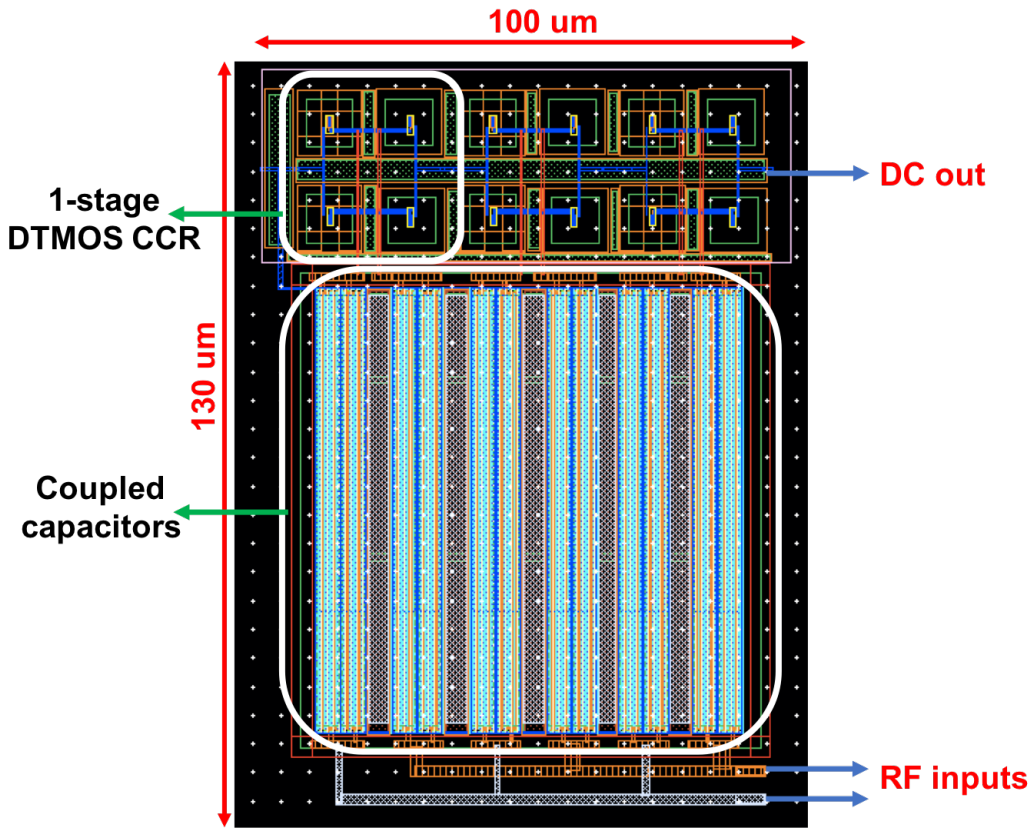

Figure 3.20: Layout of 3-stage DTMOS CCR

3.3.2 Measurement results

Measurement was implemented with a signal generator (SG) to test the performance of the rectifier circuits as a setup in Fig 3.21

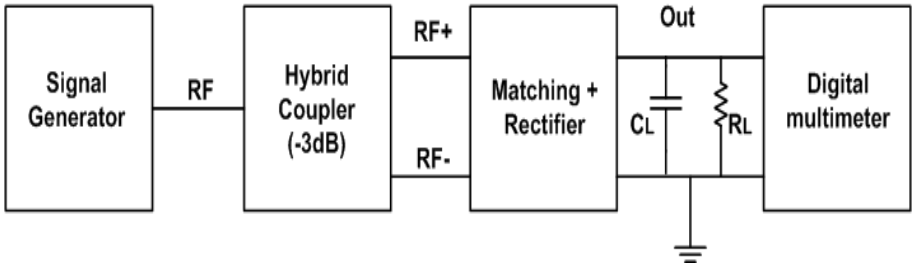

Figure 3.21: Evaluation setup with signal generator

The SG SMJ100A is used to supply RF signals to the rectifiers. The SG can generate a sine wave signal (CW) and some modulated signals such as phase-shift keying (PSK) and quadrature amplitude modulation (QAM). The

SG has one port output, so to create two symmetrical RF signals, a hybrid coupler KRYTAR4010124 is used. Matching circuits are designed to ensure matching between rectifier circuits and 50 Ω of the hybrid coupler through SMA connector. DC output of the rectifier after filtering by C_L and R_L is measured by a digital multimeter DMM7510

3.3.3 Matching circuits for 3-stage CCR chip

The SOTB rectifier chip is attached to the FR4 board for measurement, as shown in Fig 3.22.

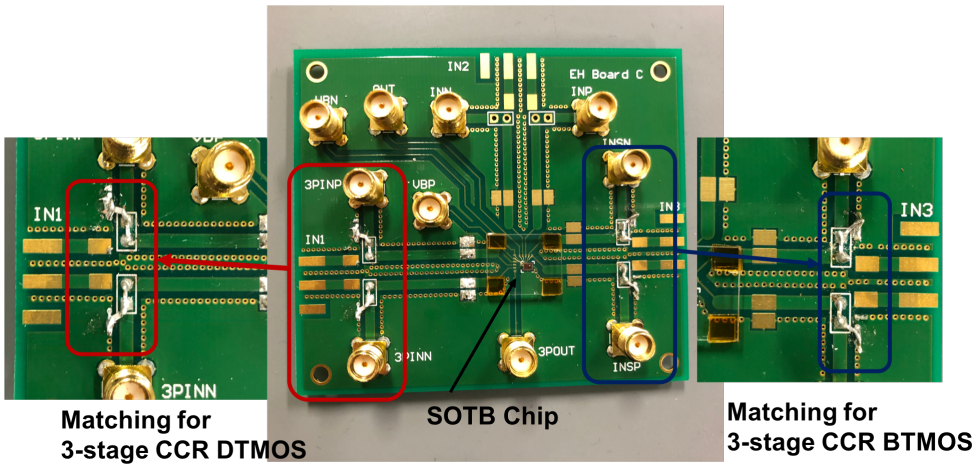

Figure 3.22: 3-stage CCR with matching circuit in FR4 board

The matching circuit is designed in L type matching to minimize components added in the system, so that minimize loss. The equivalent circuit of the total board chip is shown in Fig 3.23. The target matched frequency of the matching circuits is 950 MHz. Components used for matching with 3-stage BTMOS CCR consist of an inductor of 3.9 nH and a capacitor of 6.5 pF. Components used for matching with 3-stage BTMOS CCR consist of an inductor of 2 nH and a capacitor of 6.5 pF.

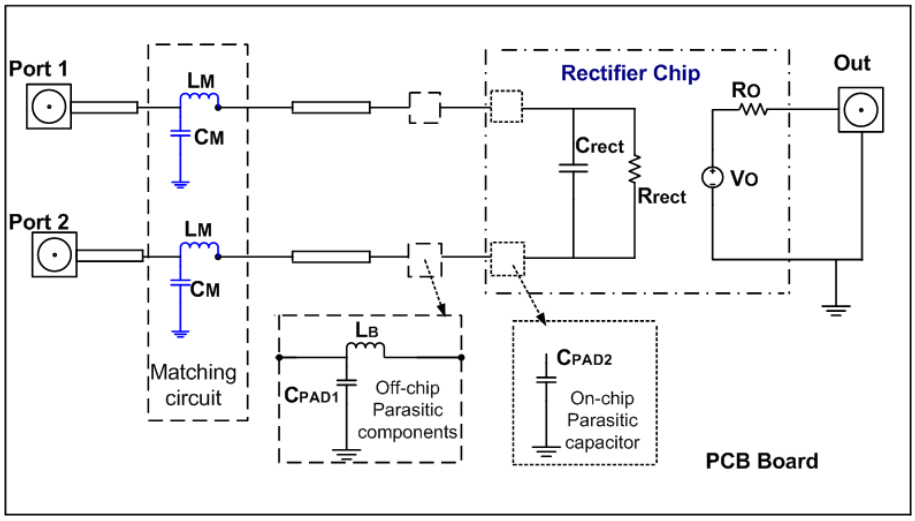

Figure 3.23: Equivalent circuit of the rectifier and matching in the PCB board

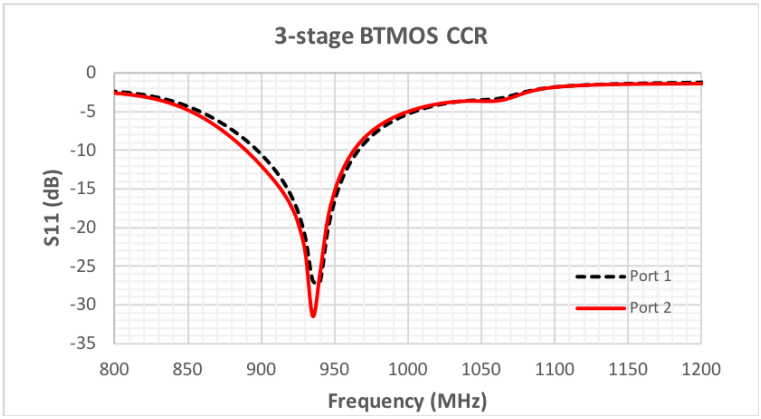

(a)

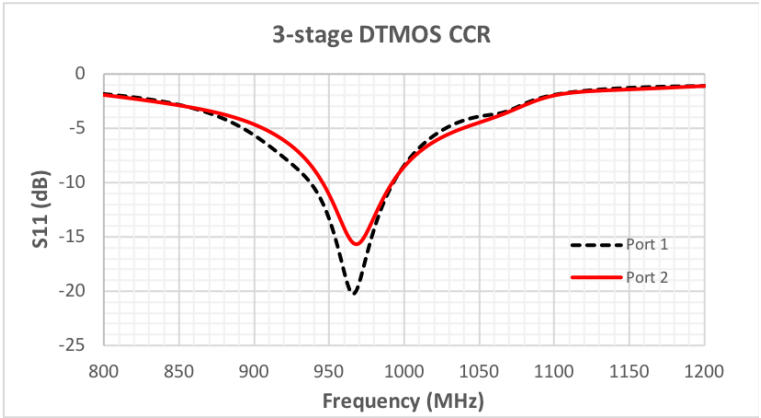

(b)

Figure 3.24: Measured S11 at two ports rectifier boards: (a) BTMOS CCR board, (b) DTMOS CCR board

Fig 3.24 (a) presents measured S11 at the two SMA ports of the BTMOS CCR board. From the figure, BW -3dB achieved from 810 MHz to 1050 MHz. At 950 MHz, S11 is -15 dB. Fig 3.24 (b) presents measured S11 at the two SMA ports of the DTMOS CCR board. From the figure, BW -3dB achieved from 820 MHz to 1080 MHz. At 950 MHz, S11 at two ports are -11 dB and -14 dB. The results indicate that the two CCR board are matched at 950 MHz.

3.3.4 Measurement results of the designed 3-stage CCR

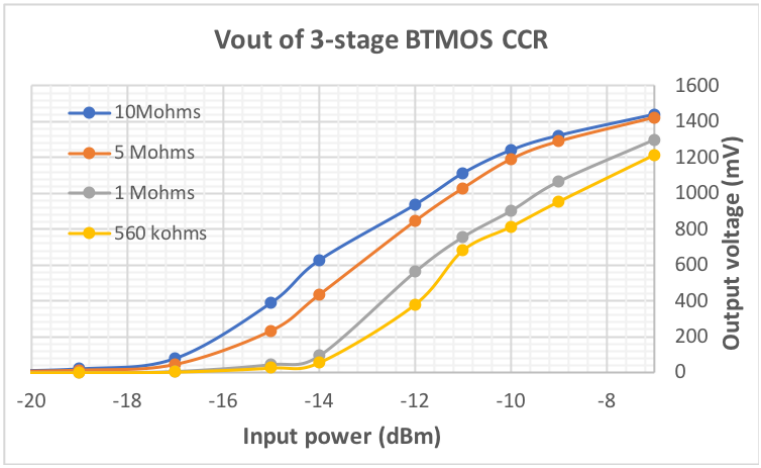

(a)

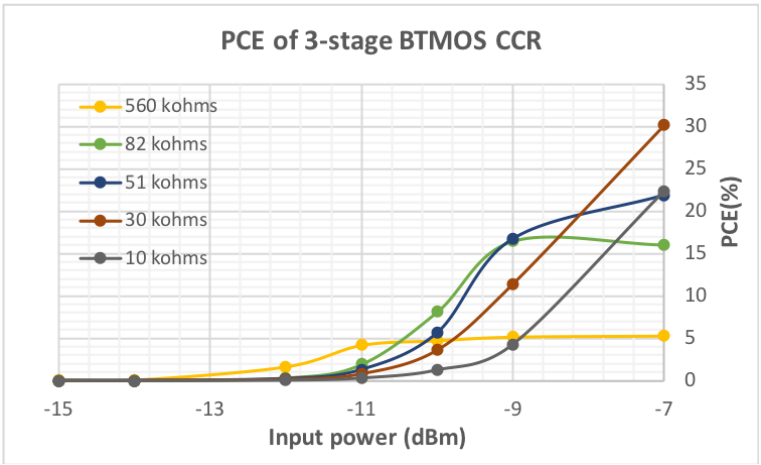

(b)

Figure 3.25: Measured results of 3-stage BTMOS CCR at 950 MHz: (a) Output voltage at different loads, and (b) PCE at different loads

3.3. Evaluated results of fabricated rectifiers

Fig 3.25 presents measured results of 3-stage BTMOS CCR at a frequency of 950 MHz. From the figure, BTMOS CCR reaches a sensitivity of 1V when input power is higher than -12 dBm. The highest PCE of the BTMOS CCR is 30 % at -7 dBm input power.

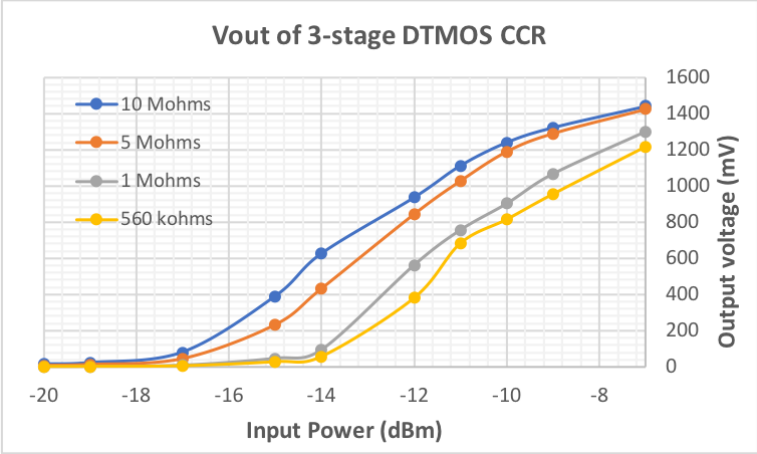

(a)

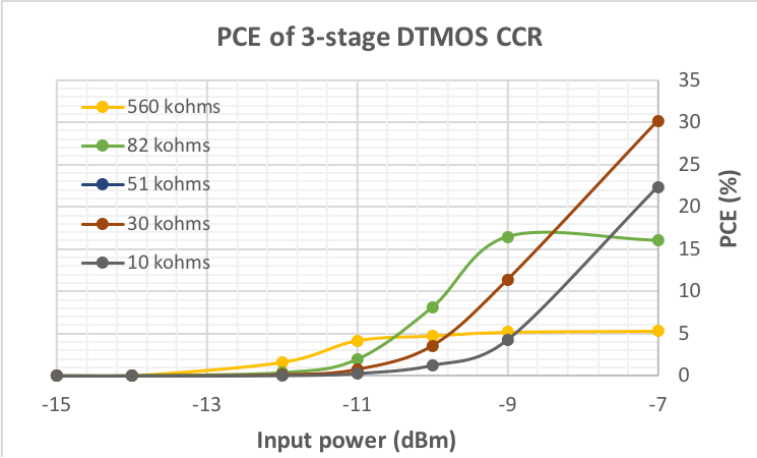

(b)

Figure 3.26: Measured results of 3-stage DTMOS CCR at 950 MHz: (a) Output voltage at different loads, and (b) PCE at different loads

Fig 3.26 presents measured results of 3-stage DTMOS CCR at a frequency of 950 MHz. From the figure, DTMOS CCR reaches a sensitivity of 1V when input power is higher than -13 dBm. The highest PCE of the DTMOS CCR is 30 % at -7 dBm input power.

Fig 3.27 indicates comparison results between the DTMOS CCR and BT-

MOS CCR. Figure (a) shows output voltages of the circuits at 10 $M\Omega$ when the CW signal excited. As shown in the figure, output voltages of DTMOS CCR are higher than that of the BTMOS CCR over the range of input power. Besides, Fig 3.27 (b) presents measured output voltages of the circuits when excited by BPSK signal, 64 QAM, and 256 QAM. From the figure, with all modulation types, output voltages of DTMOS CCR are higher that of BTMOS CCR. The result proves that DTMOS configuration, which leads to a high drain current, when applying in CCR boosts output of the circuit. Therefore, DTMOS CCR is a good choice for RFEH rectenna.

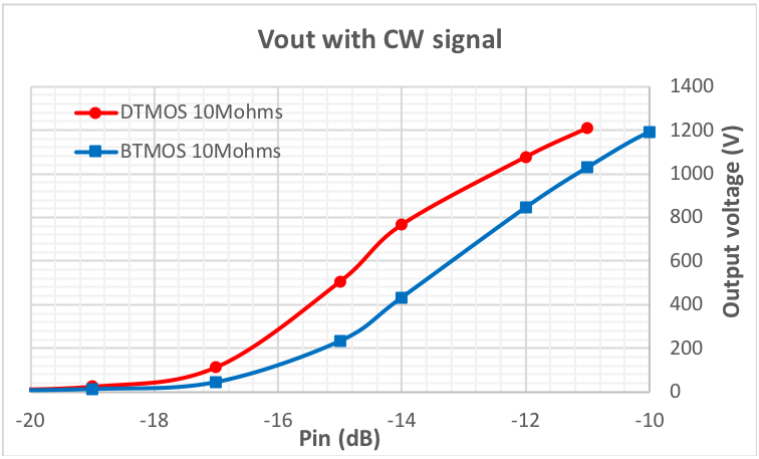

(a)

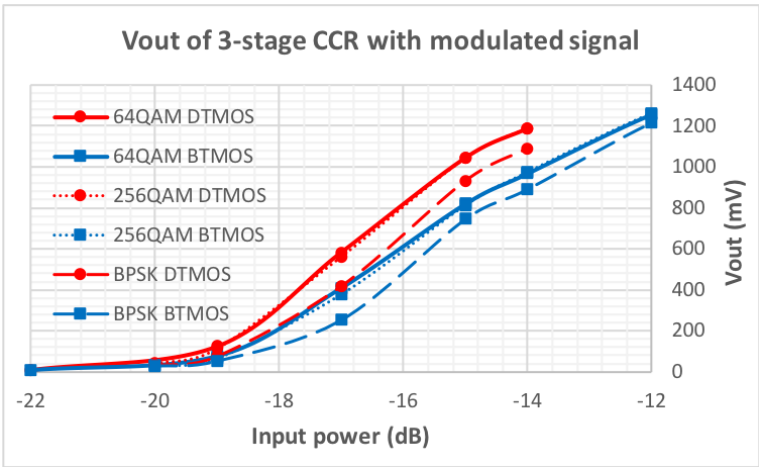

(b)

Figure 3.27: Measured output voltages of 3-stage DTMOS and BTMOS CCRs at 10 $M\Omega$ load: (a) Input is CW signal, and (b) Inputs are modulated signals

In [84–86], study about optimal waveform excitation of the rectifier are validated. The studies proved that the PCE of the rectifier increased when the rectifier is excited by the modulated signals. Fig 3.28 presents the dependence of the output power of the CCRs on the PAPR of the RF signals. As shown in the figure, the modulated signals are effective with both DTMOS and BTMOS CCR. When the PAPR increases, the output power also increases. Notably, these results got in a condition that designed BWs of the DTMOS and BTMOS are wide as the results shown in section 3.3.3

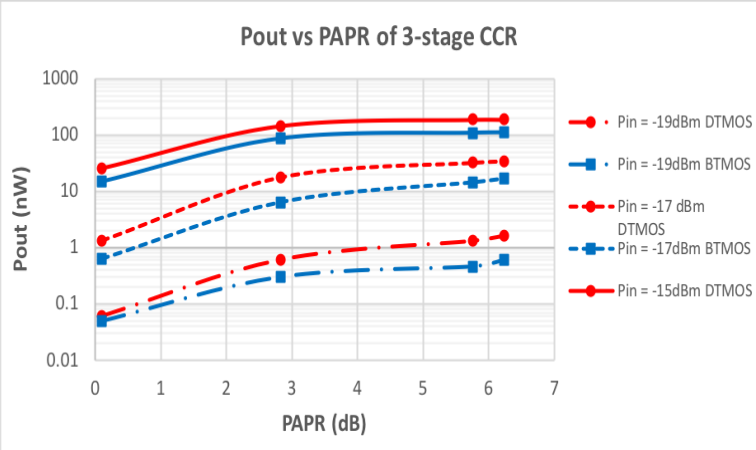

Figure 3.28: Measured dependence of output power of CCR on PAPR of RF signals

3.4 Implement of 3-stage DTMOS CCR with floating sub-circuit

3.4.1 Matching circuit for 3-stage CCR with floating sub-circuits chip

The 3-stage CCR with floating sub-circuits was designed before. In this study, we designed matching circuits for the rectifier, and RFEH rectennas utilized the rectifier. The board chip, which included the matching circuit and rectifier chip, is shown in the Fig 3.29

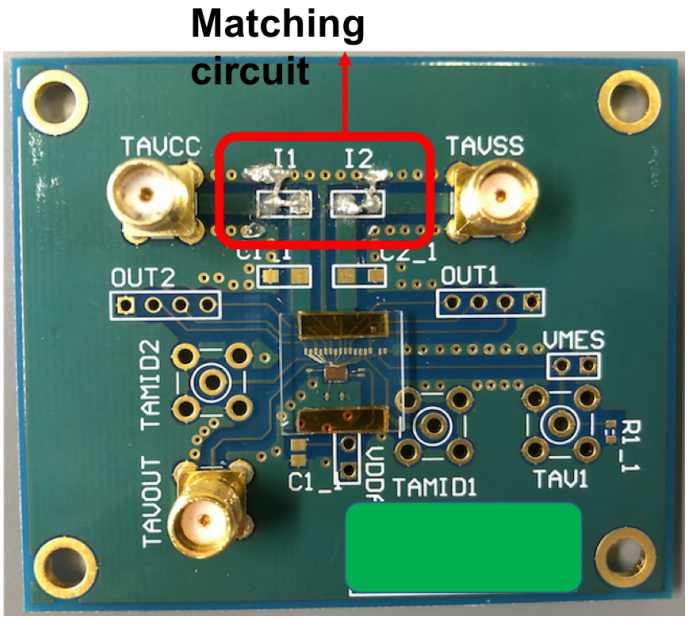

Figure 3.29: Matching circuit for CCR with floating sub-circuits for measurement with SG

L type matching circuits were designed to match the rectifier with two SMA ports. In the matching circuits, an inductor of 4.1 nH and a capacitor of 6.5 pF are chosen. Fig 3.30 presents measured S11 of the circuits at the two ports P_1 and P_2. As shown in the figure, the BW of the matching circuit is 180 MHz. The target frequency band, which is from 945 MHz to 960 MHz, is within the -10 dB loss band.

In Fig 3.30, simulated results of the total board chip are also presented. In the simulation, a harmonic balance method (HBM) of advanced design system (ADS) software (ADS) is used for simulation. In the simulation, SOTB MOSFETs are modeled by the BSIM4 model; all the parasitic components are estimated and attached. From the results indicated in the figure, it can conclude that the simulated results and measurement results of the total board chip are almost identical. Therefore, the designed calculation about the Q factor, which is calculated from the impedance of the rectifier, in section 3.2.2, is validated.

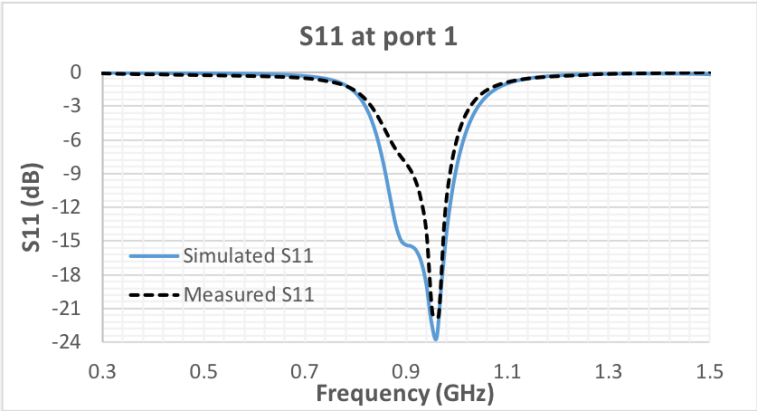

(a)

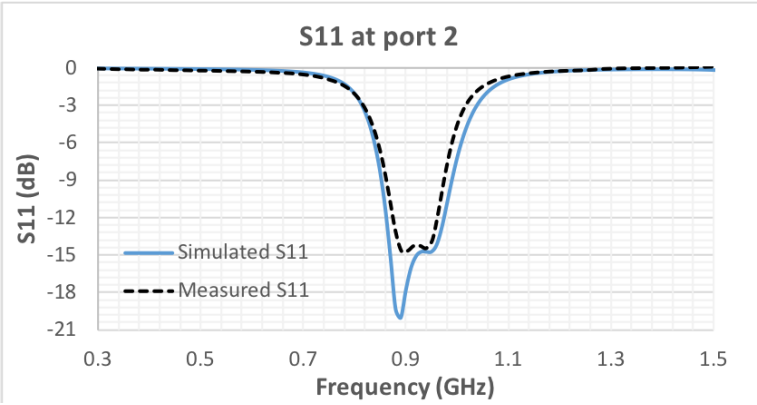

(b)

Figure 3.30: Measured S11 of 3-stage DTMOS CCR with floating sub-circuits: (a) at Port 1, and (b) at Port 2

3.4.2 Measurement results of 3-stage CCR with floating sub-circuits

Fig 3.31 presents measurement results of the 3-stage CCR with floating sub-circuits with CW signal at a frequency of 950 MHz. The circuit reaches sensitivity 1V at an input power of -14 dBm and 10 $M\Omega$ load. The highest PCE of the circuit is 52 % at -10 dBm input power and 10 $k\Omega$ load.

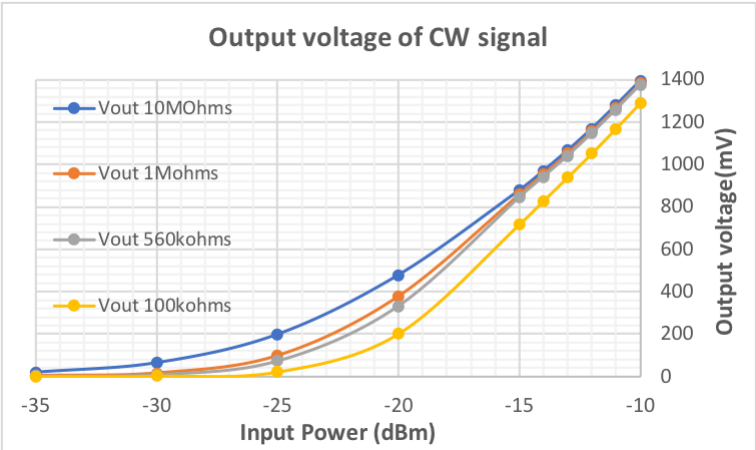

(a)

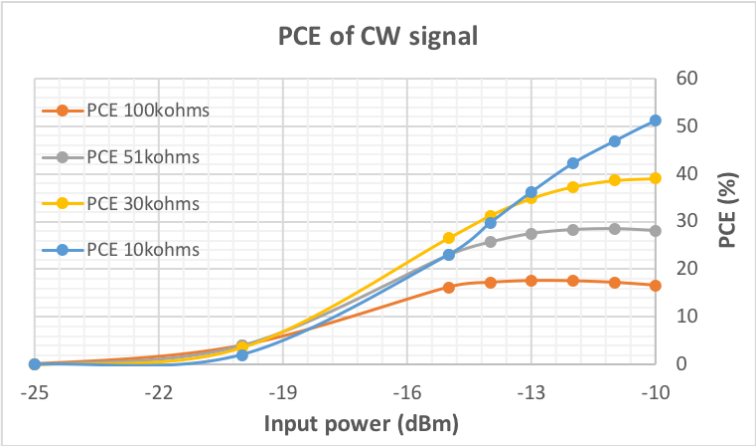

(b)

Figure 3.31: Measured outputs of 3-stage DTMOS CCR with floating sub-circuits with CW signal: (a) Output voltage, and (b) PCE

Fig 3.32 presents the measured PCEs of 3-stage CCR with floating sub-circuits in conditions of multi-type signal excited. From the figure, at -20 dBm input power and optimum loads, PCE of the case excited CW signal is 4 % but that of the case using modulated signals is 9 %, which is 2.25 time increase. At -15 dBm input power and optimum loads, PCE of the case excited CW signal is 26 % but that of the case using BPSK is 34 %, which is 1.3 time increase. The results prove that, with the designed matching circuit, the PCE of rectifier board chip increased when harvested the modulated signal at a low input power range

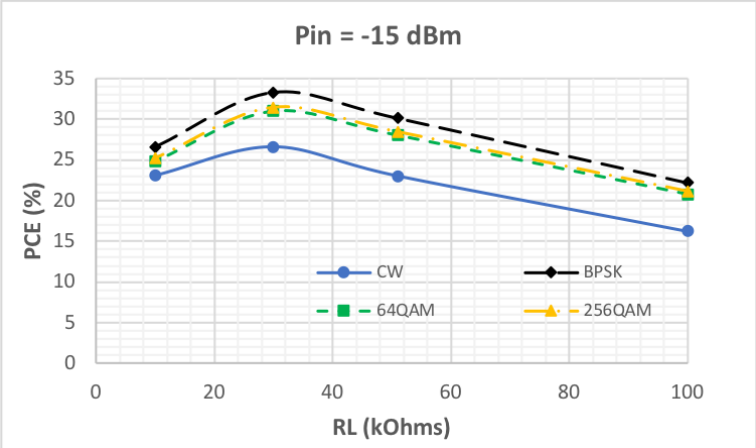

(a)

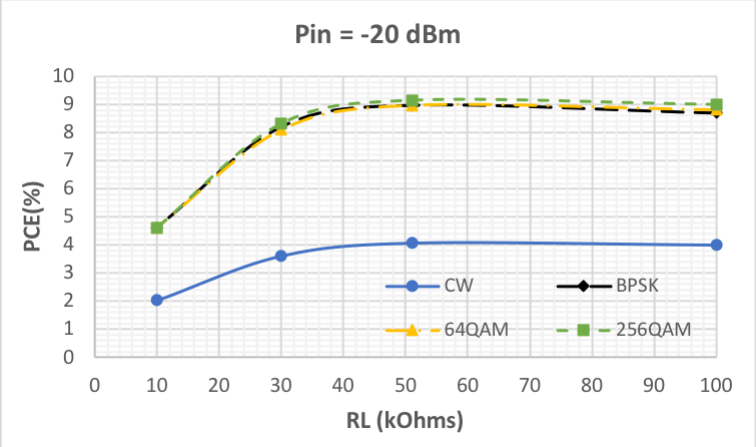

(b)

Figure 3.32: Measured PCE of 3-stage DTMOS CCR with floating sub-circuits: (a) at an input power of -20 dBm, and (b) at an input power of -15 dBm,

3.4.3 Measurement results of phase different effect

The measurement setup to evaluate the effect of the phase difference of the two RF signals is presented in Fig 3.33. The signal generator generates the RF signal to the input of a hybrid coupler, KRYTAR 4010124. The RF signal then is divided into two RF signals by the coupler and supplied to the rectifier.

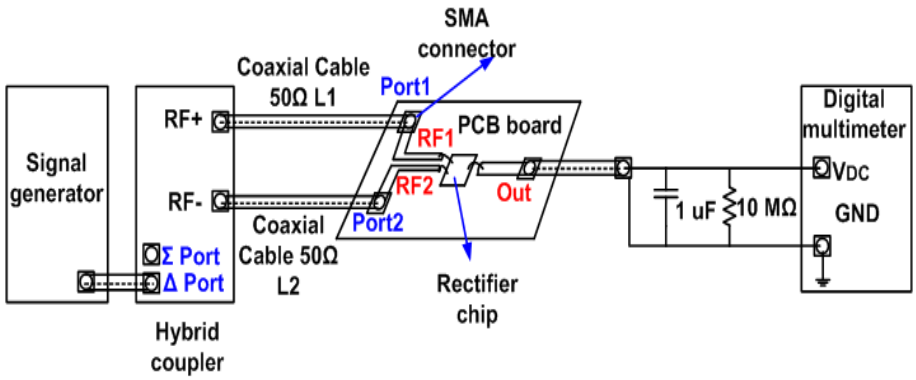

Figure 3.33: Evaluation conditions for phase effect measurement

Phase difference between points RF_+ and RF_- in Fig. 3.33 is notated by $\Delta\varphi(RF_+, RF_-)$. Phase difference between two RF signals RF_1 and RF_2, at ports P_1 and P_2 of the rectifier board, is denoted by $\Delta\varphi$. The phase $\Delta\varphi$ is the phase difference of the two RF inputs supplied the rectifier. $\Delta\varphi(RF_+, RF_-)$ and $\Delta\varphi$ are calculated by equation 3.31 and 3.32:

$$\Delta\varphi\left(RF_+, RF_-\right) = \begin{cases} 0 & for \quad \Sigma \quad port \\ \pi & for \quad \Delta \quad port \end{cases} \tag{3.31}$$

$$\Delta\varphi = \frac{2\pi}{\lambda_P}\left(L_1 - L_2\right) + \varphi\left(V_{RF+}, V_{RF-}\right) \tag{3.32}$$

where L_1 and L_2 are lengths of coaxial cables used for connecting between the hybrid coupler and the rectifier board. λ_P is wavelength of the RF signal in the coaxial cable.

From the equation 3.31 and 3.32, it can conclude that $\Delta\varphi$ can drive by changing ports of the hybrid coupler and length of the coaxial cable.

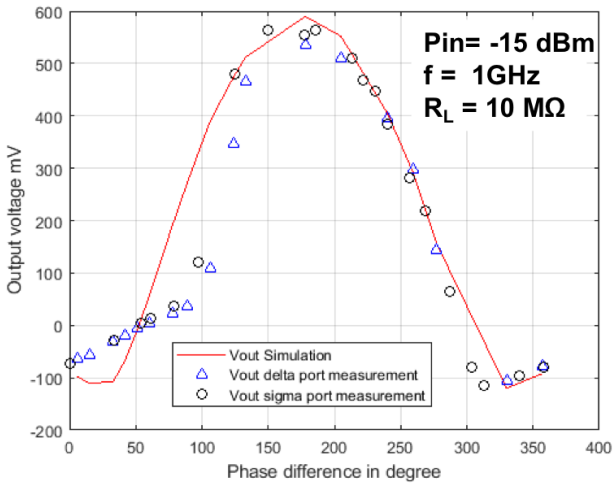

Figure 3.34: Measured and simulate results of phase difference effect into 3-stage CCR with floating sub-circuits

Fig 3.34 presents measured results about phase difference effect into 3-stage CCR with floating sub-circuits. As shown in the figure, the simulated and measured results are almost identical. The results prove the theory about the phase different effect. The output of the rectifier circuit in the cross-coupled structure depends on the phase difference between the two paired RF inputs of the circuit.

3.5 Chapter Conclusion

In this chapter, the principle specifications of the rectifier to rectify ambient RF signals are presented. In a low input level range, the high drain current is an important parameter to increase the output of the rectifier. The DTMOS structure is proved that has high drain current than BTMOS type. Besides, to harvest the ambient RF signal, an essential parameter needed to be considered in rectifier design is the Q factor. In the theoretical analysis, the Q factor is proved that it depends on the BW of the RF signal, the number of the rectifier stage. The phase difference between the two RF inputs of the rectifier is also a parameter affected by the output of the CCR.

The 3-stage DTMOS CCR and BTMOS CCR were designed and mea-

sured. The measurement results prove that DTMOS CCR achieved higher performance than BTMOS CCR. In addition, the 3-stage DTMOS CCR with floating sub-circuits is also evaluated. The measurement results indicated that the performance of the DTMOS CCR with floating sub-circuits reached the highest performance in comparison with the DTMOS CCR and BTMOS CCR. The simulated and measured results of 3-stage DTMOS CCR with floating sub-circuits are compared and proved that they are identical. Therefore, the Q factor of the circuit, which is designed as 43, is suitable to use in the RFEH rectenna to harvest the LTE signal.

In conclusion, the 3-stage DTMOS CCR with floating sub-circuits is utilized in the proposed structure of the ambient RFEH rectenna.

Chapter 4

Design of wide bandwidth RFEH rectenna to harvest RF energy in the ambient environment

In this chapter, a design methodology of the ambient RFEH rectenna system is presented. The relationships between Q factors of the RFEH system and BW of the ambient RF signal are considered. Besides, the impedance of antenna is studied. From the considerations, the RFEH systems to harvest LTE 950 MHz cell phone is proposed and designed.

4.1 Design methodology

4.1.1 Consideration of Q factor of the RFEH rectenna

The Q factor of the rectifier is considered in chapter 3. In this section, the relationships between Q factors of parts in RFEH are mentioned. The Q factors of the RFEH rectenna is defined in Fig 4.1

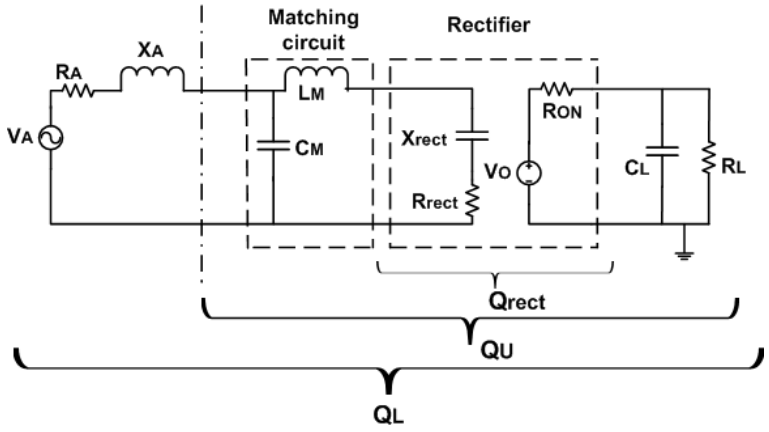

Figure 4.1: Q factor of RFEH rectenna

When the matching condition is satisfied at the target frequency, the Q factors can be calculated as equation 2.1, 3.23. In Fig. 4.1, Q_L is loaded Q factor of the total RFEH system. Because of a resonant condition, Q_L is calculated from the BW of the system as presented in equation 2.2. Besides, Q_U is an unloaded Q factor of a combined circuit of rectifier and matching circuit. The Q factor of the rectifier Q_{rect} is defined in equation 3.23. The relationships between Q_L, Q_U and Q_{rect} are shown in equation 4.1, 4.2, 4.3

$$Q_L = \frac{f_0}{BW} \tag{4.1}$$

$$Q_U = 2Q_L \tag{4.2}$$

$$\frac{1}{Q_U} = \frac{1}{Q_{rect}} + \frac{1}{Q_e} \tag{4.3}$$

where Q_e is a Q factor of external components in the PCB, which consists of transmission lines, matching components.

To reduce loss, Q_e should be maximized, resulting in high Q matching components should be chosen for the matching circuit. Besides, the matching circuit is designed in a simple structure such as L type to reduce using components for matching. The transmission lines for RF signals are designed to

be short to reduce loss. With these conditions, Q_{rect} will dominate Q_U and be moderate value to ensure the BW of the RF signal.

When all conditions are guaranteed, the BW of the RFEH system is wide enough to cover the BW of the RF signal, and the Q factor of the RFEH system is large enough to achieve satisfactory efficiency of the ambient RFEH rectenna.

4.1.2 Antenna impedance consideration

A simple model of a rectenna, as shown in Fig 4.2, is used to consider the effect of antenna impedance to the efficiency of the RFEH rectenna. As shown in the figure, antenna is modeled as a source that supplied a power P_S to the rectifier circuit, resulting in a voltage V_S in the input of the rectifier.

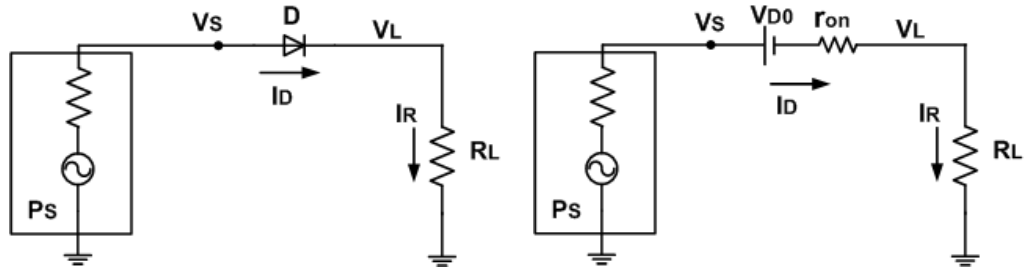

(a) (b)

Figure 4.2: Simple model of a rectenna: (a) The simple rectenna, and (b) Equivalent circuit

In the figure, the rectifier is modeled as a diode. The figure (b) presents the equivalent circuit of the figure (a) in conditions that diode is in the linear region. In this region, diode current is presented by equation 4.4

$$I_D = \begin{cases} 0 & when \quad V_D \leq V_{D0} \\ k\,(V_D - V_0) & when \quad V_D > V_{D0} \end{cases} \tag{4.4}$$

Figure 4.3 shows a piecewise-linear model of diode forward characteristic and load line of the rectenna circuit. In the figure, V_{D0} is turn-on voltage of the diode, r_{on} is on-resistance of the diode.

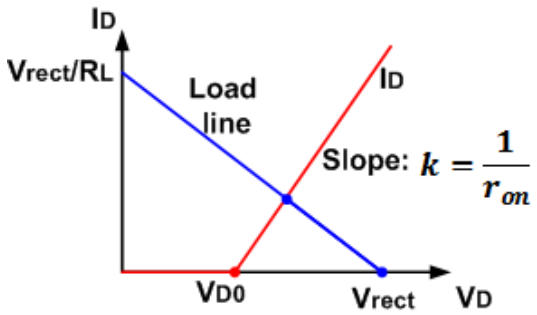

Figure 4.3: Piecewise-linear model of diode forward characteristic

The relationships between currents, voltages, powers, and efficiency of the circuit in Fig 4.2 are shown as below.

The supplied power of antenna source to the rectifier:

$$P_S = \frac{V_S^2}{R_S} \tag{4.5}$$

Input power of the rectifier circuit:

$$P_{IN\_rect} = \frac{V_S^2}{(r_{on} + R_L)} \tag{4.6}$$

Load voltage:

$$V_{Lt} = I_D R_L = (V_S - V_{D0}) \frac{R_L}{(r_{on} + R_L)} \tag{4.7}$$

Output power at the load:

$$P_{out} = \frac{(V_S - V_{D0})^2 R_L}{(r_{on} + R_L)^2} \tag{4.8}$$

From the equation 4.5 and 4.6, it can conclude that when a matching condition $R_S = r_{on} + R_L$ happen, the input power of the rectifier is maximized. at this condition the PCE of the rectenna is:

$$PCE\,(\%) = \frac{P_{out}}{P_S} 100\% = \left(1 - \frac{V_{D0}}{V_S}\right)^2 \left(1 - \frac{r_{on}}{R_S}\right) 100\% \tag{4.9}$$

Equation 4.9 indicates that in an ideal condition, when diode is lossless and turn on voltage is $V_{D0)}$ is zero, the PCE of the rectenna is 100%.

Besides, because $V_S = \sqrt{P_S R_S}$ so if P_S is unchanged, when R_S increase, V_S also increase. Hence, from equation 4.9, it can be concluded that, with a

specific diode, when R_S and V_S increase, PCE will increase if the matching condition is satisfied.

In conclusion, if input matching conditions are satisfied, the RFEH system, which has high antenna impedance, can reach higher PCE than that of the RFEH system with a small impedance antenna.

4.2 The proposed RFEH systems from 950 MHZ cell phone RF signals

As mention in chapter 2, at the environment around the laboratory, the LTE 950 MHz mobile phone signal is the strongest, so this signal is a target signal of our proposed RFEH rectenna. Base on methodology design, we propose two ambient RFEH rectennas, which are an RFEH rectenna with a 75Ω antenna and an RFEH rectenna with a 50Ω antenna. To easily distinguish, the RFEH rectenna with the 75Ω antenna is called a high impedance rectenna (HA) RFEH system, and the remained rectenna is called low impedance antenna (LA) RFEH system. The rectifier chip, which is a CCR with floating sub-circuits, showed the best implementation, so it is used in the proposed RFEH rectenna.

Fig 4.4 and 4.5 present the HA RFEH rectenna and LA RFEH.

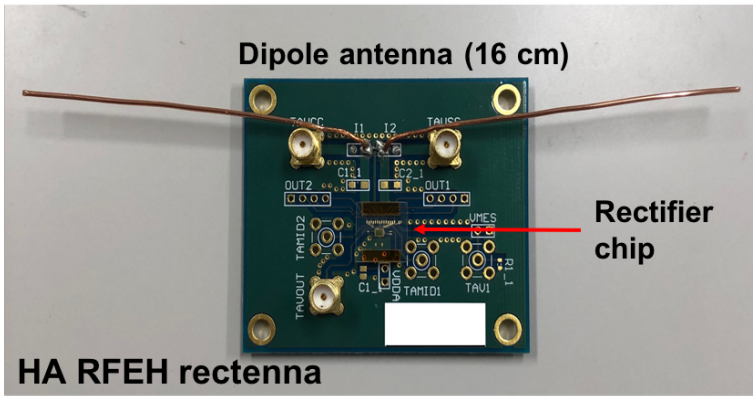

Figure 4.4: Figure of the proposed HA RFEH rectenna

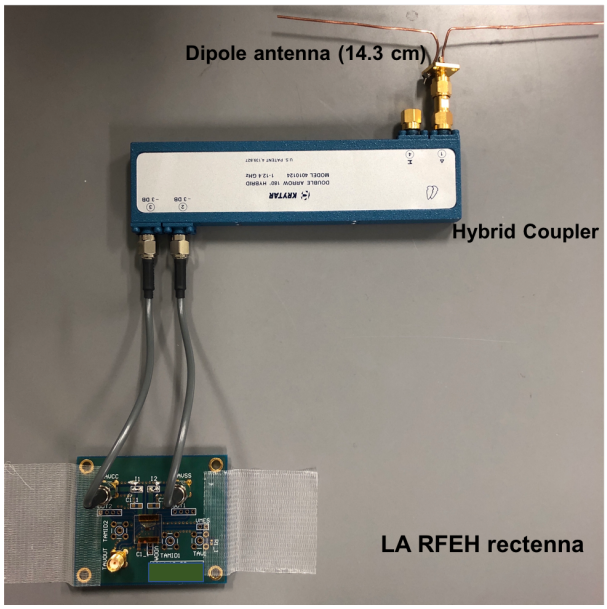

Figure 4.5: Figure of the proposed LA RFEH rectenna

In this RFEH rectennas, wired dipole antennas are used to easily change the length of the dipole, resulting in easily control the impedance of the antennas. In the HA RFEH rectenna, the antenna is directly connected with a matching circuit and rectifier circuit. In LA RFEH, the 50Ω antenna is connected with the rectifier in the PCB board, which designed and showed in chapter 3, using the hybrid coupler.

4.3 Matching circuits and antennas

4.3.1 Matching circuit and antenna for HA RFEH rectenna

The equivalent circuit of the HA RFEH rectenna is presented in Fig 4.6

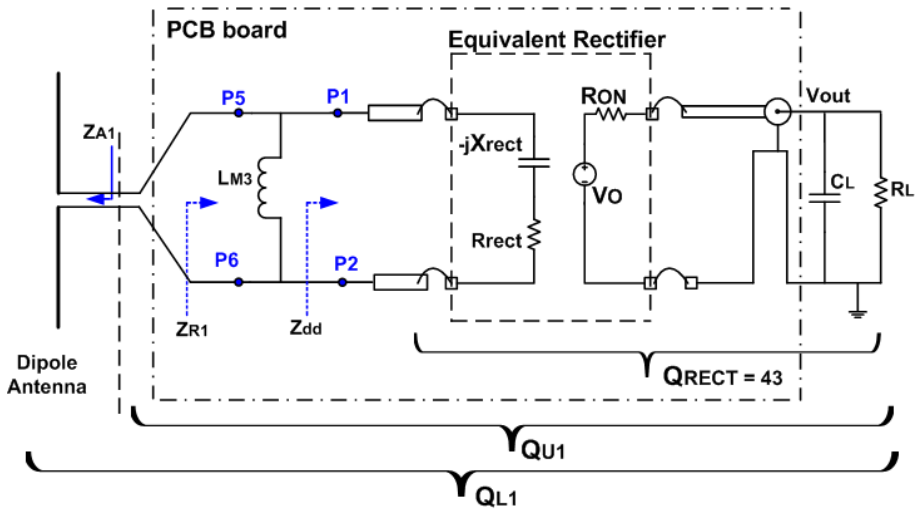

Figure 4.6: Equivalent circuit of the proposed HA RFEH rectenna

In the HARFEH, a 16 cm wired dipole antenna, which length is equivalent to 0.5 wavelengths at 950 MHz, is designed to get 75Ω impedance. In this structure, an ambient RF signal between two fingers of the dipole antenna directly supplied to two inputs of the rectifier. Besides, the rectifier structure is differential-drive structure, so the impedance of the rectifier, in this case, is differential-to-differential impedance, which called Z_{dd} in Fig 4.6. The measured impedance value is shown in Fig 4.7 (a)

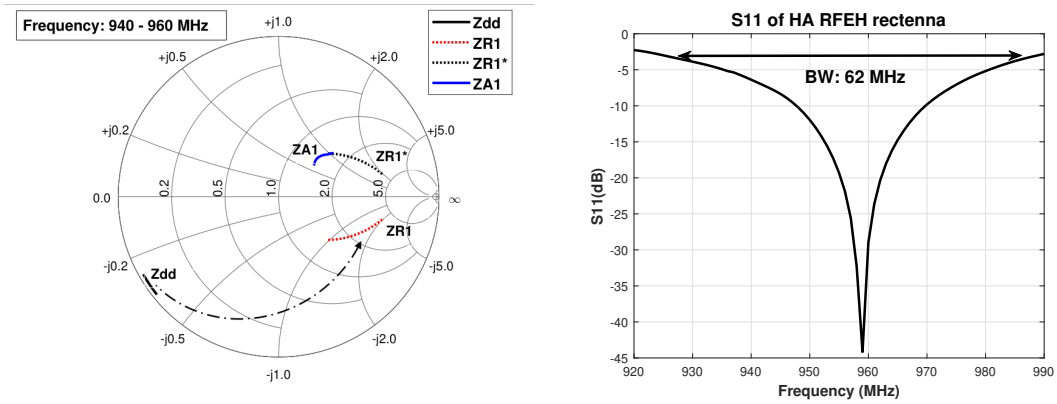

(a) (b)

Figure 4.7: Measured impedance and S11 of the HA RFEH rectenna: (**a**) Impedance, (**b**) S11.

From Fig 4.7, an inductor of 2.7 nH, which is denoted by L_{M3} in Fig 4.6, is

utilized as a matching component. The differential-to-differential impedance Z_{R1} of the system, between point P_5 and P_6, is presented in Fig 4.7 (a). The rectenna system is matched, and S11 of the HA RFEH rectenna is shown in Fig 4.7 (b).

From Fig 4.7 (b), the return loss at center frequency is $RL0 = 45 \quad dB$. Hence, from equation 2.2, a level of the return loss that used to calculate the BW is 3 dB. The figure indicates that BW of the HA RFEH rectenna at -3 dB loss is 62 MHz, which is from 926 MHz to 988 MHz. The center matched frequency is at 959 MHz. The loaded Q factor Q_{L1} and unloaded Q factor Q_{U1} calculated from equation 4.1 and 4.2 are 16 and 32, respectively.

4.3.2 Matching circuit and antenna for LA RFEH rectenna

The equivalent circuit of the LA RFEH rectenna is presented in Fig 4.8

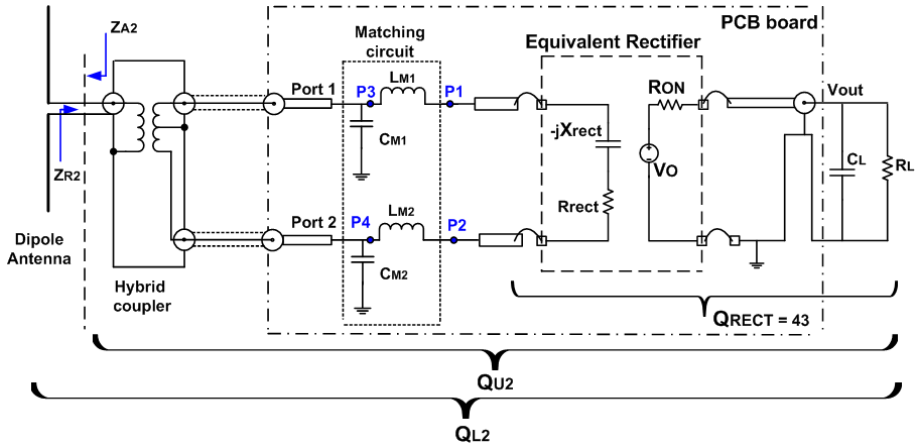

Figure 4.8: Equivalent circuit of the proposed LA RFEH rectenna

In the LARFEH, a 14.3 cm wired dipole antenna, which length is equivalent to 0.45 wavelength at 950 MHz, is designed to get 50Ω impedance. In this structure, the rectifier with matching circuits designed in chapter 3 for matching with 50Ω is utilized. The impedance of the LA RFEH system is measured and presented in Fig 4.9 (a)

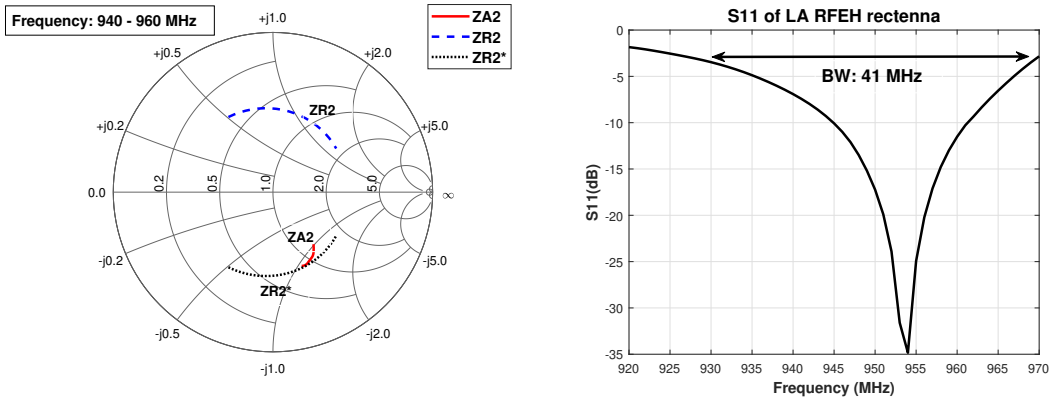

(**a**) (**b**)

Figure 4.9: Measured impedance and S11 of the LA RFEH rectenna: (**a**) Impedance, (**b**) S11.

The total impedance of a circuit part, which consisted of the rectifier, matching circuit, and hybrid coupler, is denoted by Z_{R2}. The antenna impedance is Z_{A2}. The LA RFEH is matched, and S11 of the rectenna is presented in Fig 4.9 (b).

From Fig 4.9 (b), the return loss at center frequency is $RL0 = 35 \quad dB$. Hence, from equation 2.2, a level of the return loss that used to calculate the BW is 3 dB.The figure indicates that BW of the LA RFEH rectenna at -3 dB loss is 41 MHz, which is from 928 MHz to 969 MHz. The center matched frequency is at 954 MHz. The loaded Q factor Q_{L2} and unloaded Q factor Q_{U2} calculated from equation 4.1 and 4.2 are 23 and 46, respectively.

4.4 Chapter Conclusion

In this chapter, the structure of ambient RFEH is proposed. The Q factors of the RFEH rectenna have to design from the limitation of BW of the RF signal to ensure no RF power loss. The Q factor of the rectifier should dominate the Q factor of the total system. In the two designed RFEH rectennas, the Q factors of the total system are 32 and 46, which are satisfactory with the limitation of the target Q value of 47. The bandwidth of the proposed systems are 62 MHz and 41 MHz which are cover the target bandwidth of LTE mobile

phone signal at (945 - 960) MHz band.

The two structures of rectenna, which have the same rectifier chip but different antenna impedance, were designed. The HA RFEH rectenna consists of a 75Ω antenna while LA RFEH utilizes a 50Ω antenna. The theory analysis indicates that a high impedance antenna RFEH system will gain high efficiency than the system got a small impedance antenna. The performances of this rectenna in the real ambient environment are evaluated in Chapter 5.

Chapter 5

Performance of the proposed RFEH rectennas in the ambient environment

In this chapter, the performance of the proposed RFEH rectennas are presented. First, the measurement in an anechoic chamber room was performed with the LA RFEH rectenna. After that, the two proposed systems were evaluated in a real environment in the campus of University of Electro-Communications, Tokyo, Japan. To increase the output of the RFEH, the system is designed with the use of Yagi antenna and measured with ambient RF signal.

5.1 Measurement in an Anechoic Chamber room

The proposed RFEH rectenna was first evaluated in the anechoic chamber room to check the performance of total rectenna system as shown in Fig 5.1. The LA RFEH was used for evaluation because in this system antenna type can easily change to test.

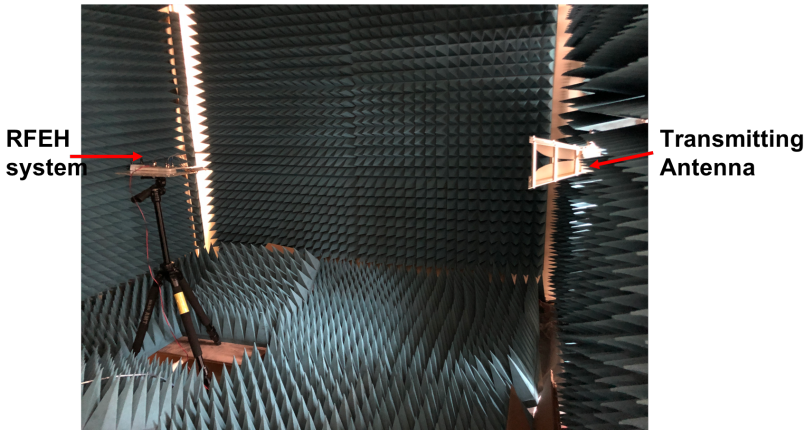

Figure 5.1: Measure the propose RFEH rectenna in an anechoic chamber

In the measurement, evaluation setup was shown as in Fig 5.2. Signal generator generated RF signal through a horn antenna. The input power of the rectenna was measure by a standard dipole antenna at 950 MHz which is CANDOX 44Sa21 as Fig 5.2 (a). Then the rectenna was put at this position for measurement.

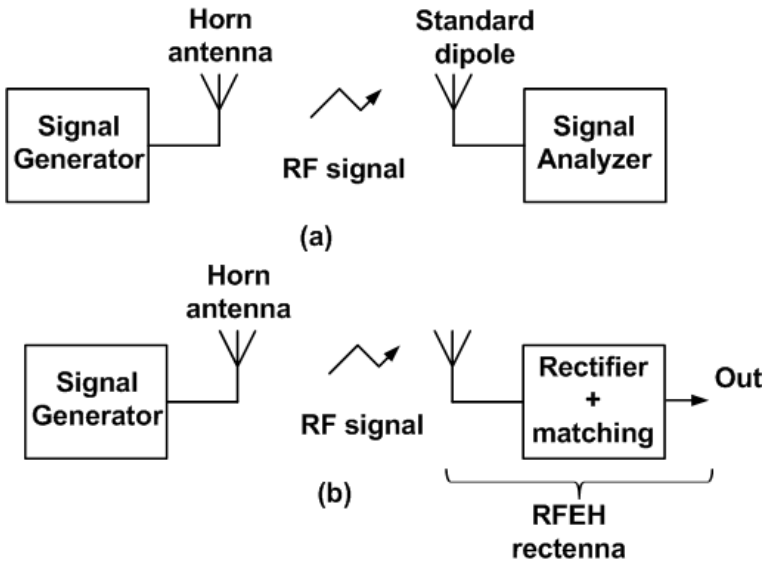

Figure 5.2: Measurement setup in the anechoic chamber

Fig 5.3 presents measurement results of the LA RFEH when system harvested a sine wave CW signal. With CW signal, the rectenna got sensitivity 1V at a level of -13 dBm input power and the highest PCE of 57 % is achieved at -10 dBm input power and 10 kΩ load.

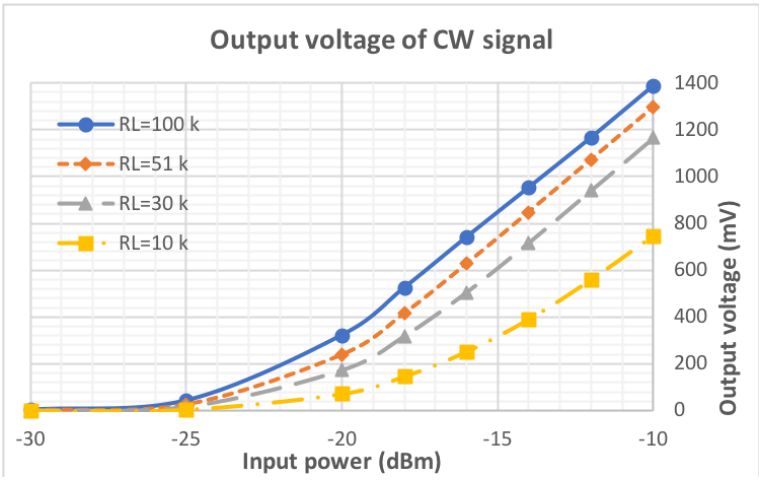

(a)

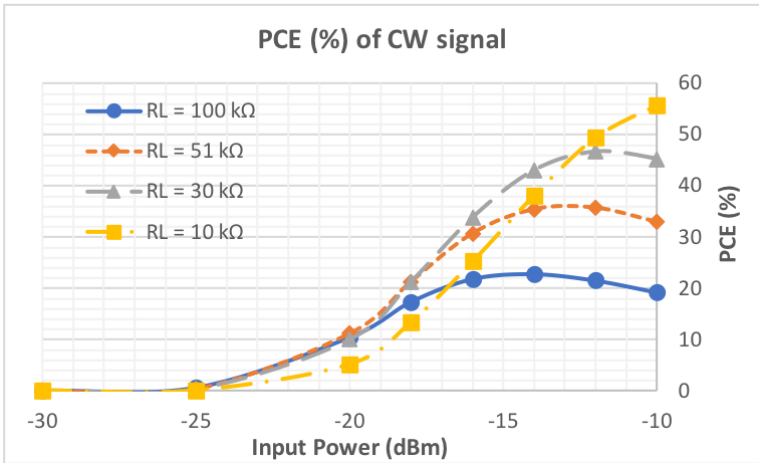

(b)

Figure 5.3: Measured output of the RFEH scheme 2 when excited by CW signal: (a) Output voltage, and (b) PCE

Fig 5.4 shows measured output voltages of the proposed rectenna at 10 MΩ with CW signal and modulated signal. Output voltages of the rectenna when harvested modulated signals are higher than that of the case harvested CW signal. The results prove that the propsed rectenna successfully achieved the target of design methodology. The system with the designed Q factor to ensure wide bandwidth system can increase outputs when harvest modulated signals

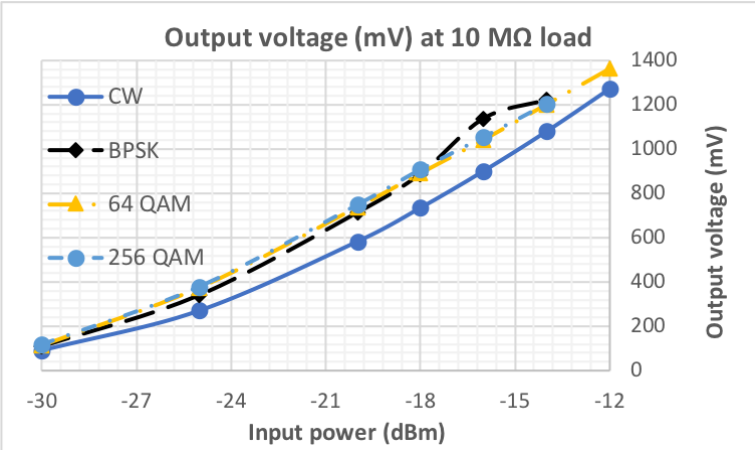

Figure 5.4: Measured output voltages of the proposed LA RFEH at 10 MΩ with CW signal and modulated signal

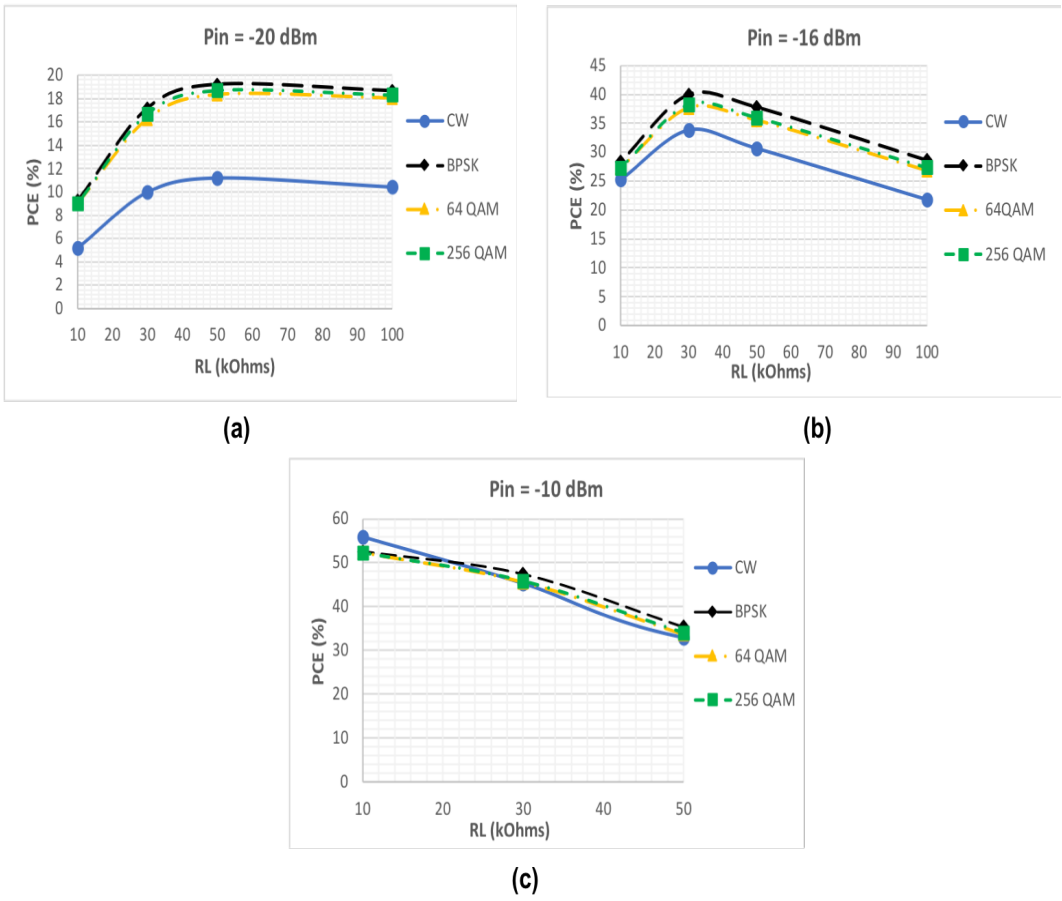

Figure 5.5: Measured PCE of the RFEH system in an anechoic chamber: (a) at -20 dBm input power, and (b) at -16 dBm input power, and (c) at -10 dBm

Fig 5.5 presents measured PCE of the system in different input powers and

loads. At -20 dBm input power level, PCE of the LA RFEH rectenna is 11 % with CW signal while that of the system with modulated signal is 19 % which is 1.7 times increase. At -16 dBm input level, the PCEs with CW signal and modulated signals are 34 % and 40 %, respectively. However, at -10 dBm input power level, PCE of the rectenna when excited by the CW signal became the highest at 57 %. The results indicated that at a level of -10 dBm, effect of modulation type to the efficiency of the rectenna is inefficient.

Fig 5.6 indicates the relationship between PCE of the LA RFEH rectenna and PAPR of the modulated signals. From the figure, it can conclude that the modulated signal bring gain for the wide BW rectenna in low input level range, which is smaller than -10 dBm. Notably, the ambient RF signal in the environment is in this range. At a level of -20 dBm input power, the PCE of LA RFEH rectenna is -19 % while at this range, the rectenna reaches 19 % when harvest real LTE signal in the environment. The results prove the efficient performance of the proposed LA REFH system in a real environment and essential agreement with the results achieved from measurement in the chamber room.

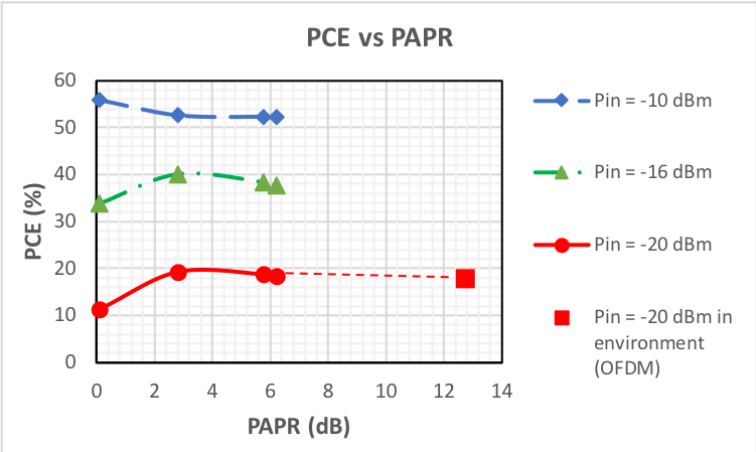

Figure 5.6: Measured dependence of PCE on PAPRs of RF signals

5.2 Indoor measurement with RF signal from ambient environment

5.2.1 RF signal in the ambient environment

Fig 5.7 presents the measurement setup in an office room at a laboratory in the University of Electro-Communications, Tokyo, Japan, which has the map is shown in Fig 2.2 in Chapter 2. The RFEH rectennas is put in the center of the office room to ensure evaluated condition is as normally daily life. The input power at measured point is measured by the reference standard dipole CANDOX 44Sa21 and a signal analyzer Agilent CXA N900A. Output voltages of the RFEH rectennas are measured by digital multimeters, and the data is stored on a computer. The time resolution of the measurement is set to a second.

(a) (b)

Figure 5.7: Evaluation setup in the office room

In the real environment, the level of RF signal is unstable and continuously changes depending on factors such as time, position, weather. In our measurement, the data is measured and stored over a long time evaluation to comprehensively express the performance of the proposed RFEH system when harvest real RF signal. The stored data then is analyzed and from the analyzed

result, the performance of the proposed system is studied. Therefore, all the measurement results, which consist of input and output data, were performed in real-time, and then distribution data is presented. In the recent context of ambient RFEH studies, the measurement conditions and results are unclearly presented, so the measurement setup of this study show a strong point of presentation.

Fig 5.8 presents measured input power of the 950 MHZ LTE mobile phone signal at measurement position. The result presents a measured data for 1 hour. The distribution data indicates that at the measurement point, the general level of the LTE signal is -19.4 dBm and the average of input power is -18 dBm.

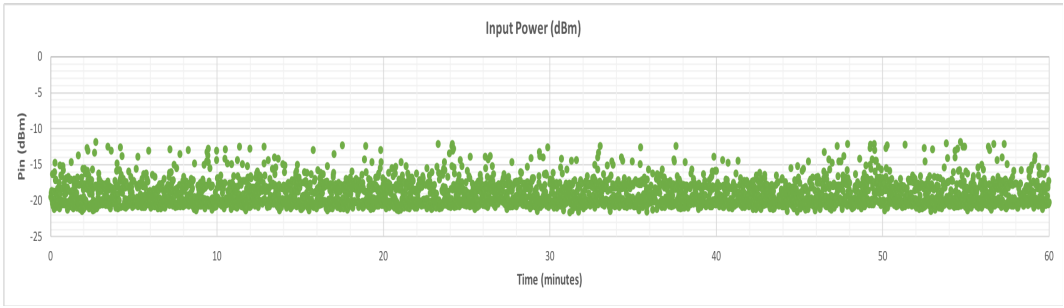

(a)

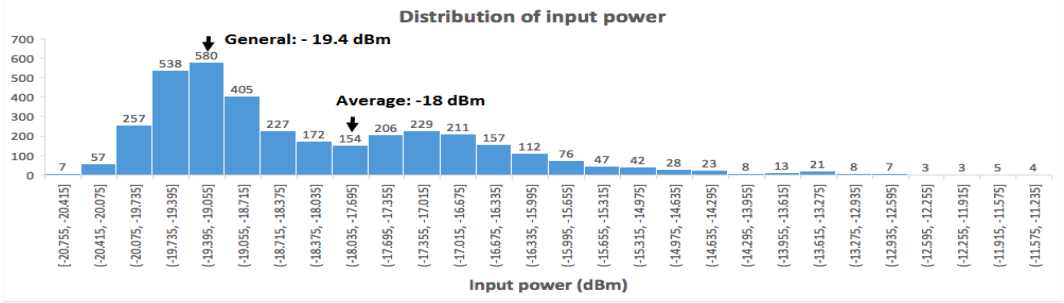

(b)

Figure 5.8: Measured input power of the 950 MHz LTE mobile phone signal at measurement position: (a) Input power, and (b) Distribution of input power

5.2.2 Performance of the HA RFEH rectenna

The performance of HA RFEH rectenna is firstly tested by measuring a voltage charge at 100 μF capacitor and open load. The measurement result is

presented in Fig 5.9. As shown in the figure, the voltage at the capacitor is charged to 1V after 15 seconds.

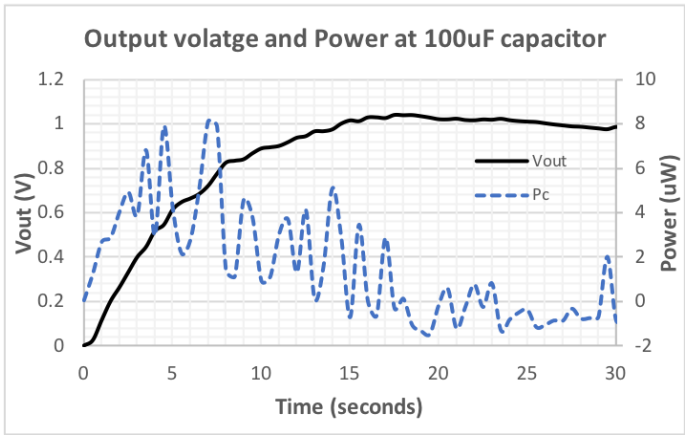

Figure 5.9: Measured output voltage of the RFEH scheme 1 at 100 μF capacitor

P_C in the figure stands for a power charged at the capacitor, which is calculated by equation 5.1

$$P_C = \frac{C\left(V_{out2}^2 - V_{out1}^2\right)}{2\left(t_2 - t_1\right)} = \frac{C\left(V_{out2}^2 - V_{out1}^2\right)}{2\Delta t} \tag{5.1}$$

In the next measurement, the output voltage of the HA RFEH system is evaluated as an hour with a load of 10 $M\Omega$. The result is presented in Fig 5.10. As shown in the figure, output voltages are in a range of 0.8 - 1.15 V

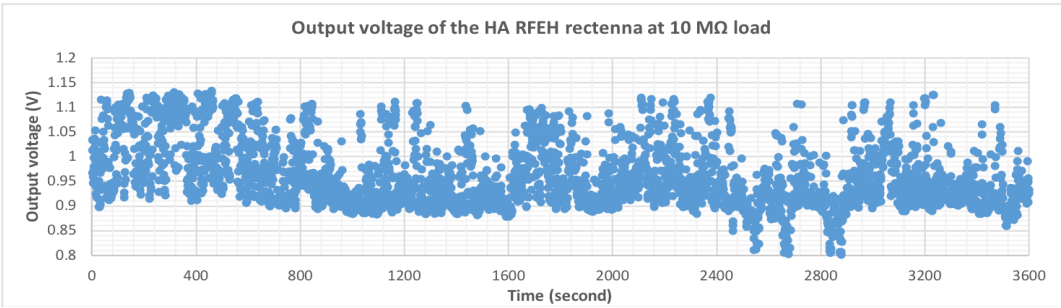

Figure 5.10: Measured output voltage of the HA RFEH rectenna at 10 MΩ as measured for 1 hour

Fig 5.11 presents output power and its distribution of the HARFEH as measured for 1 hour with a load of 100 $k\Omega$. The figure indicates that the

general DC power that the HA RFEH rectenna can generate when harvest ambient LTE signal is 2.7 μW. The average DC power that the rectenna generate through one-hour measurement is 3.63 μW.

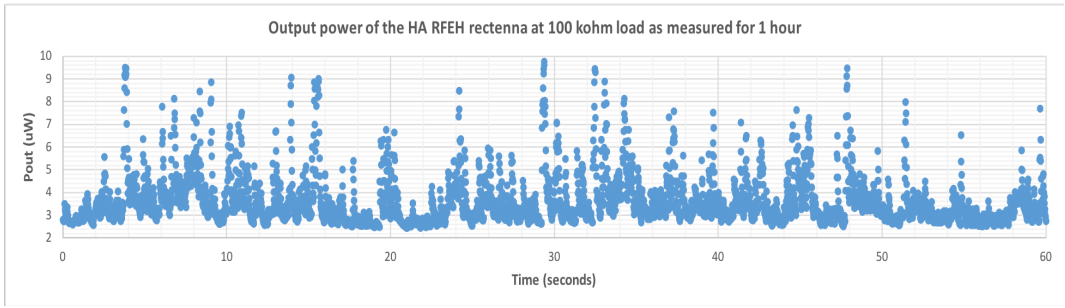

(a)

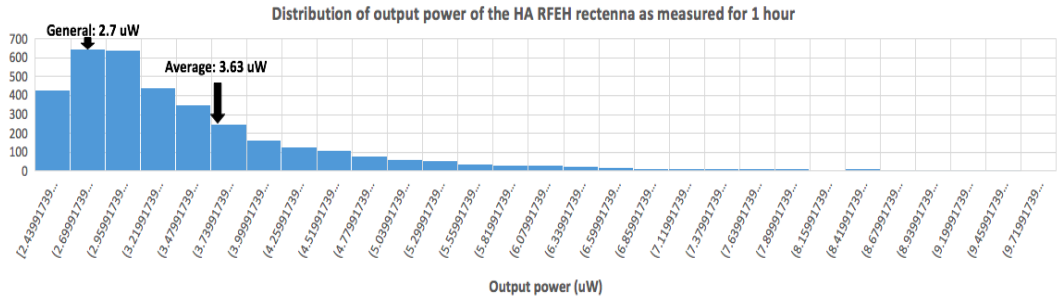

(b)

Figure 5.11: Measured output power of the HA RFEH rectenna at 100 kΩ as measured for 1 hour: (a) Output power, and (b) Distribution of output power

The HA RFEH rectenna then is evaluated in a day to test the stability performance. Fig 5.12 present output power of the HA RFEH rectenna as measured for 24 hours at a load of 100 $k\Omega$. As shown in the Fig 5.12 (a), the instantaneous value of the output power is unstable but it is in a range of (2.4 - 10) μW. Through a day, the rectenna work stably. The general DC power that HA RFEH can generate through a day is 2.44 μW, while the average generated DC output power of the system is 3.48 μW. A total DC power that the HA RFEH rectenna can generate from LTE mobile phone signal is 0.3J.

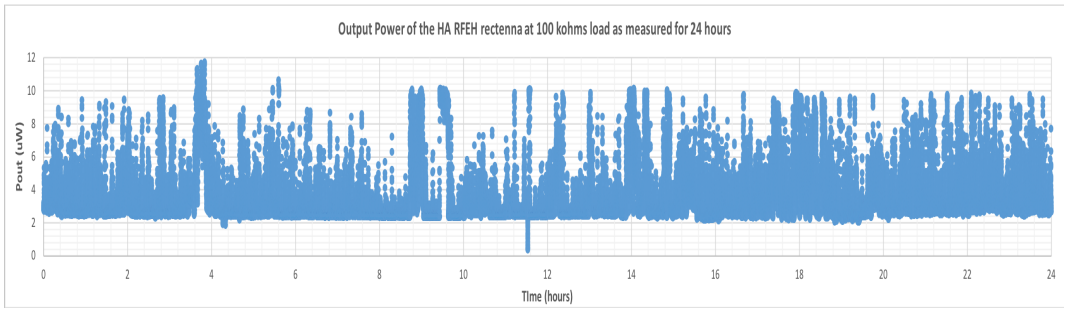

(a)

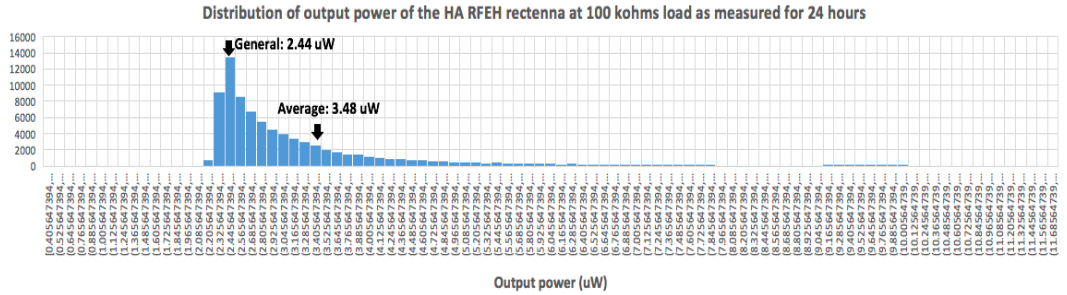

(b)

Figure 5.12: Measured output power of the HA RFEH rectenna at 100 kΩ as measured for 24 hours: (a) Output power, and (b) Distribution of output power

5.2.3 Performance of the LA RFEH rectenna

The output voltage of the LA RFEH system is evaluated as an hour with a load of 10 $M\Omega$. The result is presented in Fig 5.13. As shown in the figure, output voltages are in a range of 0.9 - 1.15 V

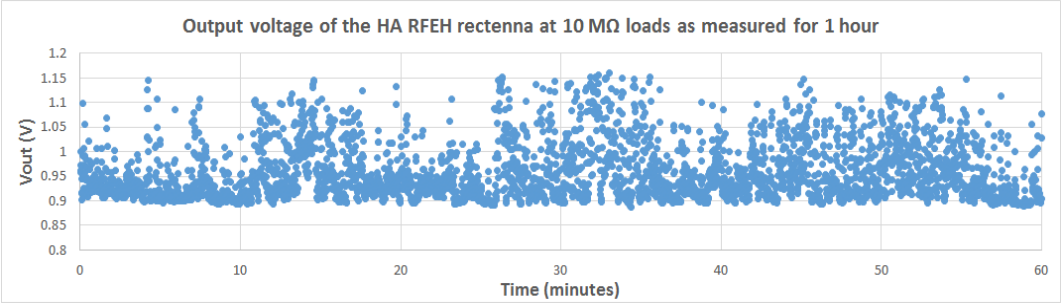

Figure 5.13: Measured output voltage of the LA RFEH rectenna at 10 MΩ as measured for 1 hour

The performance of the LA RFEH rectenna was measures in a day. Fig 5.14 present output power of the LA RFEH rectenna as measured for 24 hours at a load of 100 $k\Omega$. As shown in the Fig 5.14 (a), the instantaneous value of the output power is in a range of (2 - 8.5) μW. Through a day, the rectenna work stably. The general DC power that the system can generate through a day is 1,97 μW, while the average generated DC output power of the system is 2.77 μW. A total DC power that the HA RFEH rectenna can generate from LTE mobile phone signal is 0.238J.

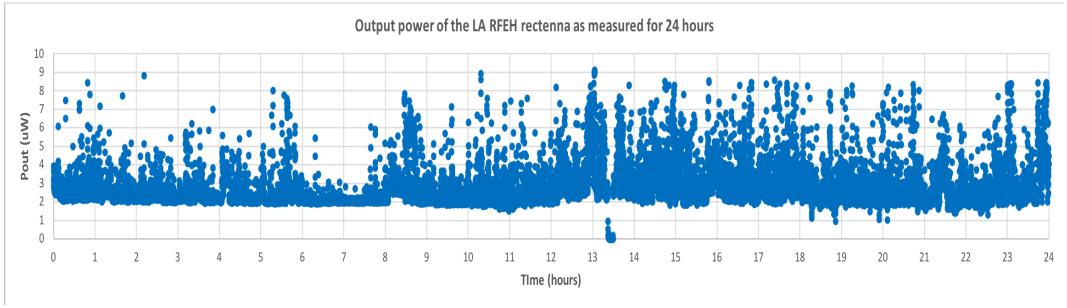

(a)

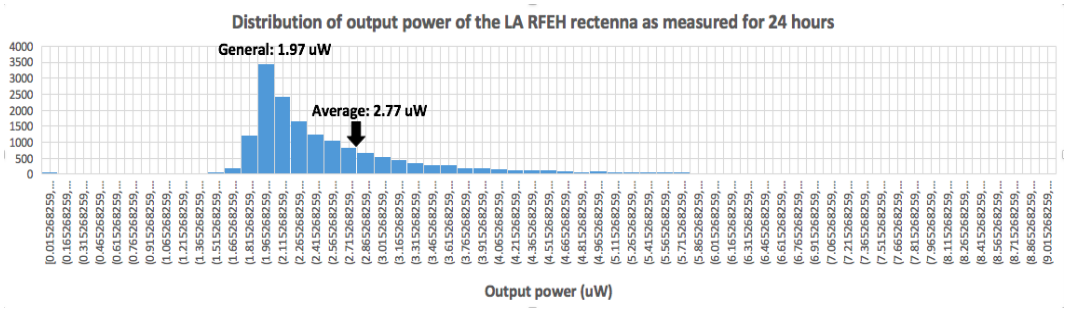

(b)

Figure 5.14: Measured output power of the LA RFEH rectenna at 100 kΩ as measured for 24 hours: (a) Output power, and (b) Distribution of output power

5.2.4 Performance of the RFEH rectenna with CCR circuit

The measurement results of 3-stage DTMOS CCR and BTMOS CCR presented in Chapter 3 with SG showed that the rectifier circuit with the ap-

plication of DTMOS on 65 nm SOTB can achieve higher performance than normal BTMOS type. In this section, the performance of DTMOS and BTMOS CCR is also tested with the real signal in the environment as shown in the Fig 5.15. The RFEH system is designed as the structure of the LA RFEH structure where the PCB board of the CCR chip is connected to 50Ω dipole by the hybrid coupler.

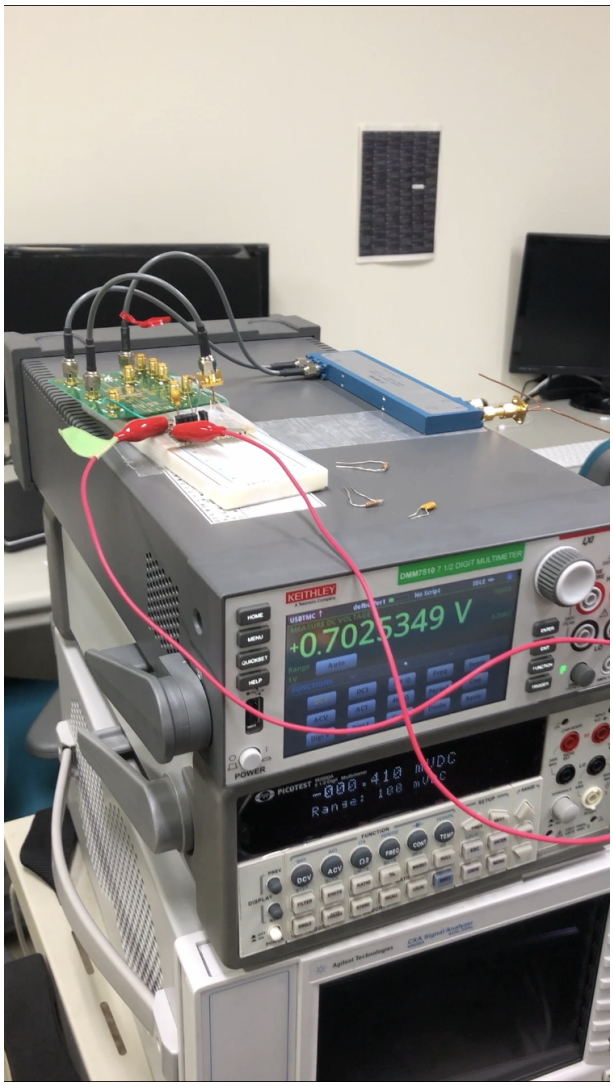

Figure 5.15: Measured the RFEH rectenna with CCR circuit

The performance of the systems are firstly tested by measuring a voltage charge at 10 μF capacitor and open load. The measurement result is presented in Fig 5.16. As shown in the figure, after 150 seconds, the output voltage of the system with DTMOS is charged to 0.55 V, while that of the system with

BTMOS is 0.35 V.

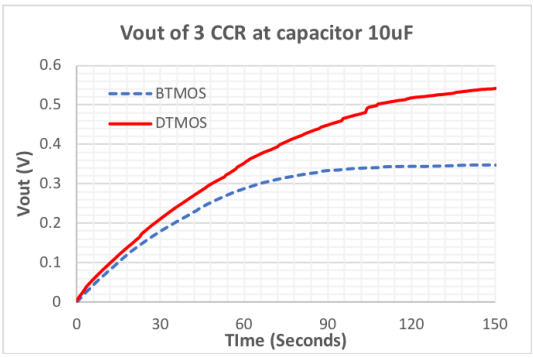

Figure 5.16: Measured output voltage of the RFEH with 3-stage DTMOS and BTMOS CCR chip at 10 μF capacitor

Fig 5.17 presents measure output power of the systems with DTMOS and BTMOS at a load of 10 $M\Omega$. As shown in the figure, output voltage and power of the system with DTMOS is higher than that of the system with BTMOS.

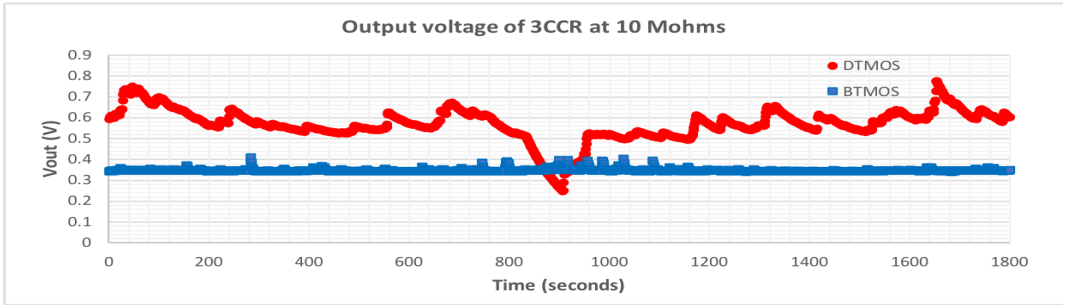

(a)

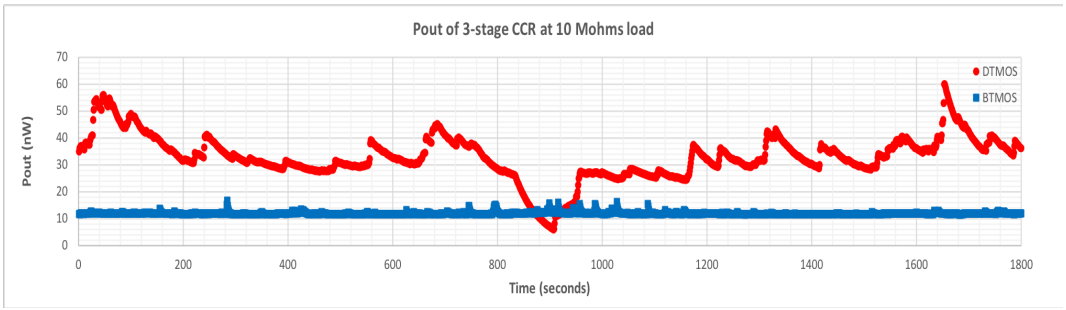

(b)

Figure 5.17: Measured outputs of the RFEH with 3-stage DTMOS and BTMOS CCR chip at 10 MΩ loads: (a) Output voltage, and (b) Output power

In conclusion, the application of DTMOS on 65 nm SOTB technology

brings higher drain current than normal BTMOS. The DTMOS rectifier shows better performance with signal from SG and real signal in the ambient environment. Therefore, DTMOS structure is a good candidate to apply in the rectifier in a low input power range for harvest ambient RF signal.

5.3 Outdoor measurement with the designed dipole rectenna

The proposed HA RFEH is measured at various buildings of the UEC to test the performance at different conditions. In our measurement, we chose three buildings in the West Campus, which map is shown in the Fig 5.18. The chosen measurement positions are at outdoor of the fifth floor of West 2, the fourth floor of West 8, and the fourth floor of West 10.

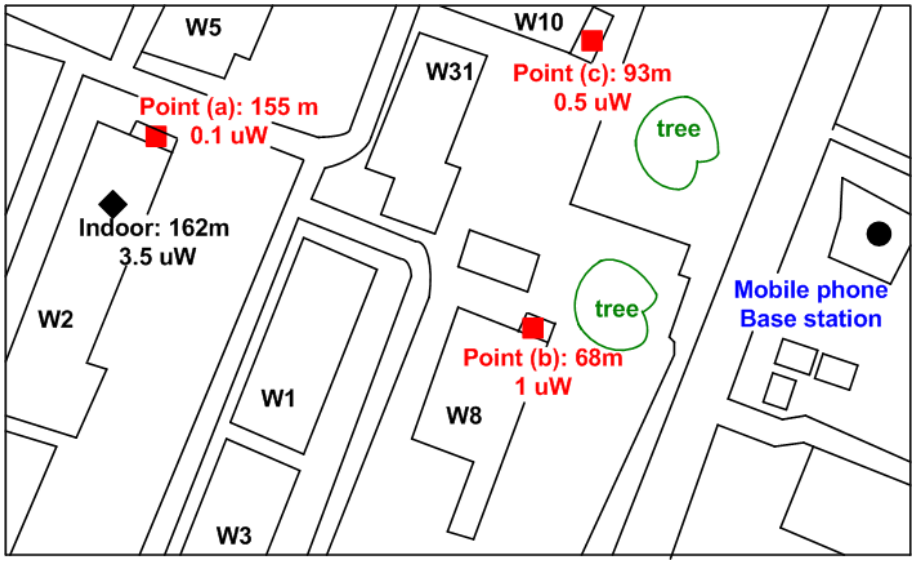

Figure 5.18: The map of the measurement at various places in the UEC

In theory, the distance dependence of received power on transmitted power of base station are shown in equation 5.2

$$P_R = P_T D_T D_R \left(\frac{\lambda}{4\pi d}\right)^2 \tag{5.2}$$

where P_T, P_R are the transmitted power and available power at received antenna, respectively. D_T, D_R are the directivity of transmitted and received

antennas, respectively. λ is the wavelength of the mobile phone signal. d is the distance between received position and base station.

The figure of the measurement at West campus of the UEC is shown in Fig 5.19

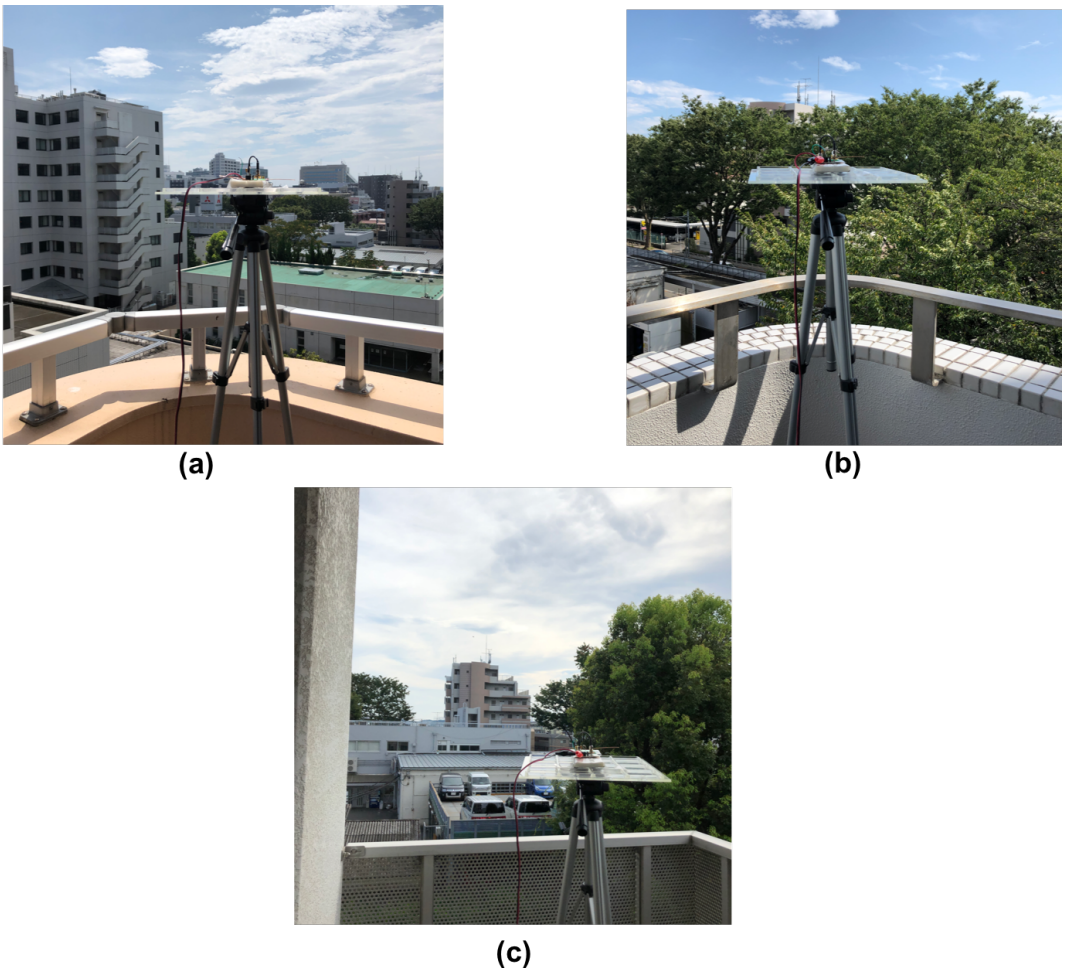

Figure 5.19: Figure of the measurement at various places in the UEC: (a) At West 2, (b) at West 8, and (c) at West 10

In real condition, the available power of the RF signal is depended on the transmit condition such as: weather, time, multi-path fading,etc. The available power P_R at received position is usually smaller than the value calculated from equation 5.2. For example, in figure 5.18, 5.19, measurement points (b) and (c) are close to the base station but there are trees in the transmit direction so the available powers at these positions are reduced.

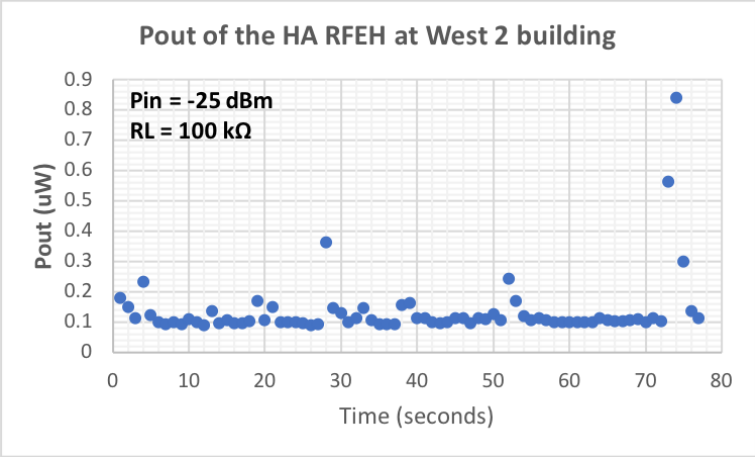

(a)

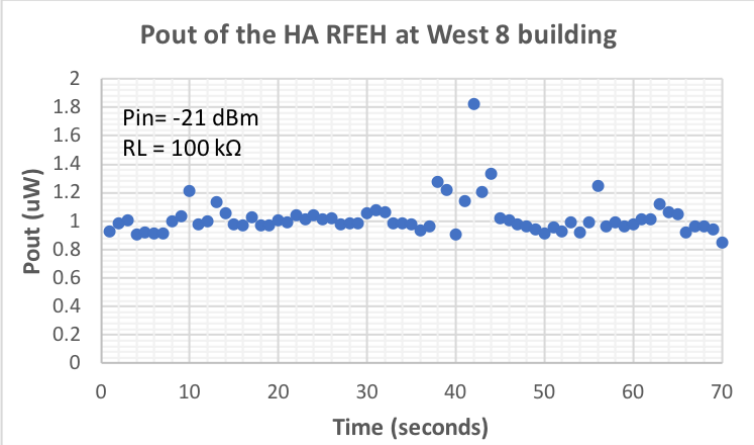

(b)

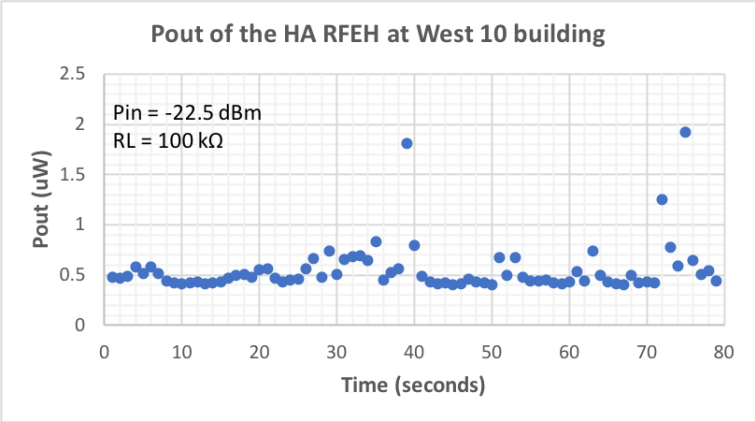

(c)

Figure 5.20: Measured output power of the HA RFEH: (a) At West 2, (b) at West 8, and (c) at West 10

The measurement results are presented in Fig 5.20. At the measured posi-

tion of West 2, the output power of the rectenna is general 0.1 μW at an input power of -25 dBm. The output power of the proposed rectenna is 1 μW at an input power of -21 dBm at the measurement place of West 8. At West 10, the rectenna generated 0.5 μW output power at an output power of -22.5 dBm.

Fig 5.21 summarizes the results of measurement in various positions in the UEC of the proposed rectenna. The figure indicates that the proposed RFEH rectenna can harvest the LTE mobile phone signal at different conditions. The results prove the efficient performance of the proposed RFEH system

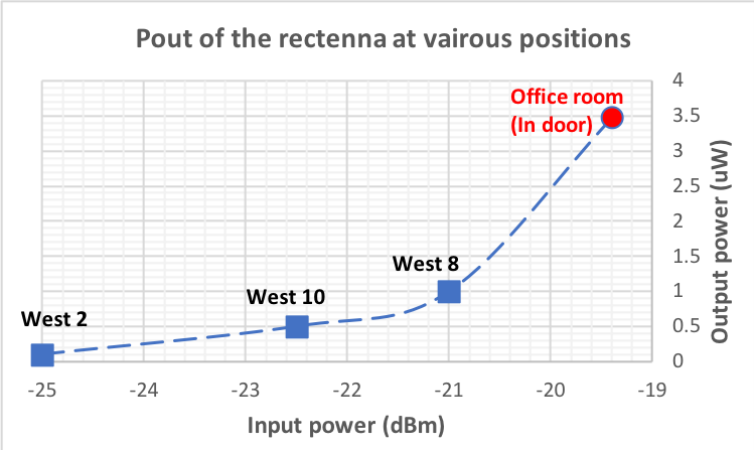

Figure 5.21: Measured output power of the HA RFEH rectenna at various positions

5.4 Measurement with the designed Yagi rectenna

The rectenna was designed with the use of a simple dipole antenna which gain is nearly 2 dBi. To improve input power of the RF signal, a high gain antenna which is the Yagi antenna is designed to utilized in the ambient RFEH rectenna. The rectenna, which is designed by our RF desig group in the laboratory, is shown in the Fig 5.22

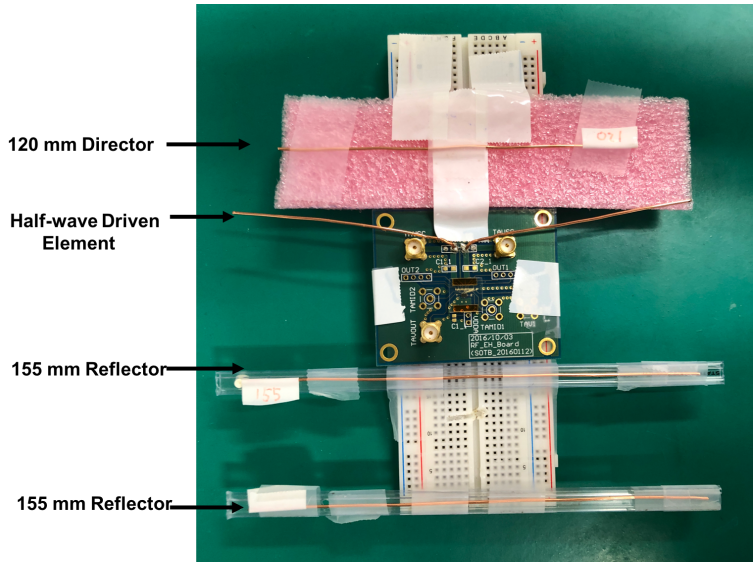

Figure 5.22: The high gain rectenna with Yagi antenna

In the system, the 75Ω half-wavelength dipole of the HA RFEH system is utilized as a driven antenna. A 120 mm wire which length is equivalent to 0.4 wavelength of 950 MHz is used as a director element. Two wires of 150 mm which is equivalent to 0.48 wave length works as reflector elements of the Yagi antenna. The specifications of the designed Yagi antenna and dipole antenna are presented in table 5.1:

Table 5.1: Specifications of the designed Yagi antenna and dipole antenna.

	Designed dipole antenna	**Designed Yagi antenna**
Gain	2 dBi	7 dBi
Size (total RFEH system)	15.5 cm x 5 cm	15.5 cm x 11.5 cm
Effective area with 950 MHz signal	0.016 m^2	0.04 m^2

The high gain rectenna is firstly tested with the experiment to light up the LED as shown in the Fig 5.23. The rectenna is put in the room center, the output of the rectenna is fed to light up the LED. As shown in the figure, the LED is lighted.

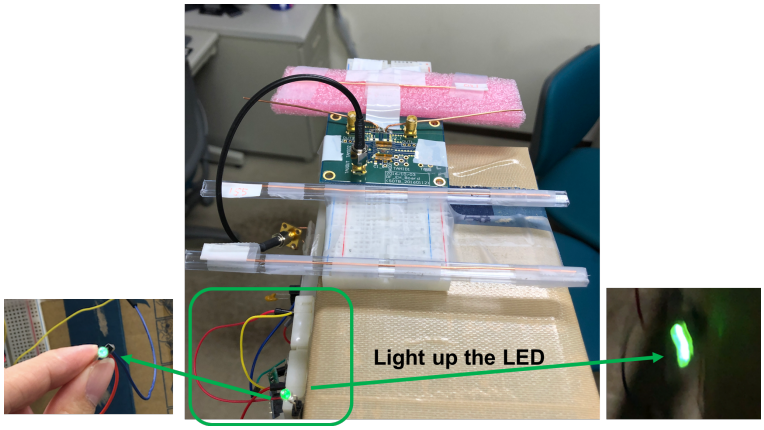

Figure 5.23: Experiment to light up the LED

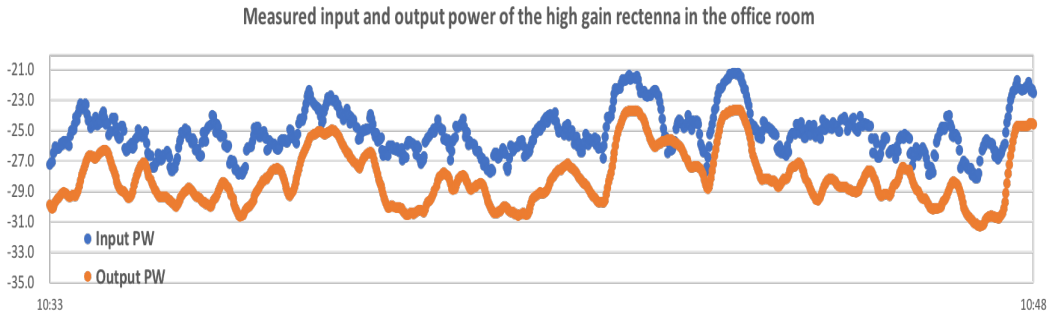

(a)

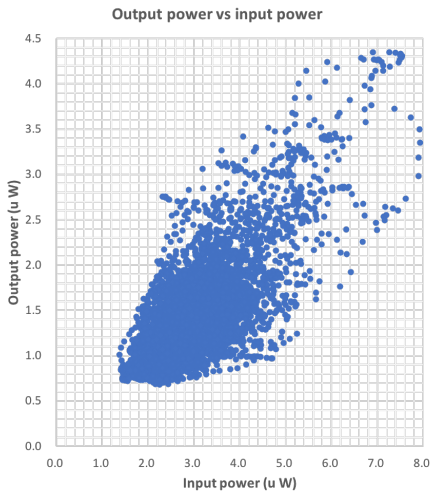

(b)

Figure 5.24: Measure the high gain rectenna at office room: (a) Input power and output power measured as 15 minutes, (b) output power versus input power

The output power of the high gain rectenna is measured at 100 $k\Omega$ load. Fig 5.24 presents the measurement results. Input power was in a range of (-21, -28) dBm, output power is in a range of (-24,-31) dBm.

Fig 5.25 presents the results at an outdoor measurement condition of the high gain rectenna. The measurement position is at outdoor stairs between fifth floor and sixth floor of W8 building, As shown in the figure, average input power is -18.6 dBm, average output voltage is 0.874V at 100 $k\Omega$ load which equivalent to 7.6 μW. The results indicate that with the high gain antenna output power of the designed rectenna increases.

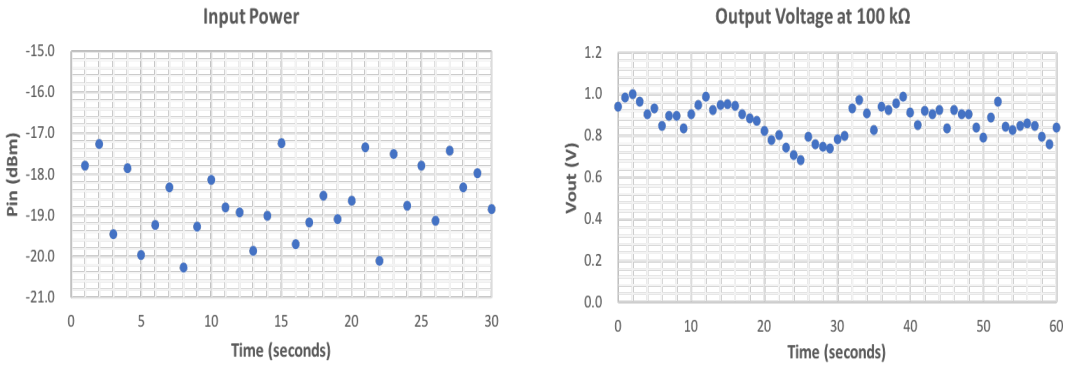

(a) (b)

Figure 5.25: Evaluate the high gain rectenna at fifth floor of W8 building in the UEC campus: (a) Measured input power, and (b) Measured output voltage at 100 $k\Omega$ load

Table 5.2 presents the measurement results of the high gain rectenna at different position at outdoor stairs of W8 building of the UEC campus. From the table, when input power is more than -23 dBm, output power of the high gain antenna reaches more than 1.4 μW. With the Yagi antenna, at an -18.6 dBm input power level, the output power of the rectenna reachhed 7.6 μW at 100 $k\Omega$ load, which equivalent current is 8.77 μA.

Table 5.2: Measurement results of the high gain rectenna at different positions out side of W8 building.

Location: stairs of W8	**Input power** (dBm)	**Output power** (μW)
Floor: 8-7	-23.2	0.71
Floor: 7-6	-21.5	3.35
Floor: 6-5	-18.6	7.6
Floor: 5-4	-19	4.19
Floor: 4-3	-21.1	3.65
Floor: 3-2	-23	1.44
Floor: 2-1	-31.7	0.01

5.5 Chapter Conclusion

5.5.1 Comparison between two proposed RFEH rectenna structures

The HA RFEH rectenna and LA RFEH rectenna have some specification as below:

- Using the rectifier chip with DTMOS CCR with floating-subcircuits on 65 nm SOTB technology;
- The HA RFEH rectenna using 75Ω antenna while the LA RFEH antenna using 50Ω antenna;
- The general DC power and average DC power that HA RFEH rectenna generated a day are 2.44 μW and 3.48 μW. The total DC power generated a day is 0.3J;
- The general DC power and average DC power that LA RFEH rectenna generated a day are 1.97 μW and 2.77 μW. The total DC power generated a day is 0.238J.

From these points, we can conclude that the HA RFEH system with higher antenna impedance show better performance than LA RFEH rectenna.

5.5.2 Comparison results between the study and other ambient RFEH studies

The output DC power of the proposed rectenna is 1 μW when the system harvest CW signal. However, with the real LTE signal in the ambient environment, a 3.48 μW DC power can generated by the proposed HA RFEH rectenna and a 2.77 μW DC power generated by the proposed LA RFEH rectenna. The output powers increase 3.5 times and 2.8 times in the real performance in environment. The results prove the efficient operation of the proposed RFEH systems when performs in the environment. Therefore, the proposed structure of the ambient RFEH system in this study is essential effectiveness.

Table 5.3 presents comparison results between specifications of the proposed RFEH rectenna in this study and the other ambient RFEH studies. Fig 5.26 presents the recent state-of-the-art in the ambient RFEH studies. From the table 5.3 and Fig 5.26, it can conclude that in the present studies, the proposed RFEH rectenna can harvest the highest output power at the same input power level range when compare to the other studies. At -20 dBm input power level, the RFEH system in [35] got 0.22 μW DC output power when harvest mobile phone signal at 845 MHz. In this studies, the proposed RFEH rectenna generated 3.48 μW, which is 15 times higher than that of [35].

Table 5.3: Comparison table.

	This work	**Kitazawa 2012 [35]**	**Kitazawa 2013 [57]**	**Stoopman 2014 [58]**	**Furuta 2016 [77]**	**Sadagopan 2018 [80]**
Technology	65 nm SOTB CMOS	Diode (unspecified)	Diode HSMS285C	90 nm CMOS	Diode HSMS285C	GP 65 nm CMOS
Rectifier stages	3-stage DTMOS CCR with floating sub-circuit	2 RF-DC stages	2-stage charge pump	5-stage CCR	1-stage and 2-stage Cockcroft-Walton	6-stage CCR
Frequency	LTE 950MHz band	845 MHz	V-High (205-225) MHz, DTV (465-545) MHz, BTS (850-900) MHz	GSM-900 (886-907) MHz	DTV 500 MHz band	Wifi 2.4GHz band
Sensitivity@ Input power, Load	0.9V@ -20dBm, 10MΩ	0.79V @ -5 dBm	na	1V @-27 dBm, $R_L = \infty$	$0.8V^*$@-15dBm, 39 kΩ	1V @ -36 dBm, $R_L = \infty$ Primary mode
Max PCE with CW	57% @ -10 dBm	19.7 % @ -5 dBm	9.1% @ -20 dBm	40% @ -17 dBm	48.9%@-15 dBm	na
P_{out} @ P_{in} in ambient environment	**3.48μW @-19.4 dBm, 7.6μW @-18.6 dBm**	0.22 μW^* @ -20 dBm	$1.9\mu W^*$ @ $-15dBm^*$	$0.16\mu W^*$ @ -4.6 dBm	$22.53\mu W^*$@-13 dBm	$3.3nW^*$ @ $-18.6dBm^*$

*: Calculated from graph

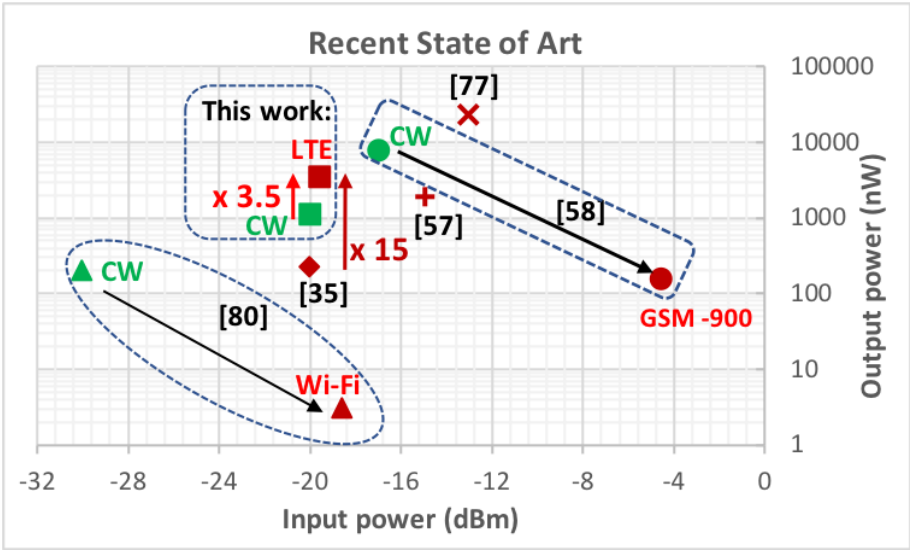

Figure 5.26: Recent state-of-the-art in the ambient RF energy harvesting

Fig 5.26 also presents a comparison between the results of this study and the study in [80]. The wireless energy harvester in [80] is a high Q co-design rectenna which Q factor of the system is 120. The rectenna generated 0.2 μW output power at -30 dBm input a CW signal, but that at -18.6 dBm input power of a real Wi-Fi signal is 3.3 nW. Whereas, to ensure a wide BW, in the proposed rectenna of this study, the Q factor is limited. Therefore, the output power of the proposed system when harvested the CW signal is 1 μW at -20 dBm input power. However, with the real LTE signal at the same level, the DC output power of the proposed rectenna is boosted to 3.48 μW, which is 3.5 time higher than that of the case harvest the CW signal. The results prove that to harvest ambient RF signal in the environment, the RFEH system must have moderate Q factor to ensure wide bandwidth system.

To increase the output power, the dipole antenna of the designed RFEH rectenna is changed to a Yagi antenna. With the Yagi antenna, the designed system produced 7.6 μW DC power. When measured at seven points, the system can generate output power at μW levels at six points.

The proposed RFEH system is evaluated at various positions in the UEC. The rectenna proved the ability to harvest the LTE mobile phone signal and supply for IoT sensor TAG with/without WuR.

Chapter 6

Conclusion and Future works

6.1 Conclusion

In this dissertation, the requirements of IoT applications are presented; hence, the ambient RFEH technique shows a prominent candidate to utilized in IoT applications. The fundamental characteristics of the RF signal in the environment affecting the efficiency of the RFEH system are presented. The required specifications of the proposed RFEH system to supply for RF sensor TAG and RF sensor TAG with WuR are proposed in Chapter 2.

In Chapter 3, principle parameters, which are drain current and Q factor, that influence the output of the rectifier, are analyzed. The 3-stage DTMOS CCR and BTMOS CCR were designed and evaluated. The measurement results proved that applying DTMOS on 65nm SOTB on the rectifier gained higher PCE than the BTMOS structure. In addition, with the wide BW designed system, the PCE of the rectifier when harvesting the modulated signals is boosted than that of the case harvest CW signal. The 3-stage DTMOS CCR with floating sub-circuit is evaluated and got the highest PCE.

Chapter 4 proposes the structures of the ambient RFEH rectenna. In the proposed structure, the Q factor of the rectifier, which dominated the Q factor of the total system, must be limited by the BW of the target RF signal in the ambient. Based on the designed methodology, the HA RFEH rectenna and LA RFEH rectenna are designed.

Chapter 5 presents the measurement results of the prosed structures in the anechoic chamber room and the ambient environment. The measurement results indicate that the PCE of the rectennas, when harvested the LTE signal in the real environment, is boosted 3.5 times in comparison to that of the case harvest CW signal. The HA RFEH rectenna achieved higher performance than LA RFEH. The output power of the proposed system reached 3.48 μW at -19.4 dBm input power of the LTE signal. The designed system with Yagi antenna generated 7.6 μW DC output power at -18.6 dBm LTE input power. The output power of this study is the highest output in comparison to other studies about ambient RFEH.

According to the architecture proposals, numerical analyses, measurement results presented in this dissertation, the following remarkable conclusions are obtained:

- By analyzing the fundamental characteristics that affect the efficiency of the RFEH system, the dissertation proposes that a wide bandwidth RFEH system with a moderate Q factor is a useful structure to harvest a real RF signal in the ambient environment.

- Measurement in the real ambient environment in the dissertation is evaluated and examined in detail and comprehensiveness in comparison with other studies. All the measurement data is evaluated, stored, and analyzed. The two proposed rectennas are evaluated through 24 hours to test the stability property of the system. The HA RFEH rectenna and Yagi-antenna rectenna are evaluated at various places in the West campus of the UEC. The rectenna proved the ability to harvest the LTE mobile phone signal in the real ambient environment.

- The output power of the proposed rectenna is 3.48 μW, which is 15 times higher than that of the other study when harvested the LTE signal at a -19.4 dBm input power. The proposed RFEH rectenna exhibits the best performance when compared to that of other realistic RFEH systems and is a potential candidate for battery-less IoT applications.

- The implement of the proposed rectenna is improved by using Yagi antenna. The designed system can generate 7.6 μW DC power at -18.6 dBm.

6.2 Applications and Future works

6.2.1 Applications of the proposed study on IoT sensors

The proposed ambient RFEH rectenna can harvest 3.5 μW power at 100 $k\Omega$ load, which equivalent to a current of 5.92 μA in the load. The total power that the rectenna system can generate a day is 0.3J. With the Yagi antenna, the designed rectenna can generate a power of 7.6 μW at 100 $k\Omega$ load which equivalent current is 8.7 μA. This DC power can store in a stored power unit to use for supplying power to a sensor node of the IoT applications.

As shown in the table 2.2, the power requirements of the RF sensor TAG and RF sensor TAG with WuR are in rage of $(1 \sim 10)$ μW. The outputs of the proposed system satisfy the requirement at both conditions indoor and outdoor measurements. The proposed system reaches the target of study.

6.2.2 Future works

Although the output power of the proposed rectenna is the highest in comparison to other studies about ambient RFEH, the proposed rectenna also exists some drawbacks that need to improve in the future, such as:

- The designed rectenna works efficiently at positions around mobile phone station. When the level of RF signal is lower than -23 dBm, the output of the proposed RFEH system is reduced. In this case, there is a need of dedicated source to transmit powered RF signal to the harvesting rectenna system.

- Size of the rectenna, which consists of the dipole antenna, is quite large.

From the above features, several studies can be extended in this work as follow:

- Design a high impedance antenna for the rectenna to achieve higher PCE.
- Design a smaller antenna size to reduce the size of the system.
- Design multi-band rectenna to harvest multi-signal in the ambient environment.

Appendix A

Full chip photos

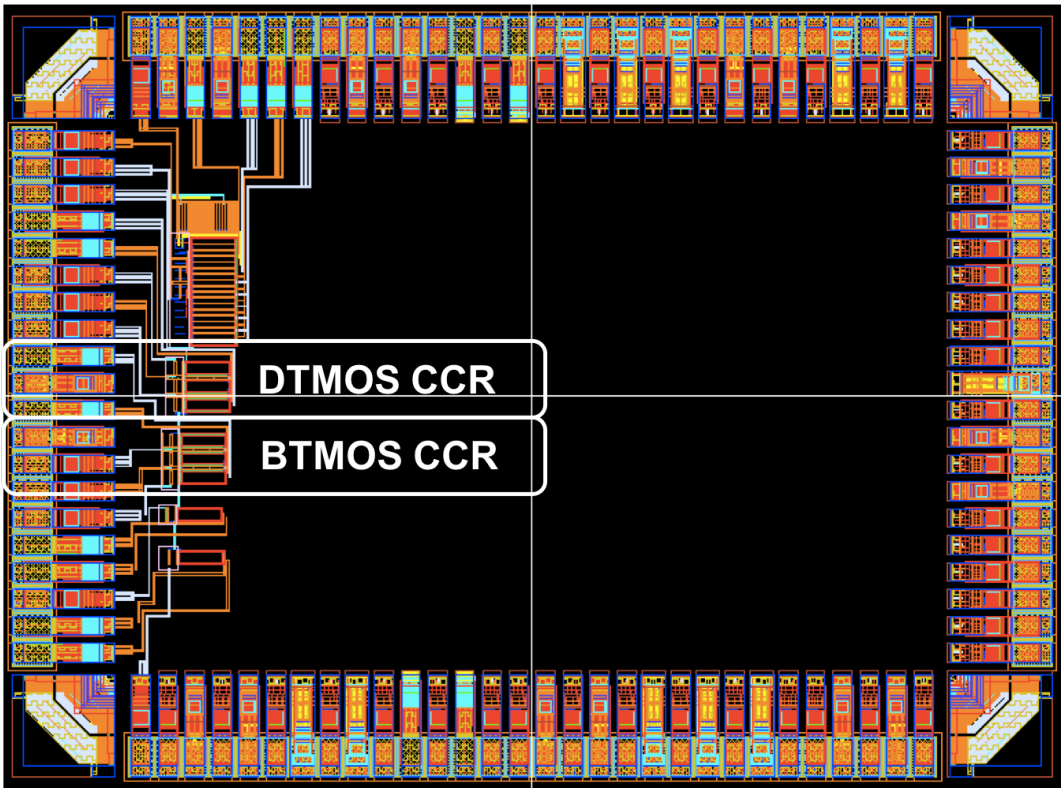

Figure A.1: The fabrication of 3-stage CCR in 65 nm SOTB technology and its layout.

Appendix B

List of Publications

B.1 Journals

[1] Thuy-Linh Nguyen, Yasuo Sato, Koichiro Ishibashi, "A 2.77 uW ambient RF energy harvesting using DTMOS cross-coupled rectifier on 65 nm SOTB and wide bandwidth system design", *MDPI electronics*, Vol. 8, No. 10, 1173 2019.

[2] Thuy-Linh Nguyen, Shiho Takahashi, Yasuo Sato, Koichiro Ishibashi, "RF energy harvesting using cross-couple rectifier and DTMOS on SOTB with phase effect of paired RF inputs", *Submitted to IEEE ECTI-EEC* , Sep., 2019.

B.2 International Conference Presentations

[1] Thuy-Linh Nguyen, Shiho Takahashi, Yasuo Sato, Koichiro Ishibashi, "RF energy harvesting using cross-couple rectifier and DTMOS on SOTB with phase effect of paired RF inputs", *IEEE ECTI-CON 2019* , July., 2019, Pattaya, Thailand.

[2] Koichiro Ishibashi, Jiro Ida, Thuy-Linh Nguyen, Ryo Ishikawa, Yasuo Satoh, Duy-Manh Luong, "RF characteristics of rectifier devices for ambient RF energy harvesting", *ISESD Conference*, OCt., 2019, Bali, In-

donesia..

[3] Shiho Takahashi, Thuy-Linh Nguyen, Yasuo Sato, Koichiro Ishibashi, "Cross-couple DTMOS rectifier with floating sub-circuit using 65 nm SOTB CMOS technology for uW energy harvesting", *TJMW-CON 2018*, July, 2018, Bangkok, Thailand.

Bibliography

[1] K. Chopra, K. Gupta, A. Lambora, "Future Internet: The Internet of Things-A Literature Review," *I*EEE COMITCon, 2019

[2] P. F. H. Sundmaeker, P. Guillemin, S. Woelffle, "Vision and Challenges for Realising the Internet of Things," *P*ub. Office EU, 2010 [Online]. Available: $http : //www.internet - of - things - research.eu/pdf/IoT_Clusterbook_March_2010.pdf$

[3] L. Atzori, A. Iera, G. Morabito, "The Internet of Things: A survey," *E*lsevier Computer Networks, Vol.54, pp.2787-2805, 2010.

[4] M. A. Razzaque, M. M. -Jevric, A. Palade, S. Clarke, "Middleware for Internet of Things: A survey," *I*EEE Internet of Things journal, Vol. 3, no. 1, pp. 70-95, 2016.

[5] Z. Ullah, S. Ahmad, M. Ahmad, A. -u. Rehman, M. Junaid, "A preview on Internet of Things (IoT) and its Application," *I*EEE iCoMET, 2019.

[6] E. J. Marinissen, et. al., "IoT: Source of Test Challenges," *I*EEE 21th European Test Symposium, 2016.

[7] S. M. Alzahrani, "Sensing for the Internet of Things and Its Applications," *I*EEE 5th FiCloundW,pp. 88-92, 2017.

[8] A. Zanella, A. Bui, A. Castellani, L. Vangelsta, M. Zorzi, "Internet of Things for Smart Cities," *I*EEE Internet of Things journal, Vol. 1, no. 1, pp. 22-32, 2104.

[9] D. Newell, M. Duffy, "Review of Power Conversion and Energy Management for Low-Power, Low-Voltage Energy Harvesting Powered Wireless Sensors," *I*EEE Transactions on power electronics, Vol. 344, No. 10, pp 9794-9805, 2019.

[10] S. Kim, R. Vyas, J. Bito, K. Niotaki, A. Collado, A. Georgiadis, M. M. Tentzeris, "Ambient RF Energy Harvesting Technologies for Self-Sustainable Standalone Wireless Sensor Platforms," *P*roceedings of the IEEE, Vol. 102, pp. 1649-1666, 2014.

[11] S. M. Demir, F. A. -Turjman, A. Muhtaroglu, "Energy Scavenging Methods for WBAN Applications: A review," *I*EEE sensors journal, Vol. 18, no. 16, pp. 6477-6488, 2018.

[12] P. M. -Y. Fan, O. -Y. Wong, M. -J. Chung, T. -Y. Su, X. Zhang, P. -H. Chen, "Energy Harvesting Techniques: Energy Sources, Power Management and Conversion," *I*EEE ECCTD, 2015.

[13] P. Jaffe, J. MacSpadden, "Energy Conversion and Transmission module for space solar power," *P*roc. IEEE, Vol. 101, no. 6, pp. 1424-1437, 2013.

[14] M. A. Green, K. Emery, Y. Hishikawa, W. Warta, "Solar cell efficiency tables (version 38)," *P*rogr. Photivoltaic, Res. Appl., Vol. 19, pp. 565-572, 2011.

[15] G. Mahan, B. Sales, J. Sharp, "Thermoelectric materials: New approaches to an old problem," *P*hys. Today, Vol. 50, no. 3, pp. 42-47, 1997.

[16] H. S. Kim, J. H. Kim, J. Kim, "A review of piezoelectric energy harvesting based on vibration," *I*nt. J. Precision Eng. Manuf., Vol. 12, no. 6, pp. 1129-1141, 2011.

[17] S. Roundy, P. K. Wright, J. Rabaey, "A study of low level vibration as a power source for wireless sensor node," *C*omput. Commu., Vol. 26, no. 11, pp. 1131-1144, 2003.

[18] G. Orecchini, L. Yang, M. M. Tentzeris, L. Roselli, "Wearable battery-free active paper printed RFID tag with human-energy scarvenger," *i*n IEEE MTT-S Int. Microw. Sym. Dig., 2011.

[19] F. Yildiz, "Potential ambient energy-harvesting sources and techniques," *J.* Technol. Studies., Vol. 35, no. 1, pp. 40-48, 2009

[20] X. Lu, P. Wang, D. Niyato,D. I. Kim, Z. Han, "Wireless Networks with RF Energy Harvesting: A contemporary Survey," *I*EEE communication surveys and tutorials, Vol. 17, pp. 757-789, 2015.

[21] A. Sample, J. R. Smith, "Experimental Results with two Wireless Power Transfer Systems," *I*EEE Radio and Wireless Symposium, pp. 16-18, 2009.

[22] M. Pinuela, P. D. Micheson, S. Lucyszyn, "Ambient RF Energy Harvesting in Urban and Semi-Urban Environments," *I*EEE transactions on microwave theory and techniques, Vol. 61, pp. 2715-2726, 2013.

[23] H. Nishimoto, Y. Kawahara, T. Asami, "Prototype implementation of ambient RF energy harvesting wireless sensor networks," *I*EEE Sens. (In Proceeding), 2010.

[24] X. Zhang, et. al, "An energy-efficient ASIC for wireless body sensor network in medical applications," *I*EEE Trans. Biomed. Circuits Syst., Vol.4, no. 1, pp. 11-18,2010.

[25] X. Lu, D. Niyato, P. Wang, D. I. Kim, Z. Han, "Wireless charger networking for mobile devices: Fundamental, standards, and applications," *I*EEE Wireless Communications, Vol. 22, no. 2, pp. 126-135, 2015

[26] J. Bito, J. G. Hester, M. M. Tentzeris, "A fully Autonomous Ultra-low Power Hybrid RF/Photovoltaic Energy Harvesting System with -25 dBm Sensitivity," *I*EEE Wireless Power Transfer Conference, 2017.

[27] T. N. T. Mohamad, J. Sampe, D. D. Berhanuddin, "RF and thermal hybrid input for ultra-low power semi-active UHF RFID tags," *I*EEE CSPA, pp. 47-51, 2018

[28] N. Shinohara, "History, Present and Future of WPT," *W*ireless Power Transfer via Radiowaves, Willey, 2014.

[29] T. S. C. Rao, K. Geetha,"Categories, Standards and Recent Trends in Wireless Power Transfer: A Survey," *I*ndian Journal of Science and Technology, Vol. 9, 2016.

[30] B. Clerckx, R. Zhang, R. Schober, D. W. K. Ng, D. I. Kim, H. V. Poor, "Fundamentals of Wireless Information and Power Transfer: From RF Energy Harvester Models to Signal and System Designs," *I*EEE Journal on selected areas in communications, Vol. 37, no. 1, pp. 4-33, 2019.

[31] M. E. -Kantarci, H. T. Mouftah, "Suresense: Sustainable wireless rechargeable sensor networks for the smart grid," *I*EEE Wireless Communication, Vol. 19, no. 3, pp. 30-36, 2012.

[32] M. E. -Kantarci, H. T. Mouftah, "DRIFT: Differentiated RF power transmission for wireless sensor network deployment in the smart grid," *i*n Proc. IEEE Globecom Workshops, pp. 11491-1495, 2012.

[33] C. Mikeka, H. Arai, A. Georgiadis, A. Collado, "DTV Band Micropower RF Energy Harvesting Circuit Architecture and Performance Analysis," *I*EEE International Conference on RFID-Technology and Appications, pp. 561-567, 2011

[34] A. S. Andrenko,X. Lin, M. Zeng, "Outdoor RF Spectral Survey: a Roadmap for Ambient RF Energy Harvesting," *I*EEE TENCON,2015.

[35] S. Kitazawa, H. Ban, K. Kobayashi, "Energy Harvesting from Ambient RF Sources," *I*EEE IMWS IWPT, 39-42, 2012.

[36] Z. Liu, Z. Zhong, Y. X. Guo, "High-Efficiency Triple-band Ambient RF Energy Harvesting for Wireless Body Sensor Network," *I*EEE IMWS-Bios, pp. 1-3, 2014

[37] P. D. Bradley, et,al., "An Ultra Low Power, High Performance Medical Implant Communication System (MICS) Transceiver for Implantable Devices," *I*EEE BioCAS, pp.158-161,2006.

[38] F. Carrara, et,al., "A 400 MHz CMOS Radio Front-End for Ultra Low-Power Medical Implantable Applications," *I*EEE ESSCIRC, pp.232-235, 2009.

[39] J. Bae, et.al, "A 490 μW fully MICS compatible FSK transceiver for implantable devices," *I*EEE 2009 Symposium on VLSI Circuits Digest of Technical Papers, pp. 36-37, 2009.

[40] X., Chen, J., Breiholz, F., Yahya, C., Lukas, H., S., Kim, B., Clahoun, D., Wentzloff., "A 486 μW all-Digital Bluetooth Low Energy Transmitter with Ring Oscillator Based ADPLL for IoT applications," *I*EEE RFIC, pp168-171, 2018

[41] S. N. Daskalakis, G. Goussetis, S., D., Assimonis, M. M. Tentzeris, A. Georgiadis, "A μW Backscatter-Morse-Leaf Sensor for Low-Power Agricultural Wireless Sensor Networks," *I*EEE Sensors Journal, Vol. 18, No. 19, pp. 7889-7898, 2018.

[42] D., W., Jee, D., Stlvester, D., Blaauw, J., Y., Sim, "A 0.45V 423nW ," *I*EEE International Conference on RFID, 2017.

[43] K. Ishibashi, J. Ida, L. T. Nguyen, R. Ishikawa, Y. Satoh, D. M. Luong, "RF characteristics of rectifier devices for ambient RF energy harvesting,", *I*SESD Conference, 2019

[44] M. Awad, P. Benech, J. -M. Duchamp, "Design of Dickson Rectifier for RF energy harvesting in 28 nm FD-SOI technology," *E*UROSOI-ULIS, 2018

[45] D. Cavalheiro, F. Moll, S. Vatchev, "Tunel FET device characteristics for RF energy harvesting passive rectifiers," *I*EEE NEWCAS,2015

[46] K. Kotani, T. Ito, "High efficiency CMOS rectifier circuit with self-Vth-cancellation and power regulation functions for UHF RFIDs," *I*EEE Asian Solid-state Circuit Conference, pp. 119-122, 2007.

[47] K. Kotani, T. Ito, "High efficiency Differential-Drive CMOS Rectifier for UHF RFIDs," *I*EEE Journal of Solid-State Circuits, Vol. 44, pp. 3011-3018, 2009.

[48] P. T. Theilmann, C. D. Presti, D. J. Kelly, P. M. Asbeck, "A μW Complementary Bridge Rectifier With Near Zero Turn-on Voltage in SOS CMOS for Wireless Power Supplies," *I*EEE Transaction on Circuit and Systems, Vol. 59, pp. 2111-2124, 2012.

[49] S. Y. Wong, C. C. Chen, "Power efficient multi-stage CMOS rectifier design for UHF RFID tags," *E*LSEVIER INTEGRATION, the VLSI journal, Vol. 44, pp. 242-255, 2011.

[50] P. Kamalinejad, K. Keikhosravy, S. Mirabbasi, V. C. M. Leung, "An Efficiency Enhancement Technique for CMOS Rectifier with Low Start-Up Voltage for UHF RFID Tags," *I*EEE International Green Computing Conference Proceedings, pp.1-6, 2013.

[51] M. Arrawatia, M. S. Baghini, G. Kumar, "Broadband RF Energy Harvesting System covering CDMA, GSM900, GSM1800, 3G Bands with Inherent Impedance Matching," *I*EEE IMS, pp.1-3, 2016

[52] N. Nguyen, N. N. Tuan, Q. C. Nguyen, V. B. G. Truong, M. Krairiksh, M. T. Le, "Multiband Antenna for RF energy harvesting," *I*EEE ISAP, 2018

[53] M. F. Shaker, H. A. Ghali, D. M. N. Elecheakh, H. a. E. Elsadek, "Multiband coplanar Monopole Antenna for Energy Harvesting," *I*EEE RFIT, 2018

[54] X. Bai, J. -w. Zhang, L. -j. Xu, "A braodband CPW fractal antenna for RF energy harvesting," *I*EEE ACES, 2017.

[55] M. Arrawatia, M. S. Baghini, G. Kumar, "RF Energy Harvesting System from Cell Towers in 900 MHz Band," *N*ational Conference on Communications, pp. 1-5, 2011.

[56] N. Tung, "Multi-band Ambient RF Energy Harvesting Rectifier for Autonomous Wireless Sensor Networks," *I*EEE TECON, pp. 3736-3739, 2016

[57] S. Kitazawa, H. Kanoda, M. Hanazawa, S. Ano, H. Ban, K. Kobayashi, "A Study on RF energy harvesting from three broadcasting and communication frequency bands," *I*EICE technical report MW2013, pp. 53-58, 2013.

[58] M. Stoopman, S. Keyrouz, H. J. Visser, K. Phillips, W. A. Serdijn, "Co-Design of a CMOS Rectifier and Small Loop Antenna for Highly Sensitive RF Energy Harvesters," *I*EEE Journal of Solid-State Circuits, Vol. 49, pp.622-634, 2014.

[59] J. Kang, P. Y. Chiang, A. Natarajan, "A 3.6 cm^2 Wirelessly-Powered UWB SoC with -30.7dBm Rectifier Sensitivity and Sub-10cm Range Resolution," *I*EEE Radio Frequency Integrated Circuits Symposium, pp. 255-258, 2015.

[60] M. Stoopman, S. Keyrouz, H. J. Visser, K. Phillip, W. A. Serdijn, "A Self-calibrating RF Energy Harvesting Generating 1 V at -26.3 dBm," *I*EEE Symposium on VLSI, pp. 226-227, 2013.

[61] F. Kocer, M. P. Flynn, "A New Transponder Architecture with on-chip ADC for long-range Telemetry Applications," *I*EEE J. Solid State Circuit, Vol. 41, no. 5, pp. 1141-1148, 2006.

[62] J. Yi, W. H. Ki, C. Y . Tsui, "Analysis and Design Strategy of UHF Micro-power CMOS Rectifiers for Micro-sensor and RFID Applications," *I*EEE Trans. Circuit System, Vol. 54, no. 1, pp. 153-166, 2007.

[63] S. Mandal, R. Sarpeshkar, "Low-power CMOS Rectifier Design for RFID Applications," *I*EEE Trans. Circuits Syst., Vol. 54, no. 6, pp. 1177-1188, 2007

[64] G. A. Vera, A. Georgaiadis, A. Collado, "Design of a 2.45 GHz Rectenna for Electromagnetic (EM) Energy Harvesting, " *I*EEE Radio Wireless Symposium, pp. 61-64, 2010.

[65] G. Papotto, F. Carrara, G. Palmisano, "A 90-nm CMOS Threshold Compensated RF Energy Harvester," *I*EEE Solid State Circuits, Vol. 46, no. 9, pp. 985-1997, 2011.

[66] J. Masuch, M. D. -Restituto, D. Milosevic, P. Baltus, "An RC-to-DC Energy Harvester for co-integration in a low-power 2.4 GHz transceiver frontend," *I*n Proc IEEE ISCAS, pp. 680-683, 2012

[67] S. Scorcioni, A. Bertacchini, L. Larcher, "A 868 MHz CMOS RF-DC Power Converter with -17 dBm Input Power Sensitivity and Efficiency Higher than 40% over 14 dBm Input Power Range," *I*n Proc. IEEE ESSCIRC, pp. 109-112, 2012

[68] D. Y. Choi,"Comparative Study of Antenna Design for RF Energy Harvesting," *H*Indawi Int. J. Antennas Propag., pp. 1-10, 2013

[69] H. Sun, Y. Guo, M. He, Z. Zhong, "Design of a High-efficiency 2.45-GHz Rectenna for low-input-power Energy Harvesting," *I*EEE Antennas Wireless Progag. Letter , Vol. 11, pp. 929-932, 2012.

[70] D. Karolak, T. Taris, Y. Deval, J. B. Begueret, A. Mariano, " Design Comparison of Low-power Rectifier dedicated to RF Energy Harvesting," *I*N Proc. IEEE ICECS, pp. 524-527, 2012

[71] M. Roberg, T. Reveyrand, I. Ramos, E. A. Falkenstein, Z. Popovic, "High-efficiency Harmonically Terminated Diode and Transistor Rectifiers," *I*EEE Trans. Microw. Theory tech., Vol. 60, no. 12, pp. 4043-4052, 2012

[72] P. Nintanavongsa, U. Muncuk, D. R¿ Lewis, K. R. Chowdhury, "Design Optimization and Implementation for RF Energy Harvesting Circuits," *I*EEE J. Emerging Sel. Topics Circuits Syst., Vol. 12, no. 1,pp. 24-33,2012

[73] B. R. Franciscatto, V. Feritas, J. M. Duchamp, C. Defay, T. P Vuong, "High-efficiency Rectifier circuit at 2.45 GHz for low-input-power RF Energy Harvesting," *I*n Proc. IEEE EuMC, pp. 507-510, 2013.

[74] S. Scorcioni, L. Larcher, A. Bertacchini, L. Vincetti, M. Maini, "An Integrated RF Energy Harvester for UHF Wireless Powering Applications," *I*n Proc. IEEE WPT, pp. 92-95, 2013

[75] X. Wang, A. Mortazawi, "High Sensitivity RF Energy Harvesting from AM Broadcasting Stations for civilian Infrastructure Degradation Monitoring," *I*n Proc. IEEE IWS, pp. 1-3, 2013.

[76] A. Agrawal, S. K. Pandey, J. Singh, M. S. Paihar, "Realization of Efficient RF Energy Harvesting Circuits Employing Different Matching Technique," *I*n Proc. IEEE ISQED, pp. 754-761, 2014

[77] T. Furuta, M. Ito, N. Nambo, K. Itoh, K. Noguchi, J. Ida, "The 500 MHz band low power rectenna for DTV in the Tokyo area. In Proceedings of the 2016 IEEE Wireless Power Transfer Conference (WPTC), Aveiro, Portugal, 5–6 May 2016.

[78] A. K. Moghaddam, J. H. Chuah, H. Ramiah, J. Ahmadian, P. I. Mak, R. P. Martins, " A 73.9%-Efficiency CMOS Rectifier Using a Lower DC Feeding (LDCF) Self-Body-Biasing Technique for Far-Field RF Energy-Harvesting Systems," *I*EEE Trans. Circuits and Syst., Vol. 64, no. 4, pp. 992-1002, 2017

[79] Y. Lu, H. Dai, M. Huang, M. K. Law, S. W. Sin, S. P. U, R. P. Martin, "A Wide Input Range Dual-path CMOS Rectifier for RF Energy Harvesting," *I*EEE Trans. Circuits and Systems, Vol. 64, no. 3, pp. 166-170, 2017

[80] K. R. Sadagopan, J. Kang, Y. Ramandass, A. Natarajan, "A 960pW Co-Integrated-Antenna Wireless Energy Harvester for Wifi Backchannel Wireless Powering," *I*SSCC 2018, pp. 136-137, 2018.

[81] T. Le, K. Mayaram, T. Fiez, "Efficient Far-Feild Radio Frequency Energy Harvesting for Passively Powered Sensor Networks," *I*EEE Journal on Solid-State Circuits, Vol. 43, pp.1287-1301, 2008.

[82] I. Chaour, A. Fakhfakh, O. Kanoun, "Enhanced Passive RF-DC Converter Circuit Efficiency for Low RF Energy Harvesting," *M*DPI Sensors, Vol. 17, 546, doi:10.3390/s17030546

[83] A. Khemar, A. Kacha, H. Takhedmit, G. Abib, "Design and experiments of a dual-band rectenna for ambient RF energy harvesting in urban environments," *I*ET Microwaves, Antenna & Propagartion, Vol. 12, pp. 49-55, 2017

[84] F. Bolos, J. Blanco, A. Collado, A. Georgaiadis, "RF Energy Harvesting From Multi-Tone and Digitally Modulated Signals," *I*EEE transaction on microwave theory and Techniques, Vol. 64, pp. 1918-1927, 2016.

[85] C. R. Valenta, M. M. Morys, G. D. Durgin, "Theoretical Energy-Conversion Efficiency for Energy-Harvesting Circuits Under Power-Optimized Waveform Excitation," *I*EEE transaction on microwave theory and techniques, Vol. 63, pp. 1758-1767, 2015.

[86] A. Collado, A. Georgiadis, "Optimal Waveforms for Efficient Wireless Power Transmission," *I*EEE Microwave and Wireless Components Letters, Vol. 24, pp.354-356, 2014.

[87] T. H. Lee, "Passive RLC networks," In *T*he Design of CMOS Radio-Frequency Integrated Circuits; 2nd ed.; Cambridge Univ. Press: Cambridge, U.K, 2004.

[88] M. A. Niknejad, "Resonance and Impedance Matching," in *E*lectromanegtics for High-speed Analog and Digital Communication circuits; Cambridge Univ. Press: Cambridge, U.K, 2007.

[89] W. D. Roehr, "Rectifier Applications Handbook: Reference Manual and Design Guide," *S*emiconductor Components Industries, LLC, Vol. Rev. 2, 2001

[90] M. Ruzbehani, "A comparative Study of Symmetrical Cockcroft-Waton Voltage Multipliers," *H*idawi journal of Electrical and Computer Engineering, Vol 2017, ID 4805268,2017.

[91] Y. C. Wong, P. C. Tan, M. M. Ibrahim,A. R. Syafeeza, N. A. Hamid, "Dickson Charge Pump Rectifier using Ultra-Low Power (ULP) Diode for BAN Applications," *J*ournal of Telecommunication, Electronic and Computer Engineering, VOl. 8, No. 9, pp. 77-82

[92] U. Alvarado, G. Bistue, L. Adin, "Low power RF Circuit Design in Standard CMOS Technology," *1* ed. Springer-Verlag Berlin Heidelberg, 2012.

[93] C. Nguyen, "Radio Frequency Integrated Circuit Engineering," *J*ohn Wiley &Sons, New Jersey, Canada, 2015

[94] Y. Yamamoto, H. Makiyama, H. Shinohara, T. Iwamatsu, H. Oda, S. Kamohara, N. Sugii, Y. Yamaguchi, T. Mizutani, T. Hiramoto, "Ultralow-voltage operation of Silicon-on-Thin-BOX(SOTB) 2Mbit SRAM down to 0.37V ultilizing adaptive back bias," *S*ymposium on VLSI Technology, pp. T212-123, 2013.

[95] V. N. Trung, V., R. Ishikawa, K. Ishibashi, "83nJ/bit Transmitter using code modulated synchronized-OOK on 65nm SOTB for normally-off wire-

less sensor networks," *I*EICE Transaction on Electronics, E101-C.472, pp. 472-479, 2018.

[96] P. R. Gray, P. J. Hurst, S. H. Lewis, R. G. Meyer, "Models for Integrated-Circuit Active Devices," In *A*nalysis and Design of Analog Integrated Circuits; Sayre D., Vargas, V. A.; Wiley: New York, 2001; pp 1-74.

[97] F. Assaderaghi, D. Sinitsky, S. Parke, J. Bokor, P. K. Ko, C. Hu, "A dynamic threshold voltage MOSFET (DTMOS) for very low voltage operation," *I*EEE Electron Device Letters, Vol. 15, pp. 510-512, 1994.

[98] S. Chouhan, K. Halonen, "The design and Implementation of DTMOS biased all PMOS rectifier for RF energy harvesting," *I*EEE International New Circuits and Systems Conference, pp. 444-447, 2014.

[99] S. Chouhan, K. Halonen, "The DTMOS based UHF RF to DC conversion," *I*EEE International Conference on Electronics, Circuits, and Systems, pp. 629-632, 2013.

[100] H. Makiyama, K. Horita, T. Iwamatsu, H. Oda, N. Sugii, Y. Inoue, Y, Yamamoto, "Design Consideration of 0.4V-Operation SOTB MOSFET for Super Low Power Application," *I*EEE International Meeting for Future of Electron Devices, 2011.

[101] N. T. Linh, S. Takahashi, Y. Sato, K. Ishibashi, "RF Energy Harvesting using Cross-Couple Rectifier and DTMOS on SOTB with Phase Effect of paired RF inputs," *I*EEE ECTI conference, 2019, on Proceeding.

[102] N. T. Linh, Y. Sato, K. Ishibashi, "A 2.77 μW Ambient RF Energy Harvesting using DTMOS Cross-Coupled Rectifier on 65 nm SOTB and Wide Bandwidth System Design," *M*DPI Electronics, Vol. 8(10), 1173, 2019

[103] B. Razavi, "Design of Analog CMOS Integrated Circuits,: *M*cGraw-Hill in Electrical and Computer Engineering, 2001

Author Biography

Thuy-Linh Nguyen received the B.S. and M.S degrees from the Vietnam National University of Le Quy Don Technical University, Vietnam, in Electronic Engineering and Technology in 2009 and 2014, respectively. In 2017, she came to Japan and became a student at The University of Electro-Communications, Tokyo, Japan. Her research interests include RF energy harvesting, wireless power transfer, low power analog IC design, RF analog circuit design.